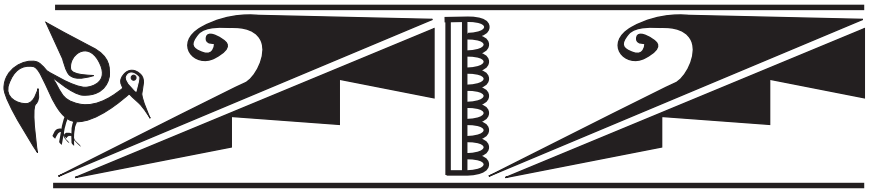

Detection & Analysis

Uncertainty Reporting in Measurements of Plutonium Solution Speciation: How Can We Do Better?

John M. Berg,
D. Kirk Veirs
Los Alamos National Laboratory, Los Alamos, NM 87545, USA

In the literature of actinide solution chemistry, it is not uncommon to find multiple published values of the same thermodynamic parameter that disagree with each other by more than their reported uncertainty ranges. This indicates an obvious historical problem with uncertainty estimates. Clearly, they have not always reflected the full uncertainty in the data and in the data analysis method. This is partly a reflection of the difficulty of propagating uncertainty in analyses of large data sets on complex chemical systems in which multiple, non-linear chemical models must be considered. It is also a reflection of the difficulty of incorporating systematic error into uncertainty analysis. Nonetheless, the chronic underestimation of uncertainty creates real problems for those who would use the parameters as part of even more complex models of real environmental or process chemical systems.

Critical reviews, when they are available, help by assessing disparate reported values and arriving at a recommended value.[1] For example, reviewers might identify and discard obvious outlying reports and then recommend acceptance of a weighted average of the remaining values. Uncertainty might be assigned to this composite by requiring that the remaining reported values be included within the uncertainty range.

This cannot be done when as few as one or two reported values are available, however. In those cases, the reviewer, or user, must either accept the uncertainty estimate in the primary literature or attempt to reassess the uncertainty from the data as it was reported. The latter is difficult since sufficient details about the uncertainty sources in the raw data are seldom available except to the authors of the primary studies. Clearly, it would be useful if uncertainty estimates could be calculated more accurately and easily by those publishing the primary studies.

Fast, modern desktop computers and statistical Monte Carlo simulations place the tools for more accurate uncertainty estimates within the hands of most researchers, without requiring expertise in analytical, statistical methods of uncertainty propagation. This is significant because Monte Carlo methods are conceptually simpler and carry less risk of errors due to misapplication than analytical statistical methods. The methods are not fundamentally new, but they have only recently begun to be applied to actinide systems.

Meinrath and coworkers has recently described the application of Monte Carlo resampling methods to U(VI) and Np(VI) carbonate complexation.[2] We take a somewhat different approach by using simulations based on an analysis of experimental sources of error, rather than resampling. The two methods are largely complimentary. Our method requires more knowledge of measurement uncertainties, but is less vulnerable to correlations within the data. Both methods should become increasingly valuable tools as computing power continues to advance.

We have applied Monte Carlo simulations to analyses of Pu(IV) complexation by two weak ligands, nitrate and chloride, in aqueous solution using visible/near-infrared (NIR) absorption spectroscopy. The resulting uncertainties we report for the formation constants, while somewhat larger than some in the literature,

CP532, Plutonium Futures – The Science, edited by K. K. S. Pillay and K. C. Kim,
2000 American Institute of Physics 1-56396-948-3

should more accurately reflect the limitations of the spectroscopic data, the experimental design, and the models used.

The choice of the model itself can also be aided and supported using Monte Carlo simulations. Uncertainty in model choice, while seldom discussed in quantitative terms, is at least as important as parameter uncertainty in analyses of complex systems. All practical models are simplifications of the interactions that occur between and within all possible chemical species. Alternative models may be tested for how well they can explain the available experimental data and, generally, one model is chosen for use in the bulk of the data analysis. However, the basis for the choice and the uncertainties in the choice of this model are not usually described in a quantitative manner. Where more than one model is a realistic possibility, this complicates the comparison of disparate reported parameter values.

Monte Carlo simulations have the potential to enable more accurate assessment of whether a given model fits the data as well as it ought, given accurate information about the uncertainties in the raw data. In general, such a quantitative assessment is not feasible using analytical statistical approaches except in simplifying cases. It is computationally intensive but conceptually straightforward using Monte Carlo simulations. We have been able to show that alternative models for weak ligand complexation of Pu(IV) that include different numbers of hypothesized complexes can be compared quantitatively using Monte Carlo simulations.

References

1. I. Grenthe, J. Fuger, R. J. M. Konings, R. J. Lemire, A. B. Muller, C. Nguyen-Trung Cregu, and H. Wanner, Chemical Thermodynamics of Uranium, (Elsevier Science Publishers, Amsterdam, 1992).

2. G. Meinrath, Y. Kato, T. Kimura, and Z. Yoshida, Radiochimica Acta 84, 21 (1999).

Production and Radiometric Measurements of the Large Particle Plutonium Oxide Non-Destructive Assay Standards

Denise L. Thronas,
Amy S. Wong,
Sandra L. Mecklenburg,
Robert S. Marshall
Los Alamos National Laboratory, Los Alamos, NM 87545, USA

Abstract

The Analytical Chemistry Group at Los Alamos National Laboratory (LANL) has produced several sets of working reference materials (WRMs) for the National TRU Waste Program (NTWP) NDA PDP(Non-Destructive Assay Performance Demonstration Program). This paper describes the first example of production of traceable, certified standards containing plutonium oxide in large particle form for the DOE complex. Discussion of the production and radiometric measurements of these NDA standards is included herein.

Introduction

The purpose of the NTWP NDA PDP is to evaluate and verify the performance of various non-destructive and gamma systems used to characterize TRU waste bound for WIPP throughout the DOE complex. This program utilizes LANL-produced certified, traceable plutonium, uranium, americium, and special large-particle WRMs representative of TRU waste forms found within the DOE complex.

In support of this program, the Analytical Chemistry Group fabricated and certified 32 large particle Pu WRMs. The large-particle WRMs were intended to evaluate the ability of NDA measurement systems to correct for measurement biases caused by the presence of relatively large particles of PuO_2. These NDA WRMs were prepared from well-characterized plutonium oxide (PuO_2) pressed into large particles (~0.5 to ~3.5 mm diameter). The PuO_2 particles were placed in a graphite matrix and encapsulated in a dual stainless steel cylinder configuration. The amount of PuO_2 in the WRM set ranged from ~1 to ~100 g of nuclear material. The WRMs were fabricated to strict quality objectives, including specified uncertainties in nuclear material content, the total contained alpha activity, and homogeneity. The WRMs are traceable to a national certifying laboratory or agency, e.g. National Institute of Standards and Technology (NIST) or New Brunswick Laboratory (NBL).

In order to meet the stringent quality objectives specified for these WRMs, a batch of PuO_2 was produced and thoroughly characterized using traceable analysis before being used as the nuclear component during WRM fabrication. The ^{241}Am, ^{244}Cm and ^{252}Cf contents of PuO_2 were characterized by radiochemical methods. The Pu material was assayed by a calorimetric analysis conducted by NIS-5 Group at LANL. Other radiometric support discussed in this paper includes the verification of the plutonium content and homogeneity of each of the WRMs.

Production of WRMs

The batch of weapon grade PuO_2 prepared specifically for the production of these WRMs by the LANL Plutonium Facility was mixed with a binder and pressed into pellets, which were calcined at 1600°C, resulting in very dense, robust pellets. The pellets were crushed and screened to form the large particles of the desired

CP532, Plutonium Futures – The Science, edited by K. K. S. Pillay and K. C. Kim,
2000 American Institute of Physics 1-56396-948-3

size, ~0.5-3.5 mm in diameter. The exact specification of this material and the WRMs are confidential information and will not be included herein.

In the fabrication of the WRMs it was important to control the inter-particle attenuation effects among neighboring PuO_2 particles. Therefore, it was necessary to place each particle in a fixed geometry relative to its neighbors within the WRM. The particles were individually embedded in fibrous graphite disks, which were then uniformly loaded into the WRM cylinder. The graphite fiber matrix was chosen because it adequately retained the plutonium particles and does not interfere with NDA measurements. The placement of each plutonium particle and loading pattern for the WRM were determined by the number of plutonium particles needed to obtain the desired weight of PuO_2 in each WRM. During WRM fabrication, each graphite wafer was meticulously loaded, weighed, and placed into the stainless steel cylinders. Welding an end cap in place then sealed the cylinders, and the inner cylinder was then welded into an outer cylinder to achieve double encapsulation.

Verification and Certification of WRMs

The Radiochemistry Team conducted verification measurements on the WRMs once they were encapsulated and decontaminated. Verification of the vertical distribution of PuO_2 (homogeneity) was performed using collimated gamma-ray intensity measurements focused on the full length of the cylinder. The WRM cylinder was placed inside a lead cage with a 13-cm wide aperture, which was 40 cm from a high purity germanium (HpGe) detector. The net area of the ^{241}Am 59.5 keV, the ^{239}Pu 129 keV, and ^{239}Pu 414 keV gamma-ray peaks were recorded. The amount of Pu in the WRMs was verified by calculating the normalized count rate per gram of Pu in each WRM based on the ^{239}Pu gamma ray peak intensity.

In addition to the verification measurements, a geometric rotational study was conducted to observe any effects of inter-particle attenuation within the WRMs. For this study, a selected WRM was rotated in 90-degree increments along its long axis and measured in each of four rotational segments. The net area of the ^{241}Am gamma-ray peak was recorded. Evaluation of the normalized count rate of Pu indicated that no inter particle attenuation effects were observable.

Certification of the WRMs was accomplished by compilation of the traceable weighing and analyses data, computation of the nuclear material quantities and total alpha activity in each WRM, and propagation of all relevant error terms to provide overall uncertainty estimates.

Conclusion

In conclusion, thirty-two large particle plutonium-based WRMs for the NDA PDP program were fabricated and certified by the Analytical Chemistry Group of LANL and distributed to eight sites within the DOE complex. All quality objectives on the WRMs were met, and the WRMs were provided with traceable certification of Pu and Am content and total alpha activity. The Radiochemistry Team supported many important aspects during the certification of these WRMs. Support included analyses of ^{241}Am, ^{244}Cm and ^{252}Cf in the PuO_2 and the final verifications of the uniformity and Pu content of the WRMs.

Analysis of Boron and Silicon in Plutonium Samples by Inductively Coupled Plasma Spectrometry

Billie A. Shepherd, Sandra L. Bonchin, Deborah J. Figg
Los Alamos National Laboratory, Los Alamos, NM 87545, USA

Inductively coupled plasma atomic emission spectroscopy (ICP-AES) and inductively coupled plasma mass spectrometry (ICP-MS) are widely employed analytical techniques. ICP has the advantage of rapid and easy sample introduction due to the high temperature of the plasma achieved. The ICP is also simple to operate and possesses low background levels for most elements. Therefore, the ICP has become one of the most common methods for trace inorganic analytical studies.

The concentration of silicon and boron is generally determined by ICP-AES or ICP-MS. The determination of silicon is difficult by ICP since background levels are often high. This may be due to the water source, the glass being used in the sample introduction, or contamination in the sample preparation process. ICP-MS is not used for Si because of direct spectral interference. The determination of boron is troublesome because of volatilization of boron from the solution.

All samples are analyzed using a Thermo Jarrell-Ash IRIS ICP-AES. Studies were performed to determine where the high silicon background was coming from. The detection limit of silicon for the ICP-AES was found to be 0.20 ppm. A comparison of the laboratory's 18 megaohm distilled water and Fisher Scientific's ultra pure distilled water was carried out. No significant difference in the silicon values between the two water sources was encountered. The next step was to look at the acids used in sample digestion for the plutonium samples and also the sample tubes used. The tubes were used "as is" and also after soaking them in 2% nitric acid for a day. The acid solutions were analyzed as soon as possible, a week later, and a month later. This was to ensure silicon was not being leached from the sample tubes. There was a notable amount of silicon in the acid solutions containing hydrofluoric acid and also a serious increase after solutions were in the tubes for a week.

The acid solutions used in the sample digestion of plutonium metals was also analyzed for silicon on a Perkin-Elmer Optima 3300 DV. There was meaningful difference between the Perkin-Elmer ICP and Thermo Jarrell-Ash ICP. The conventional setup of the sample introduction for the Thermo Jarrell-Ash ICP uses a glass spray chamber and injection tube. This system could easily contaminate the sample, especially for the determination of silicon. The normal setup of the sample introduction for the Perkin-Elmer instrument uses a Scott-type spray chamber and alumina injection tube.

A polypropylene spray chamber and alumina injection tube replaced the glass spray chamber and injection tube of the Thermo Jarrell-Ash ICP. The acid solutions were analyzed again, and the amount of silicon was significantly less compared to the results with the glass sample introduction setup. It was the determined the silicon was from the HF leaching the glassware used in the sample introduction system.

It has been found that boron can be retained by adding mannitol and cesium carbonate to the solution.[1] We have compared boron solutions with mannitol

CP532, Plutonium Futures – The Science, edited by K. K. S. Pillay and K. C. Kim,
2000 American Institute of Physics 1-56396-948-3

added, with mannitol and cesium carbonated added, and with no mannitol or cesium carbonate added. The boron solutions are analyzed on the Perkin-Elmer Optima 3300 DV. They are then heated on a hot plate. After the samples have cooled to room temperature, they are analyzed on the ICP again. Initial studies indicate mannitol does help retain boron in solution.

Reference

1. Y. K. Xiao; R. D. Vocke, Jr.; G. H. Swihart; Y. Xiao, "Boron Volatilization and Its Isotope Fractionation during Evaporation of Born Solution," Anal. Chem., 69, 5203 (1997).

Laser Induced Breakdown Spectroscopy (LIBS) Applied to Plutonium Analysis

Coleman A. Smith, Max A. Martinez
Los Alamos National Laboratory, Los Alamos, NM 87545, USA

Introduction

A Laser Induced Breakdown Spectroscopy (LIBS) system has been developed specifically for the quantitative analysis of gallium in plutonium dioxide in support of the MOX fuel development program. The advantage of this system is no sample preparation and the capability to analyze extremely small samples. Success in this application has prompted an expansion of the technique to other areas, including determination of plutonium isotopic ratios. This paper will present recent results for gallium content in PuO_2 after processing via thermally induced gallium removal (TIGR). Data will also be presented for the determination of the plutonium 239/240 isotopic ratio.

Experimental Description and Results

The LIBS system utilizes a pulsed Nd:YAG laser. Most data has been collected using the fundamental wavelength of 1064 nm, although frequency-doubled 532 nm light is also available. The laser emits 5-ns pulses, focused to a spot size of <100 μm and normally attenuated to <25 mJ/pulse. Energy densities on the order of 10^{11} W/cm^2 are produced at the sample surface, resulting in rapid ablation of material and subsequent heating to plasma temperatures. Atoms and ions within the hot plasma emit light that is collected and wavelength dispersed by a 2-meter focal length spectrometer and imaged onto a 2-dimensional intensified charge-coupled device (ICCD) camera. The current detectable wavelength range is ~300-650 nm, limited by optics coating materials and by a 2400 gr/mm grating installed in the spectrometer. Very high resolution work is possible by operation of the spectrometer in double-pass mode, for an effective focal length of 4 m. A delay generator provides high-speed gating for the ICCD so that the temporal evolution of the plasma plume can be followed. The light collection optics configuration allows for the preservation of the plume image, so that spatial information appears at the ICCD in the vertical dimension. The sample is enclosed within a vacuum chamber so that the buffer gas composition and pressure can be varied.

Results: Ga content in Pu dioxide. LIBS has been successful in the detection of gallium in PuO_2. Gallium has two emission lines of high intensity, 403.299 and 417.204 nm. The gallium line at 417.204 nm was found to be the most intense and best suited for analysis at low Ga concentrations. A nearby Pu emission line at 417.242 nm was chosen to ratio against the Ga line. Twelve Pu oxide samples were run under identical conditions, as follows: laser energy 20 mJ/pulse at 20 Hz and accumulations ranging from 2 to 20 sec, 1 μs delay and 10 μs gate (ICCD timing), and 100 torr helium buffer gas. A total of 12 samples were analyzed. All were products from small-scale TIGR runs and prepared for LIBS analysis by pressing into a thin pellet. Portions of each sample had been previously analyzed by inductively coupled plasma-mass spectrometry (ICP-MS) to yield gallium concentrations ranging from 34 to 8336 ppm. The Ga/Pu integrated peak area ratios resulting from LIBS analysis ranged from 0.288 to 9.92. Most of the data (10 of 12 points) lies below 500 ppm and is quite linear in that range. However, the ratio of integrated area appears to become nonlinear with concentration above ~1000 ppm. The nonlinearity is due largely to self-absorption of Ga emission within the plume.

CP532, Plutonium Futures – The Science, edited by K. K. S. Pillay and K. C. Kim,
2000 American Institute of Physics 1-56396-948-3

It may be possible to avoid this effect if a less intense Ga emission line can be used for analysis at higher concentrations.

Results: Isotopic ratios. The 2-meter spectrometer operating in double-pass mode as part of the LIBS system allows for resolution of the isotope shift of plutonium electronic transitions. Many Pu-239/Pu-240 isotope shifts have been catalogued (see footnote* on table below). An atomic Pu emission line occurring at 594.522 nm was chosen for analysis. The quoted isotope shift of –355 milliwavenumbers (240 – 239) appears as two distinct emission lines separated by ~7 pixels, with full-width, half-maximum (FWHM) ~3.5 pixels. Two samples containing different ratios of 239/240 were chosen for analysis. Table 1 below summarizes this data:

Table 1. Analysis of Samples Containing Different Ratios of Pu-239/240.

Sample	Observed Ratio	Known Ratio
Metal "H"	93.1/6.9	93/6
Oxide "AFR360"	51.0	49.6/51.4
Analysis Line* (nm/cm^{-1})	**240-239 Isotope Shift* (cm^{-1})**	**Intensity***
594.52202/16815.576	-0.355	8

*Pu positions are quoted from "The Atomic Spectrum of Plutonium" by Jean Blaise (Orsay, France), Mark Fred (Argonne), and Ralph G. Gutmacher (Los Alamos) in an Argonne National Laboratory Report ANL-83-95, dated August 1984. Relative intensities are in half-log units ranging from 0-9.

Summary

The LIBS system as currently configured has wide-ranging capability for elemental and isotopic analysis. Analysis for many other impurity elements in plutonium metal and oxide are possible. Data has been collected for other elements detectable at low concentrations in a plutonium matrix, including iron, nickel, aluminum, beryllium, and uranium.

Emission from Neptunyl Ions in the Near IR

H. J. Dewey,
T. A. Hopkins
Los Alamos National Laboratory, Los Alamos, NM 87545, USA

Although luminescence spectroscopy has proved a powerful diagnostic technique for the f^0 uranium(VI), it has found limited utility for compounds of neptunium, plutonium, or compounds involving the lower oxidation states of uranium. This apparent lack of luminescence from the early actinides containing one or more 5*f* electrons can be explained by the presence of *f-f* transitions at low energies and the absence of large energy gaps between neighboring electronic states. Thus, any luminescence arising from *f-f* transitions is likely to lie in the near infrared region of the spectrum. With recent improvements in near infrared detectors, we have initiated investigations into actinide luminescence in this spectral region and have begun by searching for emission from f^1 neptunyl(VI). Our hope is that, once developed, *f-f* luminescence might serve as a tool for studying actinide speciation and ultimately find utility as an analytical chemistry tool.

We have chosen to begin our studies with the $NpO_2Cl_4^{2-}$ ion because its electronic and vibrational structure has been well characterized by Denning et al.[1] Crystalline cesium hexachlorozirconate was chosen as the matrix material because it lacks any high frequency vibrational modes that could be expected to serve as acceptor modes for radiationless deactivation and also because the hexachlorozirconate sites are about the right size to accommodate the neptunyltetrachloride ions. Indeed, highly resolved emission has been reported for $UO_2Cl_4^{2-}$ doped into cesium hexchlorozirconate.[2,3]

Samples were prepared by dissolving a 2:1 mixture of cesium chloride and zirconium tetrachloride in 4M HCl solution, adding Np(VI) so that the Zr:Np ratio was approximately 50, evaporating the solution, and allowing it cool and crystallize. The remaining liquid was removed from the crystals, and they were dried and sealed in a quartz capillary tube. The capillary was sealed in a larger quartz tube for secondary containment of the radioactivity and immersed in liquid nitrogen for the spectroscopic measurements. A continuous wave argon ion laser operating on the 488 nm or the 514 nm line was used as the excitation source. Near infrared emission was collected and dispersed through a quarter meter spectrograph and detected on a 512 element InGaAs photodiode array. A representative spectrum is shown in Fig. 1. The most intense line at about 6930 cm^{-1} is assigned as the 0-0 band. Its position is in good agreement with the second excited state of $NpO_2Cl_4^{2-}$ doped into $Cs_2UO_2Cl_4$ reported by Denning et al. to be at 6880 cm^{-1}. The vibronic features to lower energy are labeled according to their displacements from the origin and should correspond to ground state vibrational frequencies. They are in reasonable agreement with ground state

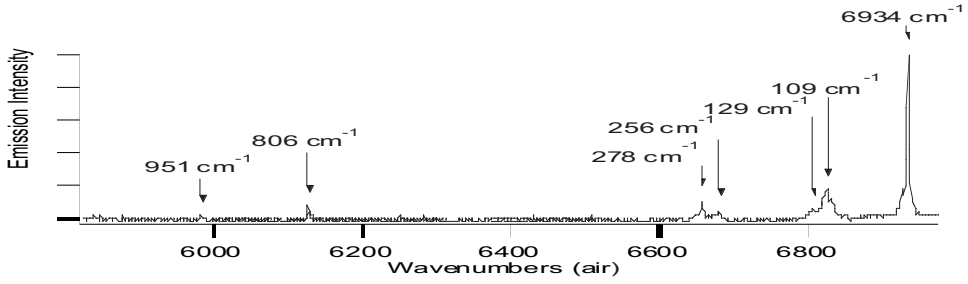

Figure 1. Emission spectrum of $NpO_2Cl_4^{2-}$ in a Cs_2ZrCl_6 matrix at 77 K.

CP532, Plutonium Futures – The Science, edited by K. K. S. Pillay and K. C. Kim,
2000 American Institute of Physics 1-56396-948-3

vibrational frequencies in crystalline $Cs_2NpO_2Cl_4$. The weak feature at 951 cm^{-1} may be a transition to the first excited state. Denning reports that this level lies between 900 cm^{-1} and 1040 cm^{-1} above the ground state when $NpO_2Cl_4^{2-}$ is doped into $Cs_2UO_2Cl_4$.

References

1. Denning, R. G.; Norris, J. O. W.; Brown, D.; *Molecular Physics* **1982**, *46*, 287-323.

2. Flint, C. D.; Tanner, P. A.; *Journal of Luminescence* **1979**, *18-9*, 69-72.

3. Metcalf, D. H.; Dai, S.; Delcul, G. D.; Toth, L. M.; *Inorganic Chemistry* **1995**, *34*, 5573-5577.

Spectroscopy of $UO_2Cl_4^{2-}$ in Basic Aluminum Chloride: 1-Ethyl-3-methylimidazolium Chloride

Todd A. Hopkins, John M. Berg, David A. Costa, Wayne H. Smith, Harry J. Dewey
Los Alamos National Laboratory, Los Alamos, NM 87545, USA

Room temperature ionic liquids have attracted much interest recently because of their potential application in green chemistry, clean technology development, and nuclear fuel reprocessing. Room temperature ionic liquids, such as mixtures of aluminum chloride ($AlCl_3$) and 1-ethyl-3-methylimidazolium chloride (EMIC), have low vapor pressures and adjustable acid/base properties, which makes for an interesting solvent environment. In $AlCl_3$:EMIC, the Lewis acid/base properties can be adjusted simply by varying the composition ratio, where mixtures with >50 mol % of $AlCl_3$ are Lewis acidic, and <50 mol % of $AlCl_3$ are Lewis basic. $AlCl_3$:EMIC also forms a low temperature glass in both acidic and basic mixtures, which provides an excellent medium for detailed spectroscopic studies. In $AlCl_3$:EMIC, the lack of actinide hydrolysis products provides a unique solvent medium to study the fundamental chemistry and spectroscopy of actinide compounds.

In this study we focus on the spectroscopic characterization of $UO_2Cl_4^{2-}$ in 40:60 $AlCl_3$:EMIC using multiple techniques. A combination of absorption, emission, excitation, two-photon excitation, Fourier transform Raman, and time-resolved emission spectra for solution (298 K) and frozen glass (75 K) samples have been measured and analyzed in terms of the electronic and vibrational structures of the $UO_2Cl_4^{2-}$ ion. The spectroscopic properties of $UO_2Cl_4^{2-}$ in single crystals are well known, and the analyses of the spectra of $UO_2Cl_4^{2-}$ in 40:60 $AlCl_3$:EMIC rely heavily on single crystal studies.[1-3] Results are also compared with absorption spectra from a previous study of $UO_2Cl_4^{2-}$ in 48:52 $AlCl_3$:EMIC (a basic ionic liquid).[4] The results from multiple spectroscopic measurements and their comparison with previous results help provide a picture of the structure and environment of $UO_2Cl_4^{2-}$ in 40:60 $AlCl_3$:EMIC.

Over the 20500-16000 cm^{-1} energy range, the 75 K emission spectrum of $UO_2Cl_4^{2-}$ in 40:60 $AlCl_3$:EMIC encompasses the magnetic-dipole allowed electronic (origin) transition, the vibronically-induced electric-dipole (*false origin*) transitions, and the first four members of a vibronic progression in the OUO symmetric stretch (g_1). The *false origins* are displaced from the origin (zero-phonon) by the ground-state frequencies of the OUO asymmetric stretch (g_2), OUO bend (g_3), and OUCl bend (g_{10}) ungerade vibrational modes of $UO_2Cl_4^{2-}$. The ground-state vibrational frequencies determined from the emission spectrum are typical for the $UO_2Cl_4^{2-}$ ion.[2] Time-resolved emission measurements show that the luminescence lifetime of $UO_2Cl_4^{2-}$ in 40:60 $AlCl_3$:EMIC is 1.6 ms at 75 K.

The one-photon absorption (OPA) and excitation (OPE), and two-photon excitation (TPE) spectra of $UO_2Cl_4^{2-}$ in 40:60 $AlCl_3$:EMIC over the ~20000-27000 cm^{-1} energy range encompass transitions from the ground state to the ten lowest-energy electronic excited states of $UO_2Cl_4^{2-}$ and numerous coupled vibronic transitions. The analysis of the OPA and OPE spectra is complicated by a high density of vibronically enabled transitions. However, the (75 K) TPE spectra show the location of 6 of the electronic excited states and their vibronic progressions in the (excited-state) OUO symmetric stretch. The excited-state vibrational frequencies and electronic structure determined from the TPE spectra are remarkably

CP532, Plutonium Futures – The Science, edited by K. K. S. Pillay and K. C. Kim,
2000 American Institute of Physics 1-56396-948-3

similar to those found for $UO_2Cl_4^{2-}$ in single crystals.[3] The one-photon absorption and excitation spectra of the $AlCl_3$:EMIC sample show enhanced electric-dipole intensity due to a deviation from a center of symmetry in the $UO_2Cl_4^{2-}$ ion. This is attributed to a hydrogen-bonding interaction between the U-O in $UO_2Cl_4^{2-}$ and the imidazolium in EMIC.[4]

References

1. Denning, R. G.; Snellgrove, T. R.; Woodwark, D. R., *Mol. Phys.* **1976**, *32*, 419.

2. Flint, C. D.; Tanner, P. A., *J. Chem. Soc., Faraday Trans. 2* **1978**, *74*, 2210.

3. Barker, T. J.; Denning, R. G.; Thorne, J. R. G., *Inorg. Chem.* **1987**, *26*, 1721.

4. Dai, S.; Shin, Y. S.; Toth, M. L.; Barnes, C. E., *Inorg. Chem.* **1997**, *36*, 4900.

ARIES Nondestructive Assay System Operation and Performance

The ARIES (Advanced Recovery and Integrated Extraction System) Project is an integrated system at the Los Alamos Plutonium Facility for the dismantlement of nuclear weapons. The plutonium produced by the ARIES process was measured by an integrated nondestructive assay (NDA) system. The performance of the NDA systems was monitored by a measurement control program which is a part of a nuclear material control and accountability system. In this paper we will report the results of the measurements of the measurement control standards as well as an overview of the measurement of the ARIES process materials.

Teresa L. Cremers, Walter J. Hansen, Gary D. Herrera, David C. Nelson, Thomas E. Sampson, Nancy L. Scheer
Los Alamos National Laboratory, Los Alamos, NM 87545, USA

CP532, Plutonium Futures – The Science, edited by K. K. S. Pillay and K. C. Kim,
2000 American Institute of Physics 1-56396-948-3

Peak Asymmetry Understanding in α Liquid Scintillation with β/γ Rejection

Jean Aupiais
Département Analyse Surveillance Environnement, Service Radioanalyses Chimie Environnement, CEA, BP 12, 91680 Bruyères-le-Châtel, France

Nicolas Dacheux
Groupe de Radiochimie, Institut de PhysiqueNucléaire, Bât 100, Université Paris Sud, 91406 Orsay Cedex, France

Introduction

The alpha liquid scintillation with β/γ discrimination is an analytical method of interest for the determination of α emitters at the trace level. Several authors already suggested its utilization for the detection of radioactivity in environmental samples due to its high sensitivity and a fast sample preparation. Nevertheless, whatever the apparatus used, it suffers a dramatic lack of resolution in comparison with the α spectrometry in a grid chamber or with PIPS detectors. The peak shape is often considered nearly Gaussian, which greatly simplifies the deconvolution process (reduction of the number of variables), even for complex spectra. This assertion is quite acceptable for very low activity measurements but can not be applied for measurements using spike standardization. Thus, it became necessary to understand why the asymmetry factor is an intrinsic property for each nuclide.

Results

The quantification of the asymmetry is calculated by using the Fischer's coefficient γ_1, which is described by the following equation:

$$\gamma_1 \frac{m_3}{\sigma_3} = \frac{m_3}{1/8\ \left(\sigma_1 + \sigma_2\right)^3} = \frac{m_3}{(FWHM/2.354)}\ ,$$

where m_3 corresponds to the third central moment (symmetry factor related to the Gaussian peak), σ is the width of the peak at 0.882↔H (FWHM is equal to 2.354↔σ and to _(σ_1+σ_2)).

For each isotope, the disintegration scheme is unique. Generally speaking, even-even nuclides have a main α emission leading to the fundamental level of the daughter nuclide, which does not produce any asymmetry in the α scintillation spectrum. On the contrary, additional α rays lead to the rearrangement of the daughter nuclide. A competition between γ-ray emissions and internal conversion occurs. The IC prevails because of the low energy of the excited level (about 50 keV). For odd-even nuclides, each nuclide is a particular case. Anyway, that means that each nuclide has its own asymmetry depending on the energy level and the conversion rate. For even-even nuclides, the internal conversion is mainly due to the L shell (about 73%) because of the low energy of the E2 transition. The internal conversion on the M shell contributes to 20% of the IC. Thus, the L and M shells contribute to 93% of the IC. In these conditions, we considered the conversion in the N and above shells negligible in comparison with the total α pulse. As a result, the figures below show clearly that the internal conversion is observed and cannot be neglected.

For instance, the γ_1 value is maximum for the main thorium isotopes like ^{228}Th (0.59 ± 0.09), ^{230}Th (0.48 ± 0.03) and ^{232}Th (0.53 ± 0.03) or uranium ones like ^{232}U (0.32), ^{234}U (0.31 ± 0.05) and ^{238}U (0.25 ± 0.05). As these nuclides usually contribute

CP532, Plutonium Futures – The Science, edited by K. K. S. Pillay and K. C. Kim,

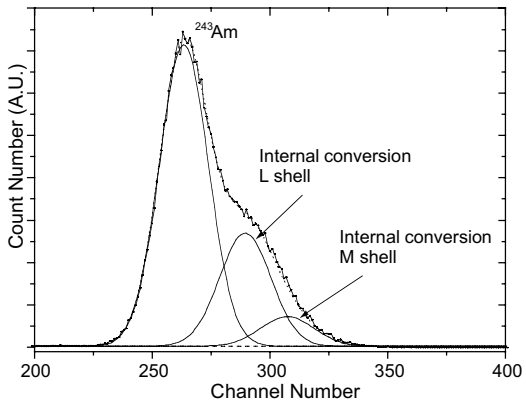

Figure 1. A Liquid scintillation spectrum of ^{243}Am.

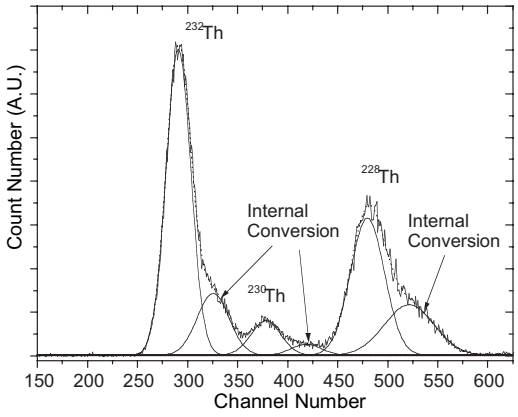

Figure 2. A Liquid scintillation spectrum of thorium isotopes.

the greater part of the natural radioactivity measured in environmental samples, it clearly appears that, for all these actinides, the use of a pure Gaussian peak should lead to great discrepancies in the results.

As an application, we attempted to measure thorium activity in two reference solutions furnished by IAEA (10.7 ± 0.2 Bq/g and 36.8 ± 1.8 Bq/g, respectively). Two determinations were carried out for each reference solution. The results are gathered in Table 1. We applied four kinds of mathematical treatment: deconvolution with Gaussian function, bi-Gaussian function Eq. (2), Gaussian function taking into account the L shell and Gaussian function taking into account L + M shells. The table shows without ambiguity that the L and M shell contributions must be taken into account for a higher accuracy. In this case, the relative error is always lower than 8%. Nevertheless, it also shows that the M shell contribution can be avoided because the PERALS resolution is not high enough to separate both contributions.

Table 1. Activity Measurement of ^{232}Th in 2 Reference Solutions.

Sample	Deconvolution process	Activity (Bq/g)	Deviation (%)
Sample 1	**Reference**	**10.7 ± 0.2**	
	Gauss	9.9 ± 0.1	8.1
	Bi-Gauss	10.2 ± 0.1	4.9
	Gauss (+ L shell)	10.8 ± 0.1	-0.9
	Gauss (+ L and M shells)	10.7 ± 0.1	0.0
Sample 2	**Reference**	**36.8 ± 1.8**	
	Gauss	33.3 ± 0.6	10.5
	Bi-Gauss	32.2 ± 0.6	14.3
	Gauss (+ L shell)	35.2 ± 0.6	4.5
	Gauss (+ L and M shells)	37.7 ± 0.7	-2.4

A New Method of Alpha Spectrometry Based on Solid-State Nuclear Track Detection: Principles, Performance, Applicability

O. A. Bondarenko,
Y. N. Onischuk,
D. V. Melnichuk,
S. Y. Medvedev,
V. M. Petrishin
Radiation Protection Institute, Kiev 254050, Ukraine

A new method for alpha particle energy determination using CR-39 is presented in this work. The method is principally based on measurement of one parameter of an etched out track, i.e., the track end diameter. It is shown that d is connected to the alpha particle range R by a simple linear relationship. An auxiliary parameter the minor axis m is involved in order to resolve the vertical incidence angle dependence of d. A special energy calibration procedure has been worked out to obtain an alpha energy spectrum avoiding explicit involvement of track detector etching velocities Vt É Vb. It is demonstrated that attainment of the good energy resolution (about 2%) for CR-39 TASTRAK detectors combining with other features provides high performance for application of this type of detectors in ultra-low alpha activity measurement of transuranic elements in biological samples.

CP532, Plutonium Futures – The Science, edited by K. K. S. Pillay and K. C. Kim,

Analysis of Aerosol Distribution inside the Object "Shelter"

O. A. Bondarenko,
P. B. Aryasov,
D. V. Melnichuk,
S. Yu. Medvedev
Radiation Protection Institute, Kiev 254050, Ukraine

Abstract

Results of the aerosol sampling inside the Object Shelter are considered in the work. The results show a consistent and significant contribution of the submicron fraction to the total aerosol activity. Different methods of interpretation of impactor data series are compared in order to indicate and detect in most effective way the submicron fraction as a separate mode of the distribution. The following methods were used—method of probabilistic-logarithmic scale, method of likelihood function, and restoration of the initial distribution using passage functions of impactor cascades. Practically all the collected data on aerosol distribution inside the Shelter show a distinct submicron component. The contribution of the submicron component into the total aerosol activity is about 40%.

Introduction

One of the most significant potential sources of personnel exposure during works performed inside the Shelter is inhalation intake and as a result doses from that intake. An important feature of internal irradiation dose formation is the fact that the doses are delivered mainly by transuranium elements (TUE). According to [1] activity of ^{241}Pu and alpha emitting TUE in 1999 were 11% and 1% correspondingly, whereas their joint contribution into the total internal dose from acute inhalation intake varies from 79% to 83% (depending on different types of systemic uptake for ^{137}Cs). At the same time the remainder of the dose, i.e., from 21% to 17%, corresponds to ^{137}Cs and ^{90}Sr, total activity of which in average was about 88%.

Activity distribution versus the aerodynamic diameter (AD) d_{ae} is an important factor that determines the dose coefficient for inhalation intake. Figure 1 shows dependence of dose coefficient as a function of AMAD in the case of acute inhalation intake of aerosols containing ^{239}Pu. Calculation was performed according to ICRP 66 [2] for the following standard options: type of systemic uptake – Slow, physical exercise level – light, breath – normal, aerosol particle density – 10 g·cm-3. As it is seen the dose coefficient varies within range of more than two orders of magnitude from its maximum (AD is about 0.6 μm) to minimum (AD equals 10 μm, i.e., optional upper limit of inhalable fraction).

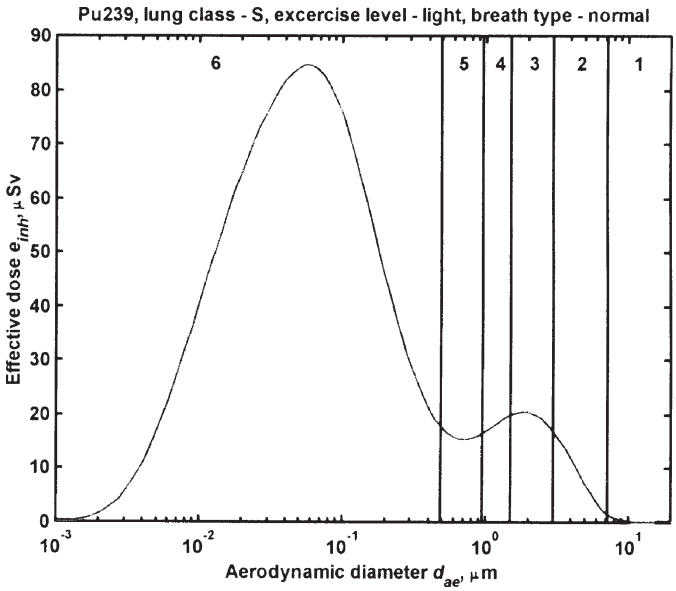

Figure 1. Dose coefficient e_{inh} as a function on d_{ae}. Acute inhalation intake of ^{239}Pu bearing aerosols.

A cascade impactor is a typical device for determination of aerosol activity distribution on AD. Five-stage impactor SA-235

CP532, Plutonium Futures – The Science, edited by K. K. S. Pillay and K. C. Kim,

(manufacturer HI-Q Environment, San-Diego, USA) used in this work has the following cut-off levels {7.2, 3.0, 1.5, 0.95, 0.49} μm for the sampling volume rate 40 Ft^3 per minute (CFM). For catching the aerosol particles passed through all the five cascades a filter paper of FP-5211 type was used as the last 6th cascade. Some important specifications of the FP-5211 filter media are as follow: 100% borosilicate glass fibres, dioctyl phthalate (DOP) smoke efficiency retention 99.994%, weight - 51 lbs/3000 Ft^2.

Values of the impactor cut-off levels for sampling rate 40 CFM are superimposed as vertical lines on Figure 1, so these lines show aerosol AD range, corresponding for the impactor cascades, a number of which are shown at the top of the figure. As Figure 1 shows, the maximum value of e_{inh} and, at the same time, the maximum uncertainty of e_{inh} are within 6th range (< 0.49 μm). Taking into account that activity of 6th submicron cascade achieves 50% (according to the measurements performed inside the Shelter [1]) the given work concerns in more detailed interpretation of this impactor data set.

Analysis of Impactor Data Set Collected inside the Shelter

For the purpose of studying parameters of aerosol distribution inside the Shelter a data set of seven impactor samples was analysed. Separate distributions of ^{137}Cs, ^{90}Sr, ^{238}Pu, $^{239+240}Pu$, ^{241}Am were used for the analysis so at the whole fifteen distributions of the Shelter aerosol activity were analysed (seven on ^{137}Cs, two on ^{90}Sr and the remaining six on TUE).

A method of interpretation of activity distribution measured by impactor in so called probabilistic-logarithmic scale [3] (PLS) is usually used proceeding impactor results. This method serves as a standard and obvious test as to what extent an obtained experimental distribution fits the theoretical log-normal distribution. Median and standard geometric deviation (SGD) of experimental data may be obtained in the result of approximation by straight line.

Figure 2 shows an example of application of this method for obtaining the distribution parameters. The following parameters of log-normal distribution were obtained at the given example: AMAD = 2.0 μm and SGD, σ_g = 6.76. It has to be noticed that parameters were obtained in such a way that SGD σ_g essentially exceeds the standard value from ICRP 66 for the corresponding AMAD value [2], namely: σ_g = 2.49 for AMAD = 2.0 μm.

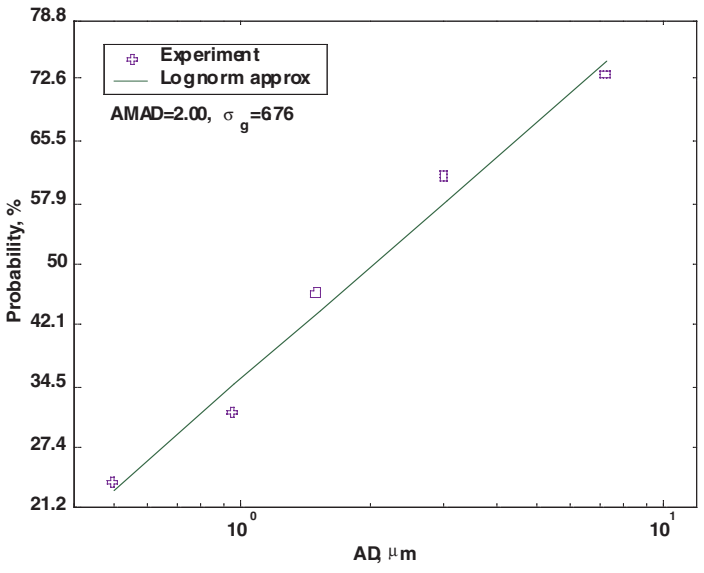

Figure 2. Approximation of the activity distribution in probabilistic-logarithmic scale. Sample code OU080998. Nuclide $^{239+240}Pu$. Obtained parameters: AMAD = 2.0, σg = 6.76.

On the one hand, for comparison, the experimental impactor data set of activity A_i can be presented as a distribution of probability density p_{ex}, with normalisation on total activity $\sum_{i=1}^{n} A_i$ and on the corresponding cascade AD range $d_{ae}^{i-1} - d_{ae}^{i}$, in the following way:

$$p_{ex}^{i} = \frac{1}{d_{ae}^{i-1} - d_{ae}^{i}} \cdot \frac{A_i}{\sum_{i=1}^{n} A_i} \quad . \tag{1}$$

At that, it has to be noticed that for determination of the 1st cascade range, corresponding to the coarsest aerosol fraction, some arbitrary value d_{ae}^{0} that is much greater than the cut-off level of the first cascade d_{ae}^{1} is introduced.

On the other hand, the average probability density of the log-normal distribution $p_{LN}(AMAD)$ with SGD $\sigma_g(AMAD)$, according to [2] for every $i = 1\ldots n$ of impactor cascades is calculated:

$$p_{LN}^{i}(AMAD) = \int_{d_{ae}^{i}}^{d_{ae}^{i-1}} P_{LN}(AMAD)d(d_{ae}) \quad . \tag{2}$$

The PLS method brings in a certain discrepancy like any approximation does. It is impossible to perform a multi-modal distributions in order to obtain information on separate distribution modes. Figure 3 explains this limitation. At that figure values are shown of the distribution of probability density averaged over impactor AD ranges for the initial experimental distribution and for the approximating log-normal distribution.

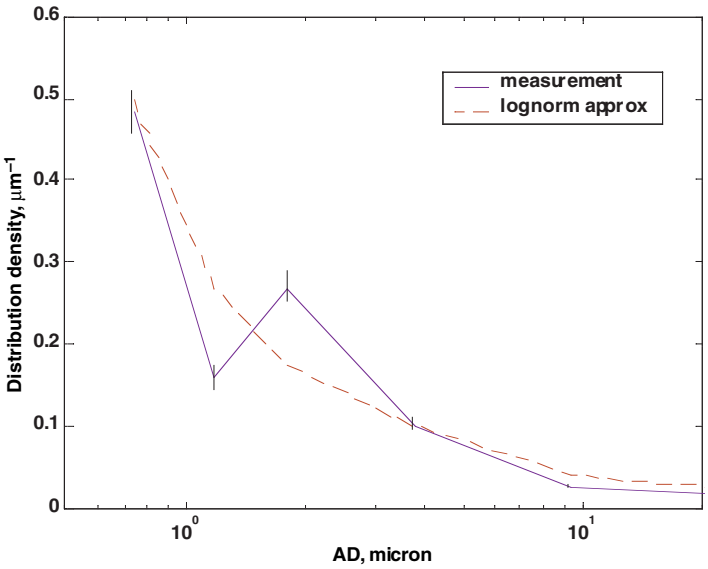

Figure 3. Comparison of distributions of probability density obtained by the PLS method and the experimental data set. Sample code OU080998. Nuclide $^{239+240}$Pu. AMAD=2.0, s_g=6.76.

As it can be seen from the comparison at Figure 3, the experimental data set shows such a shape that can be easily be interpreted a bimodal one, i.e. with two distinct submicron and micron modes.

Non-standard definition of likelihood function (LF) S can be introduced for the purpose of searching probable modes in the experimental distribution. This function is introduced as a measure of correspondence of the experimental distribution p_{ex} (obtained from (1)) and log-normal distribution $p_{LN}(AMAD)$ with SGD σ_g(AMAD) (averaged by (2)).

For calculation of LF S the next procedure is followed: for every AMAD value within the range from 0.01 to 20 μm a search of maximum multiplier s of $p_{LN}(AMAD)$ is carried out, so as value of $s \cdot p_{LN}(AMAD)$ does not exceed p_{ex} for all $i = 1\ldots n$ impactor cascades:

$$S(AMAD) = \max_{p_{ex}^{i} - s \cdot p_{LN}^{i}(AMAD) > 0, \forall i}(s) \quad . \tag{3}$$

Testing of typical experimental cases with single and bimodal distributions are given at figures 1 a-d. At the figures 1a and 1b experimental data are presented in

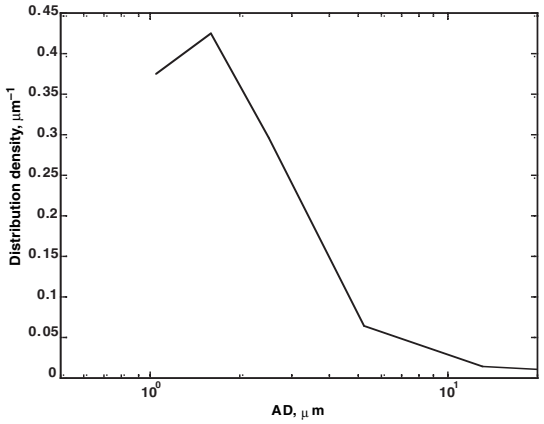

(a), OU230699 ^{137}Cs

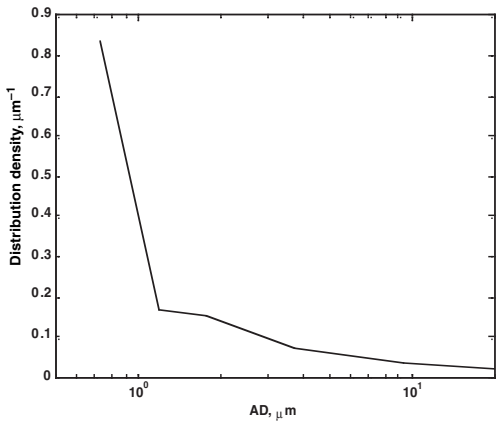

(b), OU090998 ^{90}Sr

Figure 4 (a,b). Determination of the modality for two experimental data sets: (a) and (b) – the experimental data sets as a probability density.

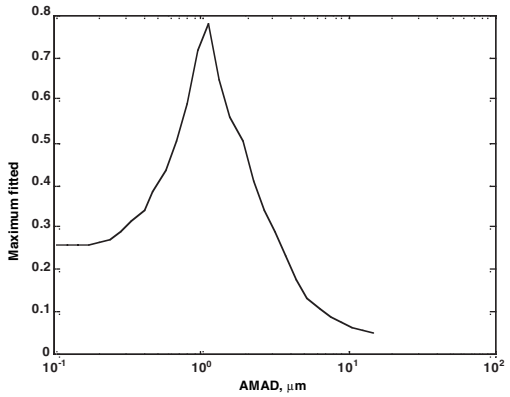

(c), OU230699 ^{137}Cs

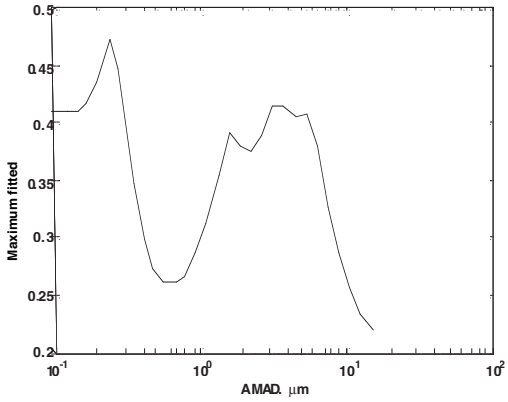

(d), OU090998 ^{90}Sr

Figure 4(c,d). Determination of the modality for two experimental data sets: (c) and (d) – corresponding likelihood functions.

terms of probability density according to (1). At the Figures 1c and 1d corresponding to these distributions likelihood functions according to (3) are presented. Figure 4 shows that LF for the first data set (OU230699 ^{137}Cs) has one maximum at AD more than 1 μm. At the same time for the second data set LF (OU090998 ^{90}Sr) has two maxima: the first one is about 0.25 μm, and the second one is about 3 μm.

Analysis of the complete 15 data series by LF method showed the only one case when a clear singular mode distribution was observed. In all the remaining cases the submicron mode is distinctly seen. For all bimodal cases SGD σ_g is relatively high (from 6.5 to 16).

Restoration of Initial Distribution Considering the Cascade Passage Factor

While the presence of two modes in aerosol distribution on AD looks well justified in the most observations, still a question can arise whether activity collected on the last (6th) cascade resulted from impactor's "faultiness." Namely, the aerosol passage factor $\eta_i(d_{ae})$ for an ideal *i*-th cascade of the impactor is described by Heaviside function:

$$\eta_i(d_{ae}) = \begin{cases} 1, d_{ae} < d_{ae}^i \\ 0, d_{ae} \geq d_{ae}^i \end{cases} . \qquad (4)$$

In practice the passage factor differs from the step function above. Figure 2 shows the passage factor for all the cascades of the impactor used in this work [4]. Thus it is evident that cascade retention dependence on AD may lead to distortion of initial distribution for considered ranges; therefore, when restoring the most probable initial distribution it is important to consider passage factor of impactor cascade.

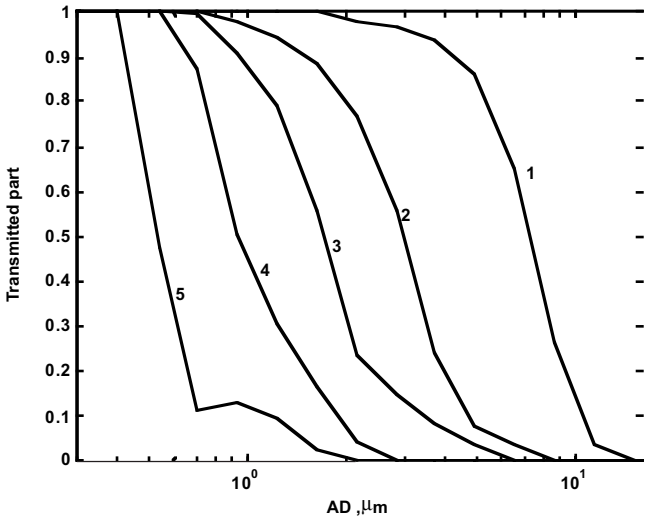

Figure 5. Actual passage factor of impactor cascades for SA-235.

In order to restore the initial aerosol distribution $p_0(d_{ae})$ considering an actual shape of the passage factor $\eta_i(d_{ae})$, the activity c_i deposited on i-th cascade can be expressed as follows:

$$c_i \int_0^{\infty} p_{i-1}(1-\eta_i)d(d_{ae}) \ , \tag{5}$$

where n = number of impactor cascades; $p_i(d_{ae})$ = aerosol distribution after passing i–th cascade, determined by recurrent relationship – $p_i - p_{i-1} \cdot \eta_i$; c_i = activity fraction, retained by i–th cascade.

The given problem is a typical case of an ill-posed inverse problem, and in general it has infinite number of solutions. One way of obtaining a single solution for the problem is in putting forward a practical assumption that the distribution of aerosol activity inside each cascade AD range is uniform. At that, equations (5) are transformed to the following system of n equations with n variables:

$$c_i = \sum_{j=1}^{n} p_{0j}(1-\eta_{ij}) \prod_{k=1}^{i=1} \eta_{kj} \ , \tag{6}$$

where η_{kj} = the passage factor for k-th cascade, averaged over interval j of AD; p_{0j} = initial distribution, averaged over interval j of AD. In matrix form equation (6) takes a following look:

$$\mathbf{C = MP_0} \ , \tag{7}$$

where

$$M_{ij} = (1-\eta_{ij}) \prod_{k=1}^{i-1} \eta_{kj} \ . \tag{8}$$

Figure 3 shows a typical result of restoration of the initial distribution. As the figure shows, application of the inverse transformation to the initial distribution makes it a bit sharper but does not qualitatively change the pattern of the distribution. And what is more, two modes become more distinct. At that the micron mode moves towards coarser AD.

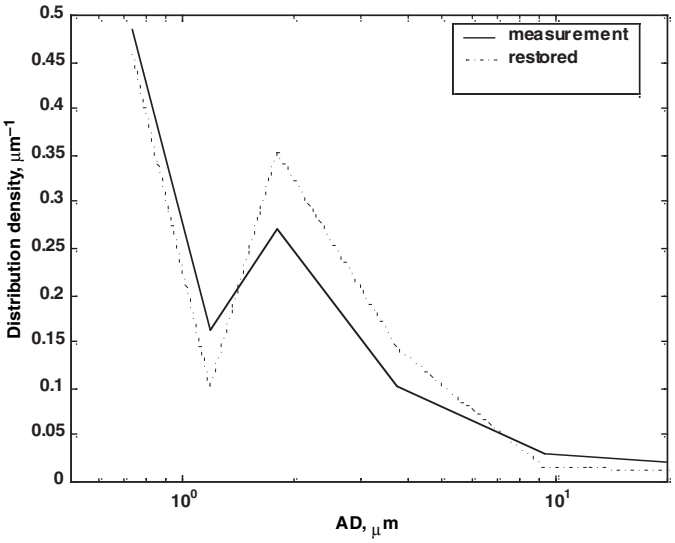

Figure 6. An example of restoration of the initial distribution on AD. Sample code OU080998. Nuclide $^{239+240}$Pu.

Discussion

For understanding the causes of the emerging multi-modal distribution, and in particular presence of submicron aerosol it is important to study the mechanisms of dust formation. So, results of research of element composition and microstructure of aerosol and other particles inside the Shelter are given in [5]. On the basis of analysis of multiple experimental observations sound scientific hypotheses on different causes of submicron particles (< 0.1 μm) origination inside the Shelter are introduced.

It is also interesting to compare the data inside the Shelter with data of other works, in particular, with data on the Exclusion Zone. So, in work [6], there are results of measurement of aerosol distribution at the territory of Radioactive Waste Depository (RWD) "Vektor." Measurements were performed for ^{137}Cs during a period from September 1998 to November 1999. The type of the impactor used was "Andersen." In presented data in two cases (2nd and 3rd) the submicron component was well separated.

Table 1. Results of measurements of aerosol distribution at RWD "Vektor." Data are presented as a part of total activity in %. [6]

	AD range, μm				
Sample description	**0 – 0.8**	**0.8 – 1.4**	**1.4 – 2.3**	**2.3 – 4.9**	**4.9 – 10**
Aug 99, techn	14	12	37	21	16
Nov 99, techn	26	18	30	12	14
Sept 98, bgnd	38	10	18	16	18

Conclusion

In all the cases of analysis of distributions of aerosol inside the Shelter presence of well distinct submicron mode was observed, except one measurement: sample code OU230699, nuclide ^{137}Cs. The contribution of the submicron component into the total activity for the Shelter aerosol varies from 20% to 60% at the average value of about 40%.

An adjusted estimate of submicron component contribution was obtained in the result of restoration of the initial distribution considering the passage factor as function of AD. The restoration does not affect the ratio of the submicron and

micron components, but the distribution shape gets sharpened, i.e., most often SGD of the micron component is decreased.

Using the standard PLS method the contribution of the submicron component may be reduced by several times in comparison to its actual contribution. On the other hand the submicron component has the higher passage factor through respirators, so usage of the PLS method can lead to significant underestimation of internal irradiation dose.

References

1. Methodological and instrumental support of internal irradiation dosimetry for personnel of the Object Shelter. Scientific report No. 8, contract No. 72-RZ/96, state register. No. 0196V024135 / Radiat. Prot. Inst., research coord. Dr. O. A. Bondarenko, Kiev, 1999. [in Russian]

2. ICRP Publication 66. Human respiratory tract model for radiological protection.– Vienna: Pergamon, 1993.– 65 p.

3. Reist P. Aerosols. Introduction to theory / Ed. B. F. Sadovskiy.- Moskow: Mir, 1987.– 280 p.

4. Graseby. Series 230. High volume cascade impactor.

5. Aerosols of the Object Shelter / A. S. Vishnevskiy, A. G. Gontar, I. E. Kuzmina, V. N. Tkach, V. V. Tokarevskiy. – Kiev, 1997. – 32 p. – (Preprint./ NAS of Ukraine, Inst. for Superhard materials of V. N. Bakulia; 97 – 1).

6. Research of dispersion, radionuclide composition and microcomponent content of aerosol and fallout in near-surface layer of atmosphere at industrial zone for the construction period of depository "Vektor." Research report, contract No. 13/153H-99, research coord. Dr. V. V. Demchuk, Kiev, 1999.

Ultratrace Analysis of Plutonium in Environmental Samples by Resonance Ionization Mass Spectrometry (RIMS)

N. Trautmann,
N. Erdmann,
C. Grüning,
J.V. Kratz,
A. Waldek
Institut für Kernchemie, Universität Mainz, 55099 Mainz, Germany
G. Huber,
M. Nunnemann,
G. Passler
Institut für Physik, Universität Mainz, 55099 Mainz, Germany

Introduction

Plutonium is present in the environment mainly as a result of global fallout from nuclear weapons tests, satellite and reactor accidents as well as releases from nuclear facilities. Sensitive and fast detection methods are required for risk assessment, low-level surveillance of the environment, personnel dose monitoring, studies of biological effects and investigations of the migration behaviour of plutonium. Furthermore, the isotopic composition is of interest to get information from what source the plutonium contamination originated. Alpha-spectroscopy is most frequently used for the determination of trace amounts of plutonium in the environment with the disadvantage that the detection sensitivity depends on the half-life of the isotope to be measured and that there are limitations in the isotopic resolution. Conventional mass spectrometry may suffer from isobaric interferences. Therefore, in the last years resonant laser ionization mass spectrometry (RIMS) has been explored as an alternative for ultratrace analysis of plutonium. This method provides a high element and isotope selectivity and a good overall efficiency, resulting in a detection limit of ~10^6 atoms (~0.4 fg). RIMS meets also the requirements of a low background and a short measuring time (1-2 h).

Description of the Experimental Setup

Until very recently our RIMS facility[1,2] consisted of three tunable dye lasers, which were pumped simultaneously by two cooper vapour lasers operating at a repetition rate of 6.5 kHz and with an average output power of 30 W and 50 W, respectively. The beams of the dye lasers were conducted through an optical fiber and focused into the region of a time-of-flight (TOF) spectrometer, where they crossed an atomic beam of plutonium produced by heating a "sandwich filament." This filament is prepared by electrolytical deposition of the chemically isolated plutonium onto a tantalum backing and subsequently coated with a thin titanium layer by sputtering. The resulting photoions were extracted by an electric field and detected after mass selection in a reflectron TOF spectrometer by a channel plate device. A mass resolution of $m/\Delta m \approx 600$ and an overall detection efficiency of 4 x 10^{-5} could be achieved. The photoionization of the plutonium atoms occurred in a three-step, three colour resonant excitation, the third step leading to an autoionizing state (λ_1=586.49 nm, λ_2=665.57 nm, λ_3=577.28 nm).
To determine the isotopic composition of plutonium, the wavelengths of the first and the third lasers had to be scanned over the region of resonance because of a substantial isotope shift in the atomic lines.

The main drawbacks of this laser system are the high maintenance efforts and its size. This has led to the development of an easy to handle solid state laser system to facilitate the application of RIMS for routine analysis of plutonium. The new apparatus consists of three titanium-sapphire (Ti:Sa) lasers pumped by a Nd:YAG laser with a repetition rate of 1-25 kHz and a power of up to 50 W. The standard TOF mass spectrometer is used for mass analysis. The three step ionization scheme with λ_1=420.76 nm, λ_2=847.28 nm and λ_3=767.53 nm for ^{239}Pu results in a detection limit of 2 x 10^6 atoms of ^{239}Pu. As in the case of the dye laser system λ_1

CP532, Plutonium Futures – The Science, edited by K. K. S. Pillay and K. C. Kim,

and λ_3 have to be tuned across the resonances of the various isotopes for the measurement of the isotope ratios.

Results and Conclusion

The former laser system has been applied for the determination of the content and the isotopic composition of plutonium[3,4] in soil samples from the Chernobyl area, Pacific ocean sediment samples, North Sea and urine samples, indicating, for instance, an isotopic composition of 97% ^{239}Pu and 3% ^{240}Pu in sediments from the Mururoa Atoll or illustrating the time behaviour of the urinary excretion of plutonium in human volunteers with ^{244}Pu. Contents of ~10^8 atoms of ^{244}Pu were determined enabling the calculation of the urinary output as a function of time and thus the uptake of plutonium in the human body. With synthetic plutonium samples of known isotopic composition it could be demonstrated that the results obtained with RIMS at the ultratrace level are within 10% in agreement with the specified values, and a detection limit of 10^7 atoms can be derived for the weakest isotope.

With the solid-state laser system dust samples from the surroundings of a nuclear power station in Germany are just under investigation. More details will be presented after the evaluation of the data.

The results have shown that resonance ionization mass spectrometry is well suited for ultratrace analysis of plutonium in environmental samples due to its high sensitivity with a detection limit down to 10^6 atoms (0.4 fg) and because of its good element and isotope selectivity. The detection limit of RIMS is by two orders of magnitude better than that of the conventional α-spectroscopy for ^{239}Pu. The reliability of RIMS has been demonstrated for a variety of samples.

References

1. W. Ruster, F. Ames, H.-J. Kluge, E.-W. Otten, D. Rehklau, F. Scherrer, G. Herrmann, C. Mühleck, J. Riegel, H. Rimke, P. Sattelberger, N. Trautmann: Nucl. Instr. Meth. A281 (1989) 547.

2. G. Passler, N. Erdmann, H. U. Hasse, G. Herrmann, G. Huber, S. Köhler, J. V. Kratz, A. Mansel, M. Nunnemann, N. Trautmann, A. Waldek: Kerntechnik 62 (1997) 85.

3. M. Nunnemann, N. Erdmann, H.-U. Hasse, G. Huber, J. V. Kratz, P. Kunz, A. Mansel, G. Passler, O. Stetzer, N. Trautmann, A. Waldek: J. Alloys Comp. 271-273 (1998) 45.

4. K. Wendt, K. Blaum, B. A. Bushaw, C. Grüning, R. Horn, G. Huber, J. V. Kratz, P. Kunz, P. Müller, W. Nörtershäuser, M. Nunnemann, G. Passler, A. Schmitt, N. Trautmann, A. Waldek: Fresenius J. Anal. Chem. 364 (1999) 471.

Rad Calc III: Radioanalysis Calculation Program for Plutonium and Americium Determination

J. M. Blackadar,
A. S. Wong,
N. D. Stalnaker,
J. R. Willerton
Analytical Chemistry Group, Los Alamos National Laboratory, Los Alamos, NM 87545, USA

Introduction

The radiochemistry team of the Analytical Chemistry Group has supported nuclear materials production and management programs at Los Alamos National Laboratory since the 1940s. Routinely, plutonium and americium contents in various matrices (such as metals, oxides, process solutions, and waste streams) are determined by direct alpha and gamma analyses.[1] Over the years, analysts have written a number of computer programs[2,3,4] to calculate analytical results. In 1999, the program was enhanced and upgraded to produce *Rad Calc III*.[5] The new program, written in Visual Basic 4.0, corrects limitations of previous versions, offers enhanced features, and incorporates user suggestions to customize the program and make it more user friendly.

Description

Rad Calc III calculates plutonium and americium contents in weapons-grade plutonium metals, oxides, and process solutions. The program also determines whether waste solutions meet the waste-discard limit for industrial, acidic, and caustic drain lines.

The user inputs the following information:

- analysis type,
- customer and sample information,
- aliquot and dilution factors, and
- counting data.

When the user presses the "Calculate" button, results appear on the screen. The user may choose to print and/or save the file for later retrieval and data transfer. Once the results have been reviewed and approved, the operator can electronically report data on the Laboratory Information Management System (LIMS) and provide a hard copy of the results to the submitter of the sample.

Rad Calc III allows data collected from multiple detectors with different counting efficiencies to be entered into the calculation. The program also contains several features, including detector background correction, detector counting-efficiency correction, plutonium alpha-specific activity calculation based on isotopic information, and data outlier test (Q test).[6]

Detailed calculations and definitions for *Rad Calc III* are described in the user manual.[5] Salient features of the program, plutonium alpha specific-activity estimates and several correction factors that influence the final calculation of plutonium and americium concentrations, are presented here. These factors include americium and plutonium activities-overlap correction, alpha counter-coincidence correction, and salt-absorption correction.

CP532, Plutonium Futures – The Science, edited by K. K. S. Pillay and K. C. Kim,
2000 American Institute of Physics 1-56396-948-3

Alpha-Specific Activity. Frequently, exact plutonium isotopic information is unknown, but an enrichment factor (wt %) for ^{240}Pu is usually associated with the samples to indicate different plutonium grades. To calculate plutonium and americium contents from gross alpha and gamma data, an estimate of plutonium alpha-specific activity is derived from more than 200 plutonium samples with known isotopic composition (Fig. 1).

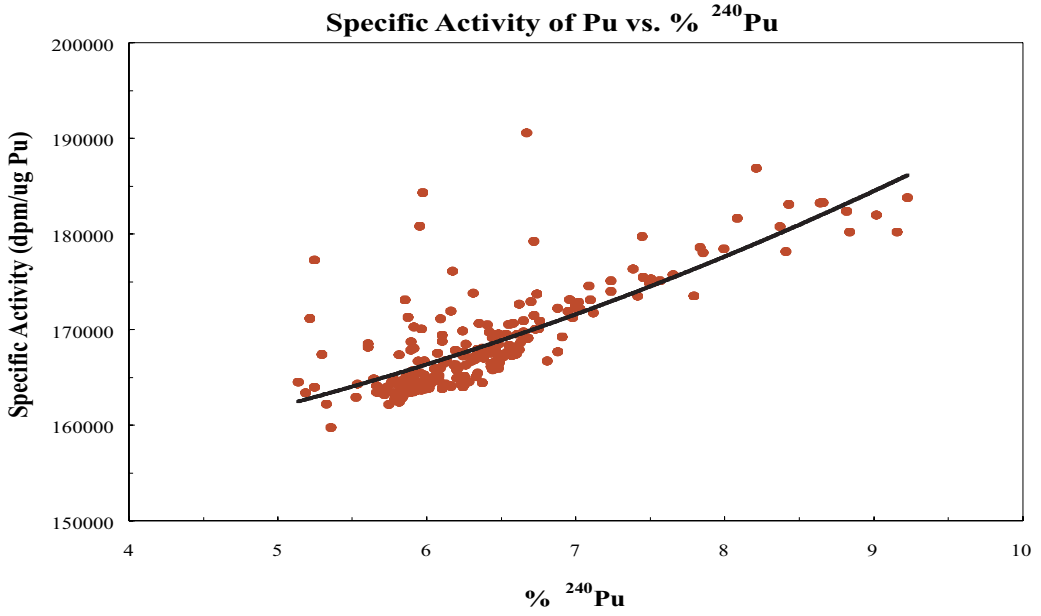

Figure 1. Specific activity of Pu vs. % ^{240}Pu.

Alpha and Gamma Activities Overlap. Sodium iodide detectors are used to perform direct gamma measurements. However, this detector does not have sufficient resolution to discriminate between the gamma rays of plutonium and americium between 40 to 80 keV. Also, gross alpha counting does not differentiate plutonium and americium activities; therefore, *Rad Calc III* uses simultaneous equations[5] to determine final plutonium and americium concentrations.

Coincidence Correction for Direct Alpha Measurement. The alpha coincidence correction is based on the fact that when two alpha particles reach the gas proportional counter at the same or nearly the same time, the two events will be recorded as a single event.

Previous experimental data[7] show that the following equation represents the determined coincidence-correction factor that can be applied to the obtained count rate.

$$CAVGA_{(cpm)} = AVGA_{(cpm)} + \frac{-AVGA_{(cpm)}}{100,000} \quad \leftrightarrow 2000 \ ,$$

where CAVGA is the coincidence corrected count rate, and AVGA is the average alpha count rate before coincidence correction.

Salt Absorption Correction. Direct alpha measurement by proportional counter involves counting alpha activity on a plate that contains a small deposited and dried aliquot of the sample solution. Experimental data showed the absorption of

alpha particles caused by the salt residue left on the plate can be described by the following equation:

$$ABS = -0.0008 \leftrightarrow SALT^2 + 0.1774 \leftrightarrow SALT \ ,$$

where SALT is the amount of salt residue in µg, and ABS is the percent of alpha absorption.

The amount of salt residue on the sample plate is estimated by visual comparison to plates with known salt deposits.

Results

The *Rad Calc III* program provides a flexible, easy-to-use calculation tool for analysts to determine gross alpha activity in waste solutions and plutonium and americium contents in plutonium materials.

References

1. Group CMB-1, *Chemical and Instrumental Methods of Analysis, Section VIII Radiochemistry*, Los Alamos Scientific Laboratory (1970).

2. G. Matlack, *Radiochemistry* programs, written in FORTRAN, BASIC, and QBASIC, Los Alamos National Laboratory (1960, mid 1980s, 1993).

3. D. Vance, *Menu 129* program, written in QBASIC, Los Alamos National Laboratory (1990).

4. P. Brug, *Rad Calc* program, written in Visual Basic 2.0, Los Alamos National Laboratory (1994).

5. J. M. Blackadar, A. S. Wong, N. D. Stalnaker, and J. Willerton, *Rad Calc III* program, Los Alamos National Laboratory, in preparation (2000).

6. R. B. Dean and W. J. Dixon, *Anal. Chem*. **23**, 636-638 (1951).

7. G. Matlack, Los Alamos National Laboratory, private communication, 1999.

A New Glovebox—Surface Science Facility for the Study of Plutonium Surface Chemistry at AWE

T. J. Piper,
D. S. Shaw,
P. Roussel,
D. A. Geeson*
Atomic Weapons Establishment, Aldermaston, Reading RG7 4PR, UK.

Maintaining a capability for the production of plutonium components, whilst continuing to underwrite the safety and quality of weapon systems, are key objectives for the Atomic Weapons Establishment (AWE), Aldermaston, UK. To support these objectives, further development of techniques for the study of plutonium materials is required in order to obtain a deeper understanding of chemical mechanisms involved.

Many of the most technologically important properties of the actinide metals e.g., corrosion resistance, weldability, specific reactivity etc., are understood by determining the surface chemical state and structure. For example, the nature of plutonium-gas reactions depends crucially upon the adsorption of reactants onto the surface oxide layer. Such adsorption characteristics are of paramount importance in determining corrosion mechanisms. In addition, the presence of adventitious impurities or contaminants can adversely affect plutonium surface reactivity. For these reasons a surface science facility has been included in a suite of analytical probes to be used in the study of the chemical and metallurgical properties of plutonium and plutonium compounds.

The instrument is a VG Scientific ESCALAB MkII electron spectrometer, extensively modified for glovebox work, and its installation and operation will be discussed in detail. It is configured to enable the following functions:

- X-ray Photoelectron Spectroscopy, (Mg/Al kα, unmonochromatised x-ray source).
- Ultra-violet Photoelectron Spectroscopy, (HeI/HeII UV source).
- Auger Electron Spectroscopy, (200 nm spot with mapping).
- Secondary Ion Mass Spectrometry, (EX05 Ar^+ ion gun with fast atom bombardment option and 800 amu quadrupole mass spectrometer).

In order to simulate production processes and in-service conditions, an extensive array of non-standard sample preparation facilities has been retrofitted to the base system. These include

- Magnetron sputter source (800W DC, 600W RF): for depositing ultra-thin films of plutonium to probe; actinide-metal interfacial reactivity, stability and corrosion resistance phenomena associated with compatibility issues, and the actinide electronic structure, which can be manipulated through control of substrate nature and deposition parameters.
- Sample heating (1000K) and cooling (77K) facilities: for simulating manufacture and service thermal environments and for thermal cycling during the argon ion etching process associated with preparation of atomically clean surfaces.
- High pressure gas reactor operating up to 30 bar at 873K.

All of these preparation techniques can be used in association with the most toxic and hazardous gaseous environments encountered during the manufacture and

CP532, Plutonium Futures – The Science, edited by K. K. S. Pillay and K. C. Kim,
2000 American Institute of Physics 1-56396-948-3

service life of a modern weapon system. The gaseous conditioning work can be conducted safely at elevated temperature and at high pressure because the vacuum system has been designed with a bespoke "hazardous gas dilution system." Safety issues associated with working on plutonium are further addressed by a "depression maintenance system" which has been incorporated into the vacuum system design. Here, personnel and the environment are afforded protection in the event of catastrophic failure of the vacuum system.

Early results from this recently commissioned facility indicate that the spectrometer has the resolving power to monitor the many oxidation states of plutonium, from which surface reactivity can be investigated. Studies have commenced on weapons grade plutonium and the diverse surface chemical composition which can be observed for "as received" material compared with material exposed to ultra high vacuum and argon ion cleaning, Figure 1. Also, surface defects and contamination arising from production processes have been studied, and the results of one such analysis are shown in Figure 2. Here, silver chloride was readily identified, using XPS and Auger techniques as the contaminant giving rise to an area of discoloration on a plutonium surface. Further work on photoemission and mass spectrometric measurements will be discussed.

In conclusion, AWE now has a unique, fully commissioned and functioning surface analysis facility. Early results indicate that the observed resolving power and sensitivity for both electron spectroscopy and mass spectrometry analyses will allow for a major contribution to be made to the UK weapons research and surveillance programmes.

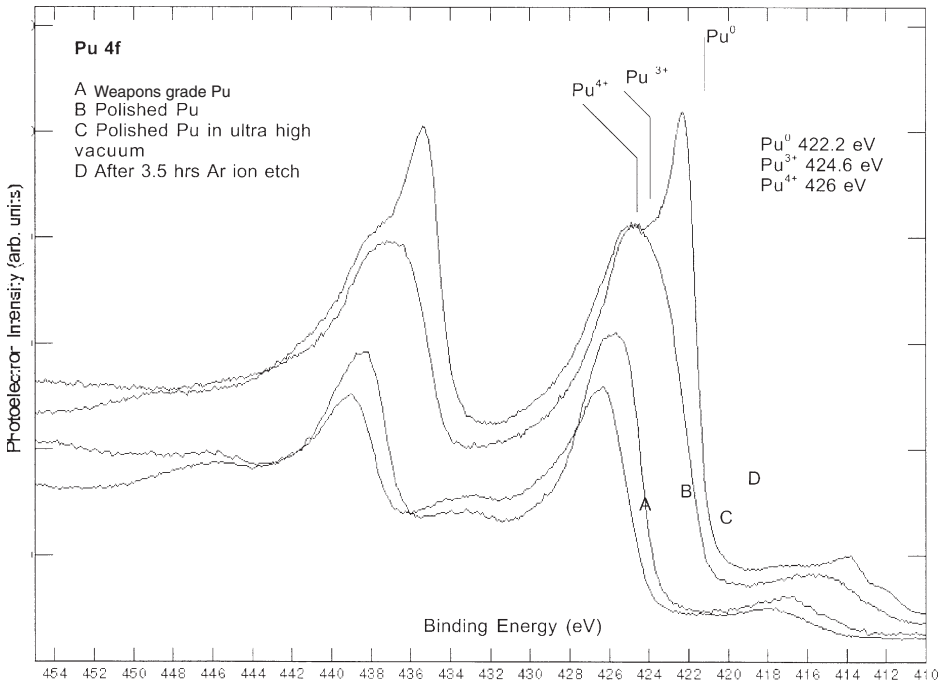

Figure 1. Photoemission measurements of the surface modifications to Weapon Grade Pu.

* To whom correspondence should be addressed.

Detection of Leaking Actinide Hexafluoride Storage Cylinders

James V. Beitz, Clayton W. Williams
Argonne National Laboratory, Argonne, IL 60439-4831, USA

The U. S. Department of Energy currently is responsible for safe storage of ~700,000 metric tons of uranium hexafluoride that, as to uranium isotopic composition, is depleted in U-235 in comparison with natural abundance uranium [1]. Due to its uranium isotopic composition, this material generally is referred to as depleted uranium hexafluoride. The bulk of this material presently is stored in ~57,000 steel cylinders in outdoor storage yards. To date, eight of these storage cylinders are known to have breached (leaked). When a cylinder breach occurs, atmospheric water reacts with the stored uranium hexafluoride principally to generate solid hydrated uranyl fluorides that contain variable amounts of hydrofluoric acid and act as a diffusion barrier that markedly slows the rate of entry of additional water.

Initial efforts to determine the luminescence properties of solid uranyl fluorides date to Manhattan Project-era work. Those studies reported that anhydrous uranyl fluoride is at best weakly luminescent [2] and an uncharacterized solid uranyl fluoride hydrate luminesced strongly at liquid air temperature following arc lamp excitation [3]. An investigation of a breached uranium hexafluoride storage cylinder by workers at the Oak Ridge National Laboratory noted that the uranyl fluoride hydrate HF-adduct plug material in the breach was visibly luminescent to the eye under sunlight illumination at ambient temperature [4]. Our past work and that of others has shown that fluoro complexes of uranyl in acidic aqueous solution at ambient temperature are among the most luminescent uranyl species known in solution phases [5].

Our spectroscopy and photophysics measurements on solid hydrated uranyl fluorides have shown that luminescence is a powerful method for detecting their presence. We report here the results of those studies and the development of a prototype luminescence imaging system that provides high sensitivity and is optimized for signature detection of hydrated uranyl fluorides. This system provides a high degree of selectivity in that its pulsed excitation source is variable as to wavelength and intensity, and detected luminescence is time-resolved using a spatial light modulator as a fast shutter and wavelength-resolved via bandpass optical filters. The features aid in signature detection of uranyl fluoride hydrates.

The characteristics of our luminescence imaging detection system have been optimized to the spectroscopy and photophysics of solid uranyl fluoride dihydrate as revealed by our investigations. Using a quantum counter method, we measured the excitation spectrum of uranyl fluoride dihydrate, which exhibits a series of peaks of similar intensity from 330 nm to 472 nm. The observed luminescence emission spectrum of this material peaks at 521 nm; the most intense peak in its spontaneous Raman spectrum occurs at 837 wave numbers when using 532 nm excitation. We have observed luminescence decay rates that sharply increase with increasing excitation light intensity at all investigated excitation wavelengths. In consequence, a high intensity light source, such as a frequency tripled, Q-switched Nd:YAG laser, is distinctly suboptimal as an excitation light source for detection of solid hydrated uranyl fluorides. A bandpass-filtered microsecond duration flash lamp or a pulsed near-ultraviolet or blue light emitting diode are markedly superior in terms of the fraction of incident excitation photons that give rise to luminescence emission.

CP532, Plutonium Futures – The Science, edited by K. K. S. Pillay and K. C. Kim,
2000 American Institute of Physics 1-56396-948-3

Our spectroscopy studies were performed under the auspices of the Division of Chemical Sciences, Office of Basic Energy Sciences, U. S. Department of Energy under contract W-31-109-ENG-38. Imaging system prototype development was carried out under the Laboratory Directed Research and Development program of Argonne National Laboratory.

References

1. For additional information about depleted uranium hexafluoride management, see http://www.ne.doe.gov and http://web.ead.anl.gov/uranium/indexie.cfm.

2. *Spectroscopic Properties of Uranium Compounds*, G. H. Dieke and A. B. F. Duncan, (McGraw-Hill, New York, 1949), pg 68.

3. D. D. Pant, Proc. Acad. Sci. India **22A**, 95 - 109 (1945).

4. *Investigation of Breached Depleted Uranium Hexafluoride Cylinders*, E. J. Barber, T. R. Butler, J. H. DeVan, J. M. Googin, M. S. Taylor, R. H. Dyer, and J. R. Russell, Oak Ridge National Laboratory Report ORNL/TM-11988, published September, 1991.

5. C. Moulin, P. Pecambox, and L. Trecani, Anal. Chim. Acta, **321**, 121-126 (1996)

Additional Bibiliography

1. J. V. Beitz and C. W. Williams, J. Alloys Comp. **250**, 375-379 (1997).

2. Z. Fizekas, T. Yamamura, H. Tomiyasu, J. Alloys Comp. **271**, 756-759 (1998.

Plutonium Process Monitoring (PPM) System

A. S. Wong,
T. E. Ricketts,
M. E. Pansoy-Hejivik,
K. B. Ramsey,
K. M. Hansel,
M. K. Romero
Los Alamos National Laboratory, Los Alamos, NM 87545, USA

Introduction

In mid-1980, Marsh and Pope developed an online gamma system to monitor americium, uranium and plutonium gamma rays during anion-exchange process for plutonium aqueous recovery operations.[1,2] It has been shown that the real-time elution profiles of actinide impurities are important for plutonium loss via breakthrough, waste minimization, and process monitoring. However, the current monitoring equipment and data acquisition software are obsolete and are frequently problematic.

In 1999, we redesigned the on-line gamma monitoring system in collaboration with Perkin-Elmer ORTEC (Oak Ridge, TN) to enhance and upgrade the current system. This paper describes the new integrated plutonium process monitoring (PPM) system for the aqueous plutonium recovery and anion-exchange processes at the Los Alamos Plutonium Facility.

Plutonium Aqueous Processes

Plutonium-bearing materials (impure oxides, ashes, residue, and other miscellaneous compounds) are dissolved in nitric acid. After the plutonium is in solution, impurities are separated using solvent extraction or anion exchange. The anion exchange process uses Reillex resin to separate americium, uranium, and trace impurities from plutonium. Then the purified plutonium is removed from solution via a Pu(III) oxalate precipitation and then is calcined to oxide.[3]

The current on-line gamma monitoring system utilizes a liquid nitrogen-cooled germanium detector with nuclear instrument module (NIM) bin based electronics to collect gamma rays from Am, U, and Pu in the processing solutions. The regions of interest for these gamma-ray peaks obtained from the data acquisition software (ORTEC Maestro) are then transferred to another software (Intellution Fix 32) to display the "real-time" elution profile. However, there is significant delay in real-time display (> 2 minutes) due to several software routines, and the customized software program is poorly documented.

Integrated Plutonium Process Monitoring (PPM) System

The new PPM system utilizes the latest digital electronics and hardware to collect data. The digital data and advance software enable us to obtain real-time information and anion-exchange elution profiles within a few seconds. The analyst may monitor the elution profiles or review stored data at a remote location via the network. Below are the hardware and software descriptions of the integrated PPM system.

Hardware. A high-purity germanium detector monitors the outlet stream from the anion exchange column as it flows through a 1"stainless steel pipe tube. The detector provides high sensitivity and best resolution in the 30 to 250-keV region of the gamma-ray spectrum. The detector is shielded with 1" lead, and the inside of the shielding is graded with copper plate. Liquid nitrogen or an electromechanical cooling unit can be used to cool the germanium detector. The advantages

CP532, Plutonium Futures – The Science, edited by K. K. S. Pillay and K. C. Kim,
2000 American Institute of Physics 1-56396-948-3

of an electromechanical cooling unit are relatively maintenance free and compact features. The unit also provides an extension of the refrigerant cooling line, which is suitable for compact, remote or distance operation. A digital spectrometer (DSPEC^{Plus}) is selected over the traditional NIM bin electronic modules or a compact analog spectrometer for acquiring Pu elution data. The digital-signal-processing-based spectrometer provides a combination of resolution, throughput, count-rate stability, and temperature stability. The major spectrometer functions are controlled and optimized by computer software, which provides easy operations for technicians. A single Ethernet cable is connected between the DSPEC^{Plus} and the computer.

Software. An ORTEC customized program written in Visual Basic integrates the detector and digital spectrometer setup, data acquisition (Gamma Vision), and real-time monitoring steps into a user-friendly software. The operator sets up the detector, DSPEC^{Plus}, and energy calibration/gain via Gamma Vision software. The elution profiles of plutonium processes are defined and stored as regions of interest (ROI) files. The analyst can set up the alarm level based on the count rate of predefined gamma-ray peaks. The software will then flag the operator with a sound and visual warning when the count rate exceeds the threshold limits. Once the basic operating parameters for the on-line gamma system are defined, the PPM software will obtain the gamma-ray counting data directly from the DSPEC^{plus} and translate the information to a trend plot (Figure 1). This type of real-time trend plot is displayed and updated within a few seconds after every predefined time interval. This new PPM program allows the operator to change acquisition time, add comments, and start/pause/resume/stop during the process run. It also allows the operator to print and save gamma-ray spectra on-demand during the elution process. Quality assurance (QA) checks are performed before each run using a built-in ^{133}Ba check source. A summarized data sheet with the QA and specific run information is printed along with the real-time trend plot at the end of each process run.

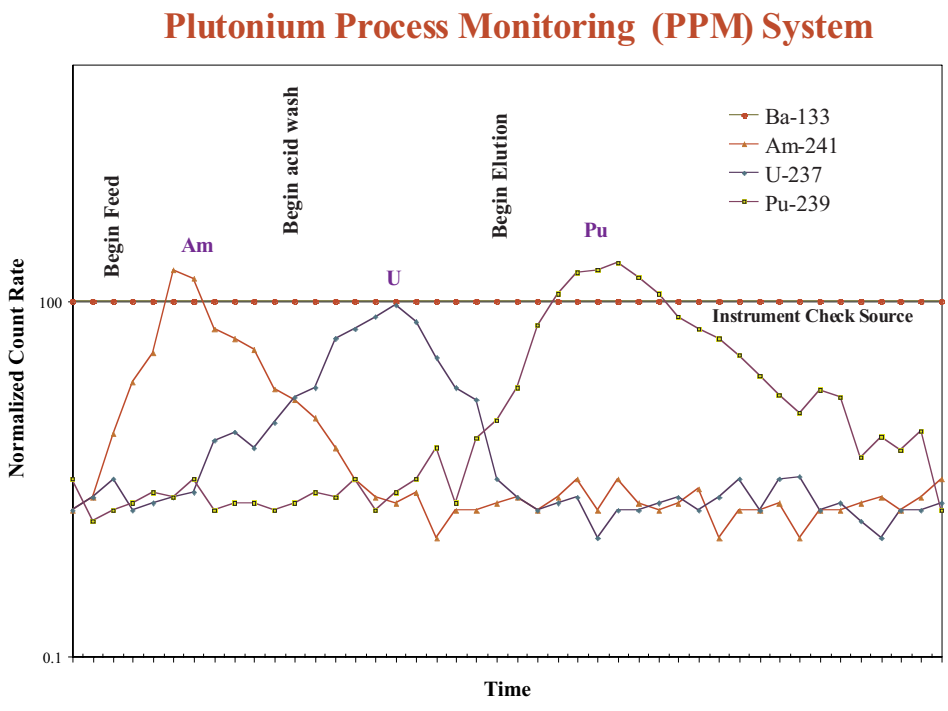

Figure 1. Simulated trend plot data.

Summary

This new integrated PPM system provides several enhanced features and flexible operations for monitoring aqueous plutonium recovery process. Further reduction of waste volume and better process monitoring during washing and elution steps are expected with the implementation of the new system.

Acknowledgment

We would like to thank Mr. Dan Upp of Perkin-Elmer ORTEC (Oak Ridge, TN) for assisting us in the design of this integrated PPM system.

References

1. S. F. Marsh and M. C. Miller, "Plutonium Process Control Using an Advanced On-Line Gamma Monitor for Uranium, Plutonium, and Americium," LA-10921, Los Alamos National Laboratory, 1987.

2. N. G. Pope and S. F. Marsh, "An Improved, Computer-Based On-Line Gamma Monitor for Plutonium Anion Exchange Process Control," LA-10975, Los Alamos National Laboratory, 1987.

3. S. L. Yarbro and S. B. Schreiber, "NMT-2 Responds as National Priorities Change," Actinide Research Quarterly, winter 1999 issue, Los Alamos National Laboratory, Los Alamos, NM.

Determining Analyte Concentrations in Plutonium Metal by X-Ray Fluorescence Using a Dried Residue Method

Christopher G. Worley, George J. Havrilla
Los Alamos National Laboratory, Los Alamos, NM 87545, USA

Introduction

Accurately determining the concentration of certain elements in plutonium is of vital importance in manufacturing nuclear weapons. X-ray fluorescence (XRF) provides a means of obtaining this type of elemental information accurately, quickly, with high precision, and often with little sample preparation.[1] In the present work, a novel method was developed to analyze the gallium concentration in plutonium samples using wavelength-dispersive XRF. A description of the analytical method will be discussed.

To achieve homogeneous specimens for accurate analysis, plutonium must be dissolved prior to XRF analysis. Because plutonium is radioactive, substantial and time-consuming, precautions are necessary to handle the solutions when introducing them into an XRF spectrometer. The plutonium must be removed from the solution prior to XRF analysis for gallium if the spectrometer is not enclosed in a glovebox. The established method for removing plutonium is ion exchange chromatography,[2] but this process is time consuming and results in some loss of gallium prior to analysis. Here, a new method was developed using solution-cast dry residues. This process has several advantages over the liquid specimen method. First, it is much faster and eliminates the potential for any residual plutonium and americium in solution to leak into the spectrometer. Also, no gallium is lost prior to analysis, and the specimen mass is small, which results in much lower radiation doses and less contamination risk in the instrument.

Description of the work

In a proof of principle study, aqueous gallium solutions were used, which reduced the considerable number of precautionary steps needed when working with plutonium. A solution of known gallium concentration was prepared, and zinc was added as an XRF internal standard (Zn Kα close in energy to the Ga Kα XRF line). A 500 mL aliquot was then deposited onto a 6 μm thick Mylar film. A small amount of Alconox soap solution was added prior to deposition on the film to act as a surfactant so that the solution would wet the film. Next, the excess solution was removed, and the wet film was allowed to air dry. A total of 10 specimens were prepared in this manner, and the dried residues were encapsulated in XRF plastic cups and analyzed.

Results

In this preliminary study, an already existing calibration based on liquid standards was used for gallium quantification. Since zinc was used as an internal standard, and the Ga/Zn peak intensity ratio was used to determine the gallium concentration, the liquid standards calibration might also be applicable to analyzing dry residue specimens. However, a critical requirement was that the background signal needed to be subtracted from the gallium and zinc peaks before using the peak ratio value since the background intensity from liquids and dry residues differed greatly.

CP532, Plutonium Futures – The Science, edited by K. K. S. Pillay and K. C. Kim,
2000 American Institute of Physics 1-56396-948-3

The Ga/Zn peak ratio was determined from each dry residue specimen, and the gallium concentration from the casting solution was then calculated. The average experimental gallium concentration was ~5% lower than the known value, and the relative standard deviation of the 10 experimental values was 1.6%. Hence, these results are quite encouraging, as dry residue standards were not used to prepare the calibration curve.

The next step will be to prepare a calibration from dry residue standards and use this calibration to calculate the gallium concentration from a casting solution. The results from this experiment will be presented. Once the accuracy and precision of this solution casting protocol is established for aqueous gallium/zinc solutions, the gallium concentration will be determined in dissolved plutonium solutions using this method. Unclassified precision data from these solutions will be discussed.

References

1. Havrilla, G. J., Chapter 24 "X-ray Fluorescence Spectrometry" in *Handbook of Instrumental Techniques for Analytical Chemistry*, Frank Settle, Ed., Prentice-Hall, Inc., pp. 459-479.

2. Martell, C. J. and Hansel, J. M., "Determining Gallium from Plutonium Using Anion Exchange and X-ray Fluorescence," Los Alamos report # LA-11435, Los Alamos National Laboratory, Los Alamos, NM (1988).

Comparison of Different Surface Quantitative Analysis Methods: Application to Corium

Nathalie Guilbaud, Delphine Blin, Philippe Pérodeaud, Olivier Dugne
DCC/DTE/SIM-CEA Valrhô BP 111, 26702 Pierrelatte Cedex France

Christine Guéneau
DCC/DPE/SPCP-CEA Saclay BP 125, 91191 Gif sur Yvette France

In the case of a severe hypothetical accident in a pressurized water reactor, the reactor assembly melts partially or completely. The formed material, named "corium," flows out and spreads at the bottom of the reactor. In order to limit and control the consequences of such an accident, it is necessary to know precisely the specifications of the O-U-Zr basic system. These specifications should lead to the understanding of physico-chemical phenomenon happening at very high temperatures, from the study at room temperature of solidified structures. Toward that goal, a corium mix was processed by a melting by electron bombing at very high temperature (3000 K), followed by a quenching of the ingot in an Isabel1[1] evaporator. Metallographical analyses were then necessary in order to validate thermodynamic databases set by the Thermo-Calc software.[2,3] The study consists of setting a global quantitative analysis method of the surface that would be fast and reliable, in order to determine a global composition of corium.

The analyzed ingot stems from a [U+Fe+Y+UO_2+ZrO_2] initial mix, whose total mass was 2253,7 grams. Yttrium was added to represent a fission product. Several successive heatings with average power were performed before a very brief level at very high temperature, so the ingot was formed progressively and without any evaporation that might have modified its initial composition. The central zone of the ingot was then analyzed by qualitative and quantitative global surface methods, which should lead to the volume composition of the analyzed zone.

The corium sample analysis happens to be very complex because of the diversity and number of the elements it contains, and also because of the presence of oxygen in a heavy uranium based matrix. Three different global quantitative surface analysis methods were used:

- Global EDS analysis (energy dispersive spectrometry), with SEM,
- Global WDS analysis (wavelength dispersive spectrometry) with EPMA, and
- Coupling of image analysis with EDS or WDS punctual spectroscopic analyses.

The difficulties met during this study come from the sample preparation (corium is very sensitive to oxidation) and the choice of acquisition parameters of images and analyses.

The studied corium sample consists of two zones that show very different morphologies and compositions. The upper oxide zone is rather homogeneous and consists of three distinct and well contrasted phases: U_6Fe (white), $(U,Zr)O_{2-x}$ (grey), and aZr(O) (black). The lower metallic phase is very heterogeneous and is composed of a high number of phases: U_6Fe, $(U,Zr)O_{2-x}$, aZr(O), $Fe_2(U,Zr)$ and many phases with different compositions of the (Fe,U,Zr) ternary.

The EDS and WDS global analysis methods were compared to the method of coupling image analysis with punctual spectroscopic analyses, which is considered to be reliable and precise, for it stands on accurate rules. Global EDS and WDS could be applied on both zones; however, the coupling of image analysis

CP532, Plutonium Futures – The Science, edited by K. K. S. Pillay and K. C. Kim,

and punctual analyses couldn't be applied on the metallic zone with accuracy because of its many phases. In order that the comparison be accurate, it was necessary to keep similar conditions for every method, such as sample preparation, the choice of the analyzed zone and magnification and global analysis parameters. Moreover, a corrective method was applied to the global results so they could be released of the influence of surface oxidation[4,5] A 10 atomic % oxygen content was indeed noticed in the white phase, which was proved to be not a $U_aFe_bO_c$ oxide, but an oxidized U_6Fe phase.[4]

The results obtained with the three methods on the oxide zone are very similar. Thus, global EDS and WDS present a good agreement, notably oxygen, generally more difficult to measure with the EDS method. Moreover, global analyses corroborate image analysis results, which are considered as more reliable. The results obtained on the metallic zone confirm the good agreement between EDS and WDS. Similar results and very good reproducibility were noticed for the three methods; therefore, EDS is the optimal method for corium analysis, since it is the fastest and easiest to perform.

This study leads to the choice of a global analysis method for the corium sample, which presents a good compromise between speed and reliability. However, the complexity of the analytical process shows that it cannot generalised, but will have to be adapted to the analyzed zones. A good agreement was noticed between global EDS and WDS and image analysis; this validates the use of global EDS method for the determination of corium composition.

References

1. C. Guéneau, V. Dauvois, P. Pérodeaud, C. Gonella, O. Dugne, *Liquid immiscibility in a (O,U,Zr) model corium*, Journal of Nuclear Materials 254 (1998), p.158.

2. C. Guéneau, Rapport scientifique DCC 1997, CEA-R-5801, p. 12-17.

3. C. Guéneau, V. Dauvois, P. Pérodeaud, C. Maillault, C. Gonella, O. Dugne, Transactions Of the American Nuclear Society, 1999 Annual Meeting, Boston, Massachussetts, June 6-10, 1999, Volume 80, TANSAO 80, p.176.

4. O. Bonino, C. Fournier, C. Merlet, C. Fucili, O. Dugne, *Contribution des effets de surface des matériaux uranifères aux résultats d'analyse quantitative par microsonde électronique en dispersion de longueur d'onde*, DCC/DTE/SIM, rapport scientifique CEA (1999).

5. R. T. DeHoff, F. N. Rhines, *Microscopie quantitative*, Edition Masson et Cie, 1972.

Qualification of the Bubble Detector as Neutron Dosemeter at the MOX Plant of BELGONUCLEAIRE

P. Kockerols,
F. De Smet,
A. Vandergheynst
BELGONUCLEAIRE, Europalaan 20, 2480 Dessel, Belgium

BELGONUCLEAIRE operates a mixed uranium/plutonium oxide (MOX) fuel fabrication plant located in Dessel, Belgium. BELGONUCLEAIRE began producing MOX fuel for fast breeders and light water reactors in 1973. Fabrication was initially performed within the framework of demonstration programs. In 1986, after the MIMAS (acronym for MIcronization and MASter blend) fabrication process developed by BELGONUCLEAIRE had been fully demonstrated, commercial-scale production was begun. Since then, the plant has been operated at a nominal annual capacity of around 35 metric tons (HM).

Due to the increasing contribution of the neutron dose to the total dose of the BELGONUCLEAIRE personnel and the introduction of the ICRP 60 recommendations,[1] the use of a more reliable personal neutron dosemeter has become even more important.

A Canadian[2] dosimeter manufactured by Bubble Technology Industries seemed to be a very interesting alternative to the albedo dosimeter used in the past. An extensive investigation program was carried out at BELGONUCLEAIRE to determine the effectiveness of the new dosimeter in the fuel fabrication plant environment. A series of tests were conducted to get a better understanding of this type of dosemeter.

Static and Dynamic Tests

The operational research on neutron bubble detectors at BELGONUCLEAIRE started with a number of static and dynamic tests. During the static tests a number of bubble detectors were mounted on a polyethylene phantom. Measurements were realized on several places in the MOX plant and compared with a reference neutron monitor.

For the dynamic tests a number of operators were equipped with two bubble detectors together with the official albedo neutron dosemeter used at BELGONUCLEAIRE. The bubbles of the detectors were counted daily and reset to zero by compressing the formed bubbles. After each month a comparison was made between the reading of the two bubble detectors on the one hand and the result of the albedo dosemeter on the other hand. During this phase a review was also carried out of the worldwide experience with the bubble detectors. [3,4,5]

Temperature Influence

Because it was known that the sensitivity of bubble detectors is temperature dependent, much attention was paid to this issue in the second phase of the evaluation program. During this second phase a large number of temperature measurements were carried out in order to determine the temperature at which the dosemeters are worn by the operators.

CP532, Plutonium Futures – The Science, edited by K. K. S. Pillay and K. C. Kim,

Long-Running Tests and Impact of Neutron Spectra

In a third and final phase of the evaluation program a number of long-running test campaigns of 4 months were carried out. Every working day for 4 months a large number of operators carried 1 bubble detector together with the official albedo neutron dosemeter. To speed up the process of counting the bubbles and to avoid errors, an automatic reading device (BDR-III) was installed and tested. In the third phase the temperature dependence was further investigated, and a number of calibrations[6] were carried out.

Another important issue during the third phase was the evaluation of the impact of the neutron spectra and the new neutron quality factor[7] on the calibration factor of the bubble dosemeters. Measurements and calculations of the neutron spectra were performed, and on this basis a correction of the calibration factor of the bubble dosemeters was determined.

As a result of these investigations and the global positive experience with the bubble detectors a qualification report was established and presented to the Belgian Nuclear Authorities. In 1997 BELGONUCLEAIRE introduced the bubble detector as the official neutron dosemeter for operational personnel in the MOX plant. Up to now, after 3 full years of operation, no major technical problem has been faced, and the previous global positive experience has been confirmed.

References

1. International Commission on Radiological Protection. 1990 recommendations of the International Commission on Radiological Protection, Oxford: Pergamon Press; ICRP Publication 60; 1991.

2. Ing, H.; Noulty, R. A.; Mc Lean, T. D., Bubble detectors - a maturing technology. Radiat. Meas. 27:1-11; 1997.

3. Buckner M. A., Sims C. S., The spectral nexus: understanding the response of the BD-100 bubble detector, Oak Ridge National Laboratory, Oak Ridge, TN.

4. Hoffman J. M., Harvey W. F., Foltyn E. M., Bubble dosimetry experience at the Los Alamos National Laboratory, Los Alamos, NM, 1992.

5. Lafon G. Dosimétrie de neutrons: performances des dosimètres à bulles, comparaison avec d'autres détecteurs usuels, CEA/INSTN, 1992.

6. Vanhavere F., Thierens H., Loos M., Testing the temperature compensated BD-PND bubble detector, SCK/CEN, 1995.

7. International Commission on Radiological Protection. Conversion coefficients for use in radiological protection against external radiation. Oxford: Pergamon Press; ICRP Publication 74; 1996.

Microscopic Determination of the Size Distribution of $Pu0_2$-Rich Zones and Pores in MOX Pellets with an Image Analysis System

J. Vandezande,
H. Pauwels,
A. Vandergheynst
Belgonucleaire,
Europalaan 20,
2480 Dessel, Belgium

Introduction

Various testing methods are used for the quality control of the MIMAS MOX fuel (MIMAS is an acronym for MIcronisation & MASter blend). The MIMAS fuel is made of a dispersion of a mix of 30% PuO_2 / 70% UO_2 in a UO_2 matrix.

As a reminder, the MIMAS process developed by BELGONUCLEAIRE is the MOX leading fabrication process (over 95% of the MOX-fueled reactors in Europe are loaded with MIMAS fuel) and has been selected as the reference process for the US MOX plant to be built in Savannah River for the US weapon plutonium disposal program.

In this paper, a method based on image analysis is presented for the microscopic determination of the PuO_2-rich zones and pores in MOX pellets. Both features are related to the microstructure of the fuel and its in-pile behaviour.

Visualization

To make the PuO_2-rich zones visible a replica technique (alpha-autoradiography) is used; the sample (donor) affects the structure of another surface (receptor). For alpha-autoradiography, contact is made between the polished ceramographic sample and a cellulose nitrate film during a given period. The film is sensitive to alpha particles, emitted by the plutonium and americium, resulting in a change of transparency of the film. The pore structure is determined directly on the unetched sample.

Evaluation

After the visualization of the sample structure, the sample is evaluated with an image analysis system. A CCD-camera projects microscopic images to the system via a frame grabber. For each item to be evaluated, an image is acquired.

Since blurred edges (transitions) can occur in an image due to the bandwidth restrictions of electronic and optical systems, edge transitions between a light and a dark region extend over several pixels with descending (ascending) grey values. This can lead to a so-called halo effect (rings around a region). To avoid this effect, a function is applied to sharpen the region edges.

In order to be able to measure the regions, segmentation is used to generate binary regions. First, the number of regions is calculated with a fixed threshold value, determined by experience. If the number of regions is larger or smaller than a predetermined maximum or minimum, the threshold value is changed automatically until this condition is fulfilled. Figure 1 shows an example of an image after segmentation.

The threshold value is calculated by maximization of the interclass variance: the image is partitioned into two connected sets (classes) of grey values. The objective

CP532, Plutonium Futures – The Science, edited by K. K. S. Pillay and K. C. Kim,

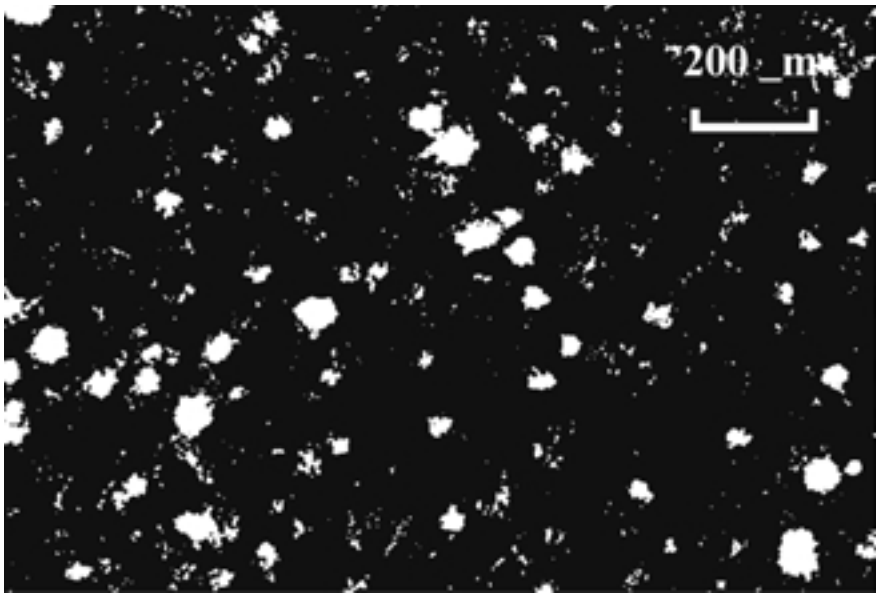

Figure 1. Pu distribution after image segmentation.

is to separate the classes as much as possible and to regroup them as much as possible around their centers.

Since the areas on the film, which are affected by the plutonium and the americium, are slightly larger than the PuO_2 grain sections, black regions from separate PuO_2 grains may get connected. To undo these connections, the regions are partitioned into different size groups and eroded and dilated a number of times, depending on their size.

After the measurement of the properties, the Johnson-Saltykov method is used to determine the size distribution of particles in unit volume of an aggregate from a distribution of section areas. This model assumes that the 3-D particles are spherical in shape and each 3-D particle size distribution can be represented by a discontinuous distribution. The latter makes the calculation less time-consuming and less complex. There is no sequential dependence upon previous calculations of other particle sizes so errors will not propagate through the calculation.

Saltykov sets the interval limits of both the sphere diameters and the section area diameters equally spaced on a logarithmic scale. This ensures that the finest subdivisions occur at small diameters, where they are needed. If necessary, the scale can be extended easily in the direction of either larger or smaller diameters.

Conclusions

This way of determining the Pu distribution and pore structure makes statistical analysis possible since large areas are studied. This makes the method more accurate and representative.

Once the image is acquired, the automated part of the analysis is perfectly reproducible.

Finally, the acquisition and the analysis of images are non-time-consuming activities so the results are rapidly available.

Bibliography

1. KS 400 Imaging System Release 3.0 User's Guide, B40-615e (August 1998).

2. Michel Coster et J.L. Chermant, Précis d'Analyse d'Images, ISBN 2-87682-020-X.

3. Ervin E. Underwood, Particle-Size Distribution.

4. D. B. Rayaprolu and D. Jaffrey, Comparison of Discrete Particle Sectioning Based on Section Diameter And Section Area, Metallography 15:193-202 (1982).

Plasmon Resonance Spectroscopy of Plutonium Metal

Roland K. Schulze, J. Doug Farr, Jeffrey C. Archuleta
Los Alamos National Laboratory, Los Alamos, NM 87545, USA

Introduction

We have measured the plasmon resonance response of the cleaned and well characterized surfaces of various plutonium thermal allotropes using electron energy loss spectroscopy (EELS).[1,2] The energy of the plasmon resonance in the plutonium is highly dependent upon the electronic structure of the solid, and in particular, the electron density or number of electrons available for conduction. Using this method we probe directly for the first time the number of free electrons, and the possible changes in the degree of f-electron localization between the various Pu allotropes.

Experiment

A coupon of high purity zone refined a-plutonium (330 ppm total impurity) was further cleaned by many argon ion sputter/anneal cleaning cycles (up to 420°C) in ultra high vacuum ($5x10^{-10}$ T). Surface purity was examined by Auger spectroscopy, with no detectable contaminants present immediately after cleaning. Material purity and vacuum quality was such that over the course of a set of measurements (120 minutes) with the sample in the β-phase at 156°C for example, less than 0.1 monolayer of oxygen surface impurity is observed. EELS spectra were acquired with primary electron beam energies of 150, 200, 500, 700, and 1000 eV, and with the sample at three different temperatures: 156°C (β-Pu), 250°C (γ-Pu), and 410°C (δ-Pu). The low energy EELS measurements were made first in the course of measurements, as these were most sensitive to surface impurities. The EELS measurements were made in backscatter mode with the primary electron beam normal to the surface and a scattering angle of 137.7°. This in part satisfies the condition of minimizing the excitation of surface plasmons. Using the universal curve, the range of primary electron energies from 150 to 1000 eV yielded an average sampling depth into the surface of 2.8 to 6.0 Å. The electron beam is less than 20 mm in diameter thus insuring that spectra were acquired on a limited area.

Results and Discussion

EELS spectra were acquired for the three Pu thermal allotropes mentioned. As an example, Figure 1 shows the set of spectra for the thermal d-Pu. The spectral set at the bottom include the elastically scattered electron peak. In all cases the centroid of the elastic peak has been located at 0.0 eV loss energy. In the top set of spectra the elastic peak has been removed and the plasmon resonance region expanded vertically by a factor of 7. For all three allotropes measured, three bulk plasmon resonance (PR_b) peaks and one surface plasmon resonance (PR_s) peak are clearly resolved and identified. The surface plasmon resonance peak is observed between 4 and 6 eV in only the 150 and 200 eV EELS spectra. At primary beam energies above this, the bulk plasmon resonance features are enhanced due to a greater sampling depth, and the surface features are no longer seen. The bulk plasmon resonance is most easily tracked using the first well resolved peak at about 11 eV loss energy. Note that the energy of this peak also changes as a function of primary beam energy. This is consistent for the three Pu allotropes measured. This

CP532, Plutonium Futures – The Science, edited by K. K. S. Pillay and K. C. Kim,
2000 American Institute of Physics 1-56396-948-3

Figure 1. EEELS thermal δ-Pu.

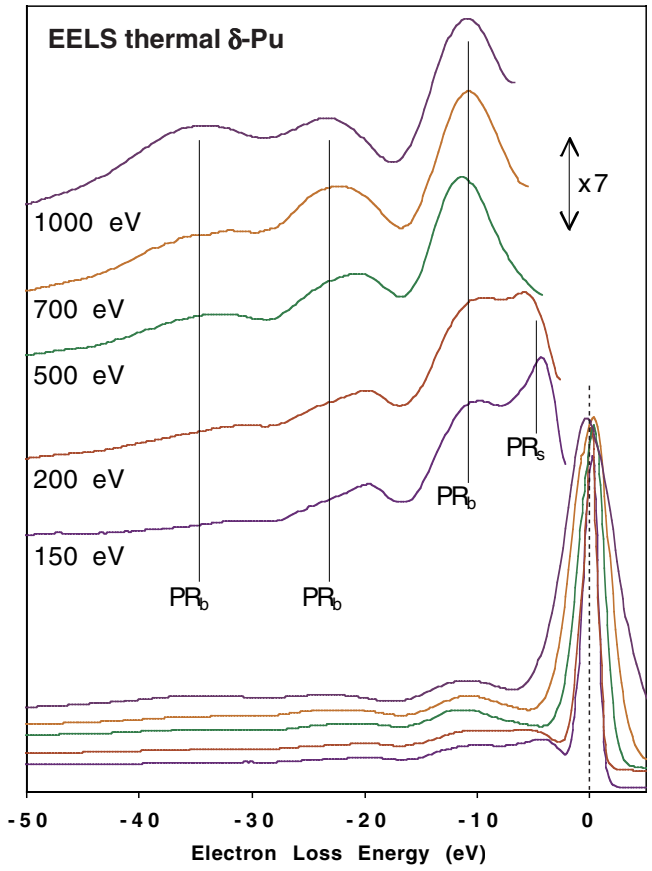

Figure 2. 700 eV EELS thermal Pu allotropes.

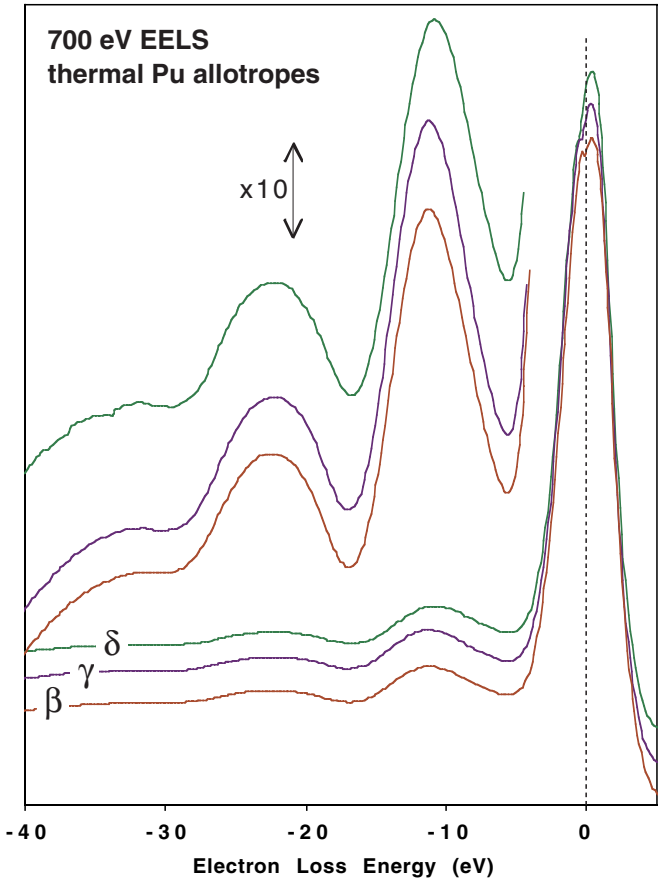

behavior and the shift in energy of the surface plasmon resonance peak is clear evidence that there is a reconstruction of the surface crystal structure from that of the bulk for the β, γ, and δ phases of Pu. At EELS energies higher than 500 eV, the bulk plasmon resonance peak locations do not change energy, indicating that approximately the top 5 Å of the surface are reconstructed, with bulk-like electronic structure at greater depths. Figure 2 shows the 700 eV EELS measurement for the thermal β, γ, and δ phases of Pu. The spectral set at the bottom once again include the elastic peak, with the upper spectral set a 10 times expansion of the bulk plasmon resonance region. The first bulk plasmon resonance peak appears at slightly different energies depending upon the allotrope, and the 700 and 1000 eV measurements are alike. The bulk plasmon resonance energies, taken as the average of the 700 and 1000 eV measurements, are 11.18 eV for the β, 11.16 eV for the γ, and 10.81 eV for the δ. Using the relationship[1]

$$\hbar\omega_p \hbar\sqrt{\frac{4\pi e^3 n}{m_3}} \ ,$$

where $\hbar\omega_p$ is the plasmon resonance energy, n the volume density of free electrons, and m_e the electron mass, we have calculated the volume density of free electrons in each allotrope. In electrons per nm^3 these are 90.7 for the β, 90.3 for the γ, and 84.8 for the δ. Correcting for the atomic density in each allotrope we obtain electron densities of 2.03 for the b, 2.09 for the g, and 2.11 for the d in free electrons per atom. The implications of these results in terms of the electronic properties of Pu and in the changes of electronic structure between the allotropes will be discussed.

References

1. H. Raether, Springer Tracts in Modern Physics 38 (1965) 85 and J. Daniels, C.V. Croixmarie, A. Mocellin, D. WarinCommissariat à l'Energie AtomiqueCEA-CADARACHE DRN/DEC/SPUA, France

2. J. Daniels, C. V. Festenberg, H. Raether, and K. Zeppenfeld, Springer Tracts in Modern Physics 54 (1970) 78.

Atomic H(D) Adsorption on Polycrystalline UO_2 and UO_2(111) Surfaces

M. R. Voss,
M. T. Paffett
Los Alamos National Laboratory, Los Alamos, NM 87545, USA

The chemical reactions of U-containing surfaces with water, oxygen, and hydrogen are important to the corrosion of nuclear materials and to gas generation reactions that have been identified in the long-term storage of these materials. In addition, the role of H atoms arising from radiolysis of adsorbed water may play a crucial role in hydrogen gas generation in actinide oxide storage environments. In this fundamental study, we examine the role of surface structure and order in the chemical reactivity of H atoms and adsorbed water with model UO_2 surfaces. The chemical behavior of highly defected and/or polycrystalline UO_2 surfaces is directly compared with that seen from a highly ordered UO_2(111) surface thus providing insight into molecular-scale processes important to understanding site reactivity.

Utilizing a unique platinum tube atomic hydrogen source, we have investigated the reactions of deuterium atoms with a UO_2 thin film grown on a polycrystalline uranium sample by oxygen dosing and at a UO_2(111) single crystal surface. The polycrystalline UO_2 sample was studied in a relatively "smooth" condition following annealing to 500 K and in a surfaced roughened condition produced by sputtering with Xe^+ ions. Both samples showed evidence of surface hydroxyl formation in the valence band region by UPS (ultraviolet photoelectron spectroscopy, data not shown for brevity). Core level XP spectroscopy (X-ray photoelectron spectroscopy), however, demonstrated peak broadening in the U 4f and O 1s levels and was more pronounced on the roughened surface (Figure 1). The appearance of surface hydroxyls is indicated by the presence of O 1s core level photoelectron peaks at higher binding energy than that typically seen from the oxide surface.

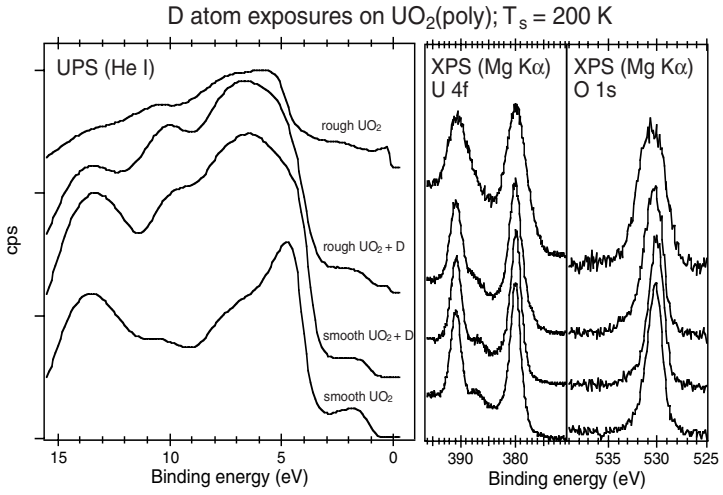

Figure 1. (Left) UPS spectra and (Right) XPS spectra of the U 4f and O 1s levels before and after exposures of D atoms to annealed and Xe^+ sputtered polycrystalline UO_2.

Results on the UO_2(111) single crystal were analogous to those observed on the smooth, annealed polycrystalline UO_2 surface. Successive D atom exposures below a surface temperature of 300 K led to the growth of three additional photoelectron peaks indicative of surface hydroxyls and adsorbed water.[1,2] As on the smooth polycrystalline surface, no peak broadening was observed for either the U 4f or O 1s spectral features upon D atom addition to the well-annealed UO_2 (111) surface (Figure 2).

CP532, Plutonium Futures – The Science, edited by K. K. S. Pillay and K. C. Kim,
2000 American Institute of Physics 1-56396-948-3

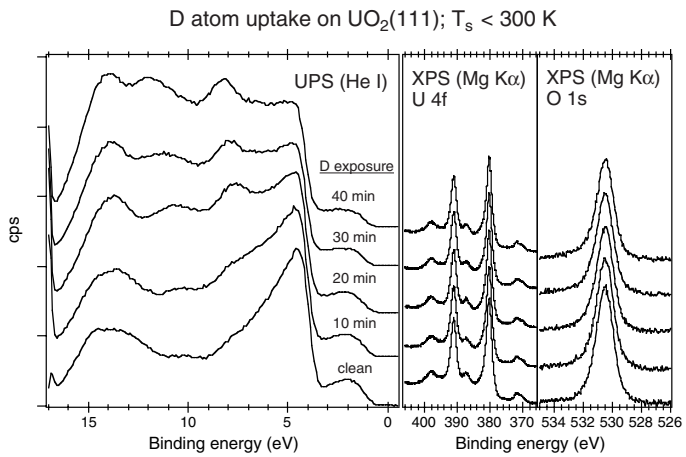

Figure 2. UPS and XPS spectra after exposures of D atoms to UO_2(111) below 300 K.

The UPS data, however, clearly demonstrate the formation of surface hydroxyls arising from addition of H atoms to the surface oxide lattice. The spectral features that account for hydroxyl formation include peaks at 8 and 11.4 eV binding energy attributed to the 3s and 1p orbitals of adsorbed hydroxyl.[3] The very narrow O 1s XPS feature on the right hand side of Figure 2 is clearly anomalous in that the existence of surface hydroxyls appears to be transparent from a conventional XPS line shape analysis. Reasons for this anomalous observation and the role of defect sites will be discussed. Molecular scale differences between the hydroylated surface prepared following deuterium atom exposure at the single crystal versus a polycrystalline surface are clearly identified from spectroscopic core level line shape analysis. These spectroscopic observations suggest the presence of coordinatively unsaturated oxide centers that are observed in conventional XPS measurements that indicate unique molecular site hydroxyl formation.

References

1. Benndorf, C., Nöbl, C., Rüsenberg, M. and Thieme, F. *Surf. Sci.* **1981**, *111*, 87.

2. Manner, W. L., Lloyd, J. A. and Paffett, M. T. *J. Nucl. Mater.* **1999**, *275*, 37.

3. Thiel, P. A and Madey, T. E., Surface Science Reports, **1987**, *7*, 211.

Accelerator Mass Spectrometry Measurements of Actinide Concentrations and Isotope Ratios

Jeffrey E. McAninch, Terry F. Hamilton
Lawerence Livermore National Laboratory, Livermore, CA 94550, USA

Accelerator mass spectrometry (AMS) is an established technique for high throughput measurements of long-lived radioisotopes at very low abundance. At the Center for Accelerator Mass Spectrometry (CAMS) at Lawrence Livermore National Laboratory (LLNL), we are extending our AMS capabilities to the measurement of Plutonium and other actinides for application in a number of fields such as environmental fate and transport and bioassays of potentially exposed populations.

AMS is an attractive alternative for plutonium measurements in that it offers high efficiency, high rejection of interferences, low susceptibility to matrix components, and large dynamic range. These advantages reduce demands on the sample preparation chemistry, which is a limiting factor for most other analytical methods for these radionuclides. The present work has four major components: 1) development of the necessary sample preparation protocols to prepare a sample which is suitable for AMS measurement; 2) design and installation of a Heavy Element Spectrometer (HES) capable of transporting and resolving isotopes near 250 AMU; 3) development of AMS measurement protocols to optimize the sensitivity and isotope ratio precision; and 4) verification of the methods through measurements of test samples and reference materials.

Sample preparation to date has been based on standard alpha spectrometry protocols with only minor modifications. Following purification in an ion exchange column, samples are combined with 1 mg iron (as iron nitrate in solution), dried, baked to 800°C, combined with ~1 mg Nb powder, then pressed into standard AMS sample holders. The HES (shown in the figure) relies on a combination of magnetic and energy analysis, followed by particle identification.

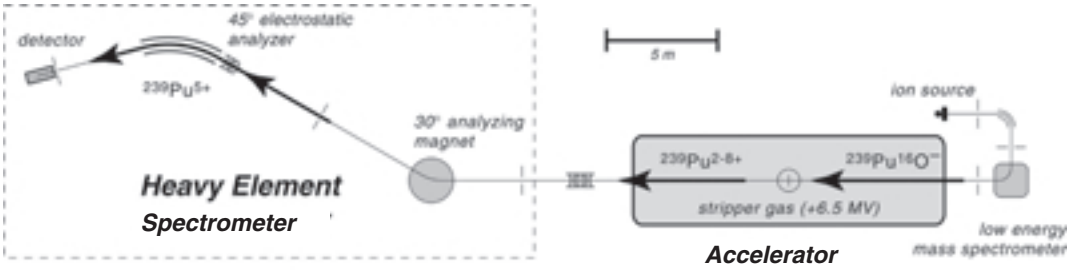

Magnetic analysis is provided by a 30° bending angle, 1 m bending radius magnet with a design resolution M/DM >600. Even with this resolution, scattering and energy spread in the ion beams exiting the accelerator allow some ions of incorrect mass (e.g., ^{238}U during ^{239}Pu analyses) to pass through the magnetic analysis stage. Further suppression of these backgrounds is therefore provided by an energy analysis stage consisting of a 4.4 m radius, 45°, cylindrical electrostatic analyser (ESA) with a rated maximum field of 50 kV/cm.

Finally, the filtered ions are counted and identified in nuclear physics-type ion detectors, which provide some identification by energy, mass, and atomic number.

CP532, Plutonium Futures – The Science, edited by K. K. S. Pillay and K. C. Kim,
2000 American Institute of Physics 1-56396-948-3

Work to date has been performed with a prototype version of the HES. Total system efficiency (detected counts per Pu atom in the sample) with this prototype is $>2\times10^{-5}$. Measurements of ^{239}Pu, ^{240}Pu and ^{241}Pu activities and ^{240}Pu/^{239}Pu isotope ratios in IAEA reference materials agree well with IAEA reference values and with alpha spectrometry and recently published ICP-MS results. The final HES has recently been completed, and testing is now underway. We will present the measured parameters of the HES, and the results of measurements of a variety of environmental, test, and reference samples. Ultimately, this spectrometer and the related sample preparation protocols are expected to provide a sensitivity for ^{239}Pu, ^{240}Pu, ^{241}Pu, ^{242}Pu and ^{244}Pu of better than 1×10^{6} atoms per sample, at a cost and throughput similar to or better than that of traditional alpha spectrometry. Additional testing to determine the suitability of the HES for analyses of ^{237}Np, uranium isotopics, and other actinides are underway.

Determination of Mercury in Radioactive Samples by Cold Vapor Atomic Fluorescence Spectrometry

Michael N. Jasperson, Lawrence R. Drake
Los Alamos National Laboratory, Los Alamos, NM 87544, USA

Plutonium processing and the analysis of radioactive samples generate significant quantities of residue and waste of various matrices. There are strict guidelines in place for the handling, storage, reprocessing, and disposal of these process remains. Characterization of residues and waste streams may require a quantitative determination of Hg at ppb and sub-ppb levels. The detection of Hg at these levels requires a sensitive yet stable method of analysis.

The method utilized was cold vapor atomic fluorescence (CVAF). All samples were analyzed using the PS Analytical CVAF Hg Analyzer. This system is illustrated in Figure 1 and consists of an autosampler, a vapor generator with peristaltic pump and gas/liquid separator, an atomic fluorescence detector, and a personal computer.

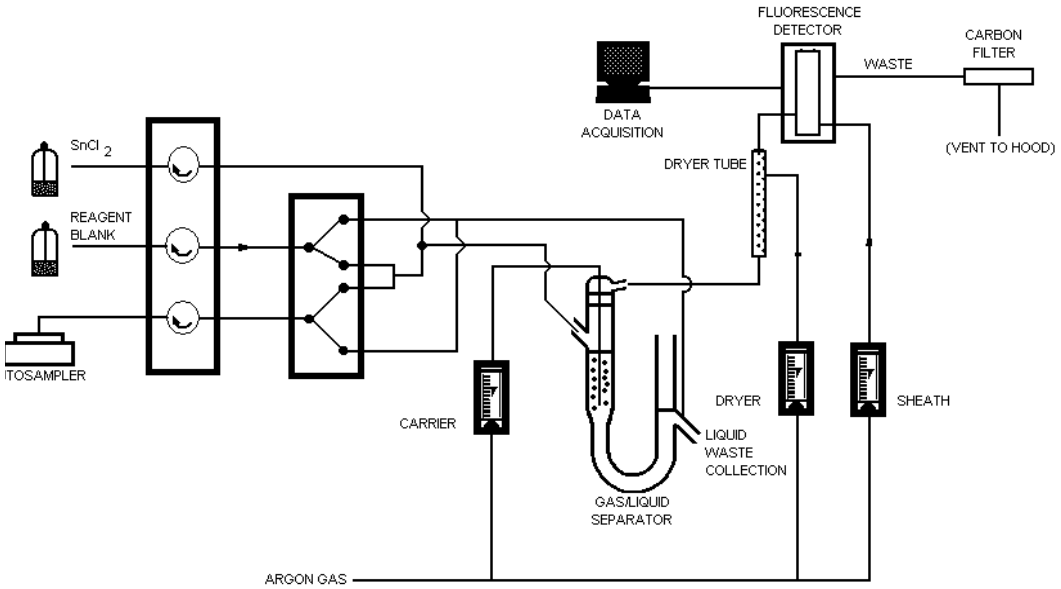

Figure 1. PSA CVAF Hg Analyzer.[1]

The sample is introduced from the autosampler to the vapor generator, where a reaction with stannous chloride in the presence of hydrochloric acid reduces the Hg in the sample to elemental Hg vapor. The Hg vapor is purged from the gas/liquid separator using high purity Argon. The vapor is then carried through a drying tube to remove water prior to its introduction to the fluorescence detector. Detection of Hg vapor is based on atomic fluorescence at 253.7 nm. Instrument detection limits range from 3-10 ppt and a typical calibration curve, based on least-squares regression, consist of six points from 0-1.0 ppb. Quality control includes initial and continuing calibration verification at 0.5 ppb, initial and continuing calibration blanks, and preparation blanks.

CP532, Plutonium Futures – The Science, edited by K. K. S. Pillay and K. C. Kim,
2000 American Institute of Physics 1-56396-948-3

The most recent data concerning improved analytical techniques, waste handling and residue disposition, and sample storage considerations will be presented. Sample preparation methods for the various matrices analyzed will be summarized. The advantages and disadvantages of CVAF over other available technologies will be discussed. In addition, current and future research plans will be addressed.

Reference

1. Billy B. Potter, Introduction to the USEPA, Method 245.7, Determination of Mercury by Automated Cold Vapor Atomic Fluorescence Spectrometry.

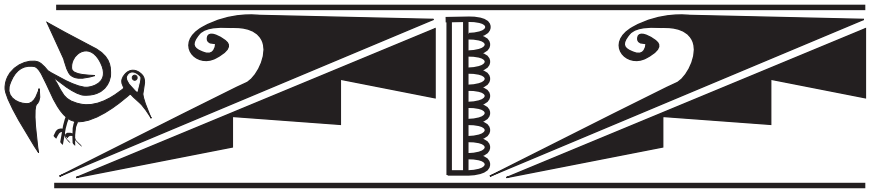

Pu & Pu Compounds

Single Crystal Growth of $(U_{1-x}Pu_x)O_2$ Mixed Oxides

J. Rebizant,
E. Bednarczyk,
P. Boulet,
C. Fuchs,
F. Wastin
European Commission, Joint Research Centre, Institute for Transuranium Elements, D-76125 Karlsruhe, Germany

Introduction

The uranium and plutonium mixed oxides $(U_{1-x}Pu_x)O_2$ have been used as nuclear fuels for more than thirty years in fast neutron and light water reactors. To prepare these plutonium fuels, in the most commonly used fabrication process, PuO_2 is first mixed with depleted uranium dioxide. The resulting primary blend is then used to prepare mixed oxide (MOX) fuels. This plutonium recycling strategy has been an industrial reality in Europe for many years. More recently, transmutation of long-lived nuclear wastes[1,2] (Am, Cm and Np) and development of new concept of plutonium fuels have renewed the interest in these systems and led to new fundamental studies. Moreover, the chemistry of PuO_2 itself is the subject of renewed interest.[3]

Single crystals of MOX are certainly required for more detailed studies. To our knowledge, no single crystal growth of transuranium mixed oxides was reported. Then, continuing our efforts on pure actinide oxides started some twenty years ago,[4] we successfully grew crystals of $(U_{1-x}Pu_x)O_2$, $(U_{1-x}Np_x)O_2$, $(U_{1-x-y}Pu_xNp_y)O_2$ and $(U_{1-x-y}Pu_xAm_y)O_2$. Here, we concentrate on the $(U,Pu)O_2$ system.

Experimental results and discussion

Several methods are used to grow actinide oxides single crystals.[5] In the seventies, large plutonium dioxide single crystals were obtained by high-temperature solution growth.[6] For UO_2,[7] $(U_{1-x}Th_x)O_2$[8] solid solutions and NpO_2,[4] single crystals were grown by chemical transport reactions. This last method was used to grow the crystals presented in this work.

$(U_{1-x}Pu_x)O_2$ pellets were used as starting material. These MOX powders were obtained by stoichiometric coprecipitation by ammoniac, calcination under air at 800°C followed by reduction under Ar/H_2 (5%) at 800°C. Powders were then pelletized and sintered at 1700°C for 6h in Ar/H_2 atmosphere. The composition of MOX powders was checked by chemical analysis.

Charges of ~5g of starting material were crushed and welded in a quartz tube (25 mm diameter, 180 mm length) with $TeCl_4$ (4.5 mg/cm^3) as transport agent in a 10^{-6} Torr vacuum. The feed substances were maintained at 1050°C and transported under the influence of the gradient temperature into the growth region at 950 C for 14 days. Cubic or octahedral single crystals of 2-3 mm^3 and up to 10 mm^3 were obtained for UO_2, $(U_{0.95}Pu_{0.05})O_2$, $(U_{0.88}Pu_{0.12})O_2$, $(U_{0.8}Pu_{0.2})O_2$, $(U_{0.7}Pu_{0.3})O_2$, $(U_{0.6}Pu_{0.4})O_2$, $(U_{0.5}Pu_{0.5})O_2$. For pure PuO_2 only small crystals could be produced. Typical examples are illustrated in Figure 1.

The single crystals were examined with an Enraf-Nonius CAD4 diffractometer using Mo Ka radiation. Lattice parameters were determined on crushed single crystals with a Siemens D500/D501 diffractometer and analysed by the Rietveld profile refinement method. The stoichiometric composition of the crystals was checked by chemical analysis.

The lattice parameters follow perfectly a Vegard law (Figure 2) and are in good agreement with previous results.[8] They suggest a O/M ratio very close to 2.00.

CP532, Plutonium Futures – The Science, edited by K. K. S. Pillay and K. C. Kim,

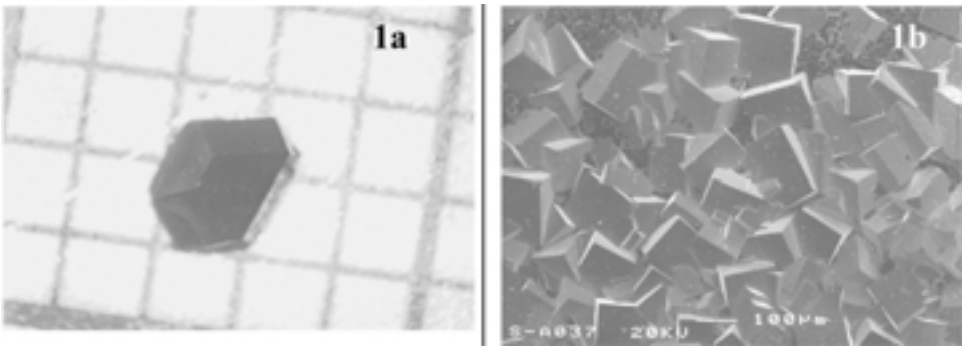

Figure 1. Rebizant, et al., (a). Single crystal of $(U_{88}Pu_{12})O_2$ isolated from the grown bloc by mechanical fragmentation; (b). Scanning electron microscope image of PuO_2 single crystals as grown after chemical transport reaction.

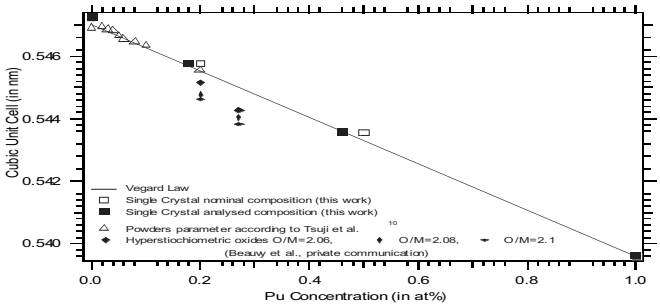

Figure 2. Rebizant et al., Lattice parameters of $(U_{1-x}Pu_x)O_2$ as a function of Pu concentration at room temperature.

The chemical analyses reveal a systematic stoichiometric default of about 10% of Pu between the crystals and the feed substance, which may be related to the difficulty encountered in obtaining large PuO_2 crystals.

In conclusion, we have demonstrated that it is possible to grow MOX single crystals by chemical transport reaction. Studies of these crystals may be able to remove the ambiguities encountered in the literature, which probably come from the lack of homogeneity of polycrystalline samples.

References

1. See e.g., A. Languille et al., J. Alloys and Compounds 271-273 (1998), 517.

2. R. J. M. Konings et al., Transmutation of Am and Tc: Recent progress of EFTTRA, Proceedings of the Fifth Int. Information Exchange Meeting on Actinide and Fission Product Partitioning and Transmutation, Mol, Belgium, Nov. 25-27, 1998.

3. J. M. Haschke et al., Science Vol. 287 (2000), 285.

4. J. C. Spirlet et al., J. of Crystal Growth 49 (1980), 171.

5. J. C. Spirlet et al., in A. J. Freeman and G. H. Lander (eds), Handbook on the Physics and Chemistry of the Actinides, Vol.1, North-Holland, Amsterdam, 1984, Chap.2.

6. C. B. Finch et al., J. of Crystal Growth 12 (1972), 181.

7. S. P. Faile, J. of Crystal Growth 43 (1978), 133.

8. T. Tsuji et al., J. Alloys and Compounds 271-273 (1998), 391.

Metallofullerenes Encapsulating Actinide Atoms

H. Nakahara,
K. Sueki,
K. Akiyama,
Y. L. Zhao
Tokyo Metropolitan University, Tokyo 192-0397, Japan

Y. Nagame,
K.Tuskada
Japan Atomic Energy Research Institute, Tokai, Ibaraki 319-1195, Japan

The fullerene, a series of all-carbon forming closed molecules, is a new material discovered in 1985. After a further discovery of a simple practical and effective production method in 1990 for synthesis of metallofullerenes, investigation on their chemical and physical properties have soon become active. What kinds of elements can be encapsulated into the carbon cages to form chemically stable species of fullerene compound in air is of particular interest. Formation of metallofullerenes stable in air has been reported so far for elements in groups 2, 3, 4, 5 and lanthanoides. But for elements in actinoides, there were reports but all failed to observe, or probably failed to produce a detectable quantity of actinide metallofullerenes. In this context, we have improved and established a method for synthesizing the metallofullerenes with actinide elements and studied some of their species and properties.

The 45 MeV ^{6}Li beams are provided from a Tandem accelerator to bombard onto the 46 mg/cm^2 metal ^{238}U target to produce ^{237}U, ^{238}Np and ^{240}Am isotopes using the reactions ^{238}U(^{6}Li,$p\alpha$2n)^{237}U, ^{238}U(^{6}Li,α2n)^{238}Np, and ^{238}U(^{6}Li,4n) ^{240}Am. After chemical separation of the ^{237}U, ^{238}Np and ^{240}Am from fission products (FPs) using a two-step ion-exchange method consisting of an anion resin followed by cation resin columns, the prepared actinide elements were quantitatively added into 0.5 g lanthanum nitrate and adsorbed into a graphite rod, which was used as an electrode for fullerene production using the arc discharge method. For a comparison with the known metallofullerenes, some FP elements as Sm, Ba, La, Ce etc. were added into the graphite rod. After a series of chemical treatment, the crude fullerene was dissolved into toluene solvent and then injected into the HPLC (high performance liquid chromatography) columns. The HPLC eluting behavior of the fullerene compounds in two kinds of HPLC columns under three different conditions were investigated.

The results indicate that the actinide metallofullerenes, for the first time, were successfully synthesized. The chemically stable species were eluted in an HPLC separation at a retention time which corresponded to the retention time of the lanthannoid(III) M@C_{82}, indicating a formation of U@C_{82}, Np@C_{82} and Am@C_{82}. These actinides metallofullerenes show generally similar HPLC behavior with the Ce@C_{82} but different from Sm@C_{82}. As the oxidation state of the metal atom in Ce@C_{82} is known to be +3 and that of the Sm@C_{82} is +2, this suggests that the oxidation state for either of U, Np and Am in the C-cages is the same, +3. Do the stable oxidation states for different actinide elements tend to be the same in the fullerene cage? The HPLC retention times in a Buckyprep/toluene system for U@C_{82}, Np@C_{82} and Am@C_{82} show a slight deviation. Discussion will be given to explore if the phenomenon originates from the effects of increasing number of f-electrons due to an interplay between the electronic sphere in the carbon cage and f-electron in the actinide metallic elements. The chemical stable uranium species were also observed at a retention time corresponding to the retention time of the dimetallofullerenes, M_2@C_{80} or $M_IM_{II}C_{80}$.

CP532, Plutonium Futures – The Science, edited by K. K. S. Pillay and K. C. Kim,

Kinetics of the Oxidation of Pu(IV) by Manganese Dioxide

A. Morgenstern, G. R. Choppin
Florida State University, Tallahassee, FL 32306-4390, USA

The chemical behavior of plutonium in natural water systems as well as in radioactive waste solutions is governed by a variety of reactions, including solubility and sorption, redox, hydrolysis, complexation with organic and inorganic ligands and formation of colloids. The oxidation state of plutonium is of major importance as plutonium has significantly different chemistry in each of its oxidation states. Knowledge of the oxidation state distribution of plutonium and of the kinetics of transfer between the oxidation states that may be involved is essential for modeling of the behavior of plutonium in aqueous systems and for design of efficient remediation procedures for plutonium containing wastes.

Manganese dioxide is present in some of the radioactive waste storage tanks within the U. S. Department of Energy complex and may influence the oxidation state of plutonium in these waste solutions. Manganese dioxide also is a common component of natural water systems in which it may influence the oxidation state and subsequently the environmental behavior of plutonium. Because of its oxidizing properties, manganese dioxide has been considered in a sediment remobilization model as contributing to the oxidation of sorbed Pu(IV) to the more soluble Pu(V).[1]

In this study an experimental procedure has been developed to monitor the oxidation kinetics of plutonium by manganese dioxide. The process consists of leaching plutonium from the solid phase followed by ultrafiltration and solvent extraction. Appropriate leaching conditions have been established using Th(IV), Np(V) and U(VI) as less redox sensitive oxidation state analogs for Pu(IV), (V) and (VI). Oxidation state speciation of the leachate was performed by removing the polymeric species of Pu(IV) from solution by ultrafiltration, followed by solvent extraction of the filtrate using thenoyltrifluoroacetone, TTA, and di-(2-ethylhexyl)-phosphoric acid, HDEHP, as extractants. The extraction uses 0.5 M TTA in cyclohexane to extract Pu(IV) from an aqueous phase containing 0.6 M HNO_3 while Pu(V) and Pu(VI) remain in the aqueous phase. A parallel extraction step using 0.05 M HDEHP in heptane extracts Pu(IV) and Pu(VI) into an organic phase at pH 0, leaving Pu(V) in the aqueous phase. The results of the two extractions allowed evaluation of the individual fractions of Pu(IV), (V) and (VI).

The oxidation of Pu(IV) by manganese dioxide was studied in 1.0 M NaCl over the pH range from 2.5 to 8.5 with variable concentrations of manganese dioxide from 0.01 m^2/L to 5.00 m^2/L. The rate of the oxidation reaction and the equilibrium ratio of Pu(IV), (V) and (VI) were found to be dependent on the pH and of the concentration of manganese dioxide. Using the kinetic data determined in this study, the influence of manganese dioxide on the oxidation state distribution of plutonium under various environmental conditions as well as in the tank waste solutions can be evaluated.

This research was supported under Grant No. 54893 Environmental Management Science Program, Office of Science and Technology, Office of Environmental Management, United States Department of Energy (DOE). However, any opinions, findings, conclusions, or recommendations expressed herein are those of the authors and do not necessarily reflect the views of the DOE.

CP532, Plutonium Futures – The Science, edited by K. K. S. Pillay and K. C. Kim,

Reference

1. Mitchell, P. E., Battle, J. V., Downes, A. B., Condren, O. M., Vintro, L. L., Sanchez-Cabeza, J. A.: Applied Radiation and Isotopes, *46(11)*, 1175-1190 (1995).

Calculation of Structural and Thermodynamic Properties of Pu-Doped Thorium Phosphate Diphosphate $Th_{4-x}Pu_x(PO_4)_4P_2O_7$

C. Meis
Commissariat à l'Energie Atomique. Centre d'Etudes de Saclay, DCC/DPE/ SPCP, Bât 125. 91191 Gif-sur-Yvette, France

Introduction

The synthesis and characterisation of the thorium phosphate diphosphate, $Th_4(PO_4)_4P_2O_7$ (TPD), has been published previously.[1,2] It has been proposed as a host phase for plutonium and actinides disposal.[3,4] However, we don't know a lot about its mechanical and thermodynamic properties as well as about their variation with respect to plutonium concentration. Furthermore, its behaviour under irradiation is unknown while the threshold displacement energies relative to the a-recoil have never been estimated. Consequently, a theoretical study on these significant questions is actually being carried out, and we present here the first results obtained.

Calculation of TPD and Pu-Doped TPD Properties

The formula and crystallography of the TPD (orthorhombic, *Pcam*, Z = 2, a = 12.8646(9) Å, b = 10.4374(8) Å, c = 7.0676(5) Å V = 949.00 Å^3) have been established by recent studies.[1] In this paper we present a first model of TPD based upon analytical potentials to describe the inter-atomic interactions, adjusted upon the last crystallographic experimental data. We have used the GULP code for this study.[5] The thorium-oxygen distances as well as the phosphate group angles of the relaxed TPD structure are given in Table 1 and compared to the experimental values[2] showing a satisfactory agreement on the whole. We have applied the established force field in order to calculate the bulk modulus B(GPa), the vibration entropy S_{vib}, the constant volume and constant pressure specific heats{C_V, C_P}, and the static dielectric tensor e_0 (Table 1). In Figure 1, the C_P is compared to the measured one,[6] in the temperature range 20°C - 800 °C, also showing a satisfactory agreement demonstrating further the validity of the established force field.

Plutonium substitutes readily for thorium and has been introduced in the modelled TPD structure using transferable potentials to get $Th_{4-x}Pu_x(PO_4)_4P_2O_7$. The substitution energy is found to be 1.8 eV, quite low compared to other plutonium doped compounds. Calculation of the Pu-doped TPD properties for $(0 < x < 1.5)$, where x = 1.5 corresponds to Pu concentration of about 25% p.w, show a decrease of the bulk modulus up to 5% while the thermodynamic properties at 300 K remain almost unchanged: $DS_{vib} \sim +3\%$, $DC_P \sim +2\%$, $DC_V \sim +2\%$ (Table 1).
For x = 1.5, the lattice volume variation is quite negligible, -0.7%, while the Helmholtz free energy slightly increases by 0.11% showing the high thermodynamic stability of the resulting structures.

The formation energy for thorium Frenkel pair defects is calculated to be 10.5 eV. Applying the R.F.O method,[7] the activation energies for the lattice migration of plutonium in the presence of thorium vacancies are estimated within the Mott-Littleton approximation[8] (Table 2).

Finally, the threshold displacement energies characterising the a-recoil damage in different crystallographic directions are currently under calculation.

CP532, Plutonium Futures – The Science, edited by K. K. S. Pillay and K. C. Kim,

Structural/thermo-dynamic properties	Experiment $Th_4(PO_4)_4P_2O_7$	Calculated $Th_4(PO_4)_4P_2O_7$	Calculated $Th_{2.5}Pu_{1.5}(PO_4)_4P_2O_7$
a (Å)	12.8646(9)	13.05982 (+1.52%)	13.0216 (-0.30%)
b (Å)	10.4374(8)	10.4915 (+0.51%)	10.4572 (-4.36%)
c (Å)	7.0676(5)	6.9234 (-2.04%)	6.9172 (-0.12%)
V (Å^3)	949.00(9)	948.62 (-0.04%)	941.91 (-0.70%)
Th(1)-O(23) (Å)	2.20(2)	2.203 (0.0%)	2.201
Th(1)-O(22) (Å)	2.44(1)/2.51(9)	2.439/2.511 (-0.1%/-0.6%)	2.428/2.504
Th(1)-O(11) (Å)	2.59(1)	2.568 (-1.6%)	2.561
Th(2)-O(32) (Å)	2.24(2)	2.246 (+0.04%)	2.243
Th(2)-O(12) (Å)	2.37(1)	2.346 (-1.1%)	2.342
Th(2)-O(33) (Å)	2.45(1)/2.52(9)	2.489/2.546 (+1.5% /0.6%)	2.482/2.540
O(12)-P(1)-O(11) (deg)	121.3(5)	118.8 (-2.0%)	118.2
O(22)-P(2)-O(21) (deg)	112.2(5)	110.4 (-1.8%)	109.5
O(32)-P(3)-O(31) (deg)	110.4(9)	111.2 (+0.8%)	110.7
Bulk modulus (GPa)	-	124	118 (-4.8%)
S_{vib}(300 K) (J/gr K)	-	0.471	0.486 (+3.2%)
C_V(300 K) (J/gr K)	-	0.390	0.397 (+1.8%)
C_P(300 K) (J/gr K)	0.380	0.397 (+4.5%)	0.404 (+1.9%)
Helmholtz free energy (kJ/gr)	-	-97.1	-97.0
ε_0	-	8.6(x) - 7.5(y) - 7.8(z)	9.9(x) - 8.5(y) - 10.4(z)

Table 1. Calculated Properties for TPD and Pu-Doped TPD at 25% p.w. (x = 1.5). The values in parenthesis correspond to the percentage variation with respect to the experimental values, for TPD, and that with respect to the calculated TPD values for the Pu-TPD.

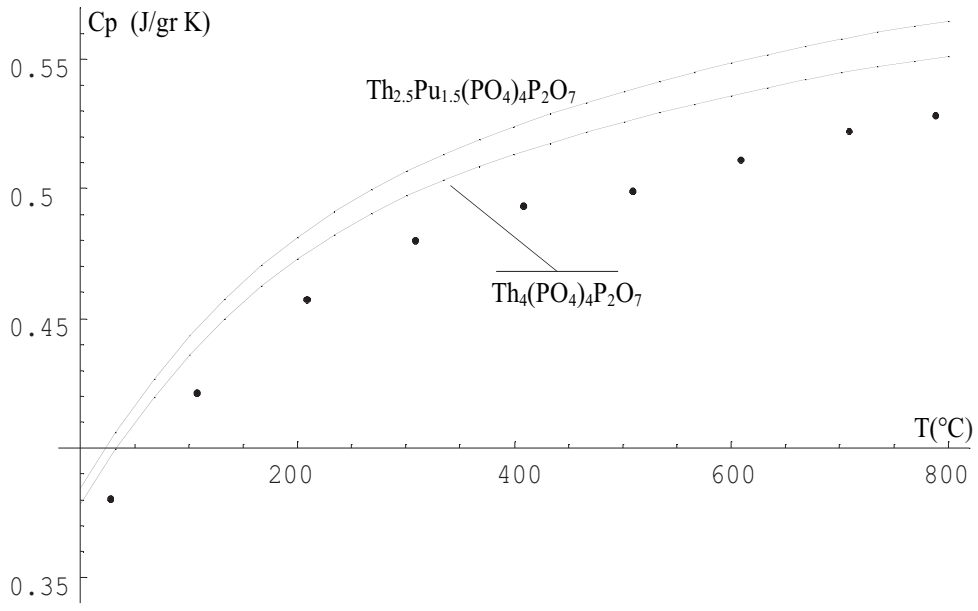

Figure 1. Calculated Cp for TPD and Pu-TPD at 25% p.w (x = 1.5). The experimental (dotted line) values of the Cp for TPD are reported.

Table 2. Migration Energies for Lattice Diffusion of Pu^{4+} Towards Adjacent Thorium Vacancies in Pu-TPD.

Pu coordinates (fractional x/y/z)	→	V''''_{Th} coordinates (fractional x/y/z)	Migration Energy (eV)
0.5173/0.0887/0.7500		- 0.4730/0.5882/0.7500	5.1
		- 0.5154/0.4165/0.2500	3.2
		- 0.9772/0.1818/0.2500	4.8
		- 0.9761/0.3267/0.7500	5.2

Results discussion

The above computational study shows that the TPD matrix preserves its essential physical properties for plutonium concentrations up to 25% p.w. Furthermore, the thorium Frenkel pairs formation energies and the activation energies for lattice migration of plutonium are considerably high. Hence, from a thermodynamic point of view the TPD is capable of confining efficiently significant quantities of plutonium (10%–15% p.w for disposal purpose). The calculation of the threshold displacement energies relative to the a-recoil damage, as well molecular dynamics cascades, presently under development, will reveal aspects of the essential behaviour of the TPD under irradiation conditions.

Acknowledgements

The author acknowledges N. Dacheux and M. Genet of the Nuclear Physics Institute, Orsay University, for supplying all the experimental data and also for the very fruitful discussions.

References

1. P. Bénard et al., *Chem. Mater*. **8**, 181 (1996).

2. V. Brandel et al., *Chem. Mater.* **10**, 345 (1998).

3. N. Dacheux et al., *J. Nucl. Mater.*, **252(3),** 179 (1998).

4. N. Dacheux et al., *J. Nucl. Mater.*, **257(2),** 108 (1998).

5. J. D Gale, *Phil. Mag*. B **73,** 3 (1996).

6. N. Dacheux and M. Genet, private communication.

7. A. Banarjee, N. Adams, J. Simons, R. Shepard, *J. Phys. Chem*. **89** (1985) 52.

8. N. F. Mott and M. J. Littleton, *Trans. Faraday Soc*. **34** (1938) 485.

Prediction of Thermodynamic Property of Pu-zircon and Pu-pyrochlore

Huifang Xu,
University of New Mexico, Albuquerque, NM 87131, USA
Yifeng Wang
Sandia National Laboratories, Carlsbad, NM 88220, USA

Due to its high durability, zircon is often present as a heavy mineral in natural environments and is the oldest mineral that has been dated on the earth. There are four zircon structure phases of $M^{4+}SiO_4$ occurring in nature: zircon ($ZrSiO_4$), hafnon ($HfSiO_4$), thorite ($ThSiO_4$), and coffinite ($USiO_4$). These phases may form solid solution. Recent interest in zircon minerals stems from the study of highly durable radioactive waste forms. Crystalline phases of $M^{4+}SiO_4$ with zircon structure have been proposed as a durable ceramic waste form for immobilizing actinides such as Pu, Np, and U. To predict the behavior of zircon-based waste forms in a geologic repository environment as well as to optimize the fabrication of those waste forms, the thermodynamic and kinetic properties for zircon mineral phases have to be determined. In this paper, we use a linear free energy relationship to predict the Gibbs free energies of formation of Pu-bearing phases (Xu et al., 1999). The calculated results show that the $PuSiO_4$ phase with zircon structure is unstable with respect to oxides of PuO_2 and quartz. However, the $PuSiO_4$ phase will be stable with respect to oxides of PuO_2 and silica glass at low temperature.

Crystalline phases of pyrochlore (e.g., $CaPuTi_2O_7$, $CaU\ Ti_2O_7$) has been proposed as a durable ceramic waste form for disposal of high level radioactive wastes including surplus weapons-usable plutonium. The Pu-pyrochlore phase is predicted to be stable with respect to PuO_2, $CaTiO_3$, and TiO_2 at room temperatures, while Th-pyrochlore phase is predicted to be unstable with respect to ThO_2, $CaTiO_3$, and TiO_2 (Table). We have postulated that the presence of a sufficient amount of $CaTiO_3$ will prevent Pu-pyrochlore from dissolution and therefore the release of Pu from pyrochlore phases in the Yucca Mountain repository.

Table. Gibbs Free Energies of Formation of Pyrochlore (kcal/mole).

M^{4+}	r_M4+ (Å)	$\Delta G_s M^{4+}$	$\Delta G_f M^{4+}$	$\Delta G_n M^{4+}$	MO_2 (Exp.)	MO_2 (Calc.)	ΔG_f Pyrochlore $CaMTi_2O_4$	$\delta\Delta G_{rxt}$ Reaction
Zr	0.79	-373.11	-141.00	232.11	-249.23	-249.21	-839.70	-1.67
Hf	0.78	-374.41	-156.80	217.61	-260.09	-259.24	-848.30	-0.24
Ce	0.94	-354.23	-120.40	233.79	-244.40	-243.28	-833.93	-1.83
Th	1.02	-344.65	-168.50	176.13	-279.34	-279.35	-864.34	3.83
U	0.97	-350.60	-124.40	226.20	-246.62	-247.40	-837.31	-1.09
Np	0.95	-353.02	-120.20	232.82	-244.22	-243.61	-834.17	-1.74
Pu	0.93	-355.45	-115.00	240.49	-238.53	-239.11	-830.42	-2.49
Am	0.92	-356.68	-89.20	267.48	-220.72	-221.35	-815.31	-5.14
Po	1.10	-339.98	70.00	409.98		-121.39	-729.36	-11.54

Reference

1. Xu, H., Wang, Y., and Barton, L. L. (1999) Application of a linear free energy relationship to crystalline solids of MO_2 and $M(OH)_4$, Journal of Nuclear Materials, 273, 343-346.

CP532, Plutonium Futures – The Science, edited by K. K. S. Pillay and K. C. Kim,
2000 American Institute of Physics 1-56396-948-3

Utilization of Principal Component Analysis on Plutonium EXAFS Data from the Advanced Photon Source

Jeff Terry,
Roland K. Schulze,
Thomas G. Zocco,
J. Doug Farr,
Jeff Archuleta,
Mike Ramos,
Ray Martinez,
Barbara Martinez,
Ramiro Pereyra,
Jason Lashley
Los Alamos National Laboratory, Los Alamos, NM 87545, USA

Steve Wasserman,
Mark Antonio,
Suntharalingam Skanthakumar,
Lynne Soderholm
Argonne National Laboratory, Argonne, IL 60439, USA

Since the 1941 discovery of plutonium (Pu) by Glenn Seaborg, this enigmatic metal has been the subject of intense scientific investigation. Despite these efforts, there is still much to be learned about the unusual physical and mechanical properties of plutonium and its alloys. In particular, unalloyed Pu undergoes six allotropic phase transformations upon cooling from the melt to room temperature. Many of these phase transformations result in large volume changes and produce low-symmetry crystal structures. These unusual characteristics have made the metallurgy of Pu and Pu alloys particularly challenging. For example, the highest density allotrope, α (monoclinic), is extremely brittle and oxidizes readily, making it a poor choice for manufacturing operations. The addition of 1 wt. % Ga stabilizes the face-centered cubic δ structure, α phase with vastly superior mechanical properties when compared to α-Pu. Phase relations within the Pu-Ga system have been studied in detail, providing an initial basis for the understanding of the metallurgical properties of the system.

However, a fundamental gap exists in our understanding of bonding properties of δ-phase Pu that has been stabilized by alloying. Most simply stated:

What is the local atomic environment of the plutonium atoms?

Does the local environment change as a function of concentration?

Does the local environment change as a function of alloying agent?

What is the local atomic environment of the alloying agent?

At present, there is a substantial controversy over the local structure of Pu alloys stabilized into the face-centered cubic structure (δ-phase) by alloying with Ga. The local structure can be determined in several different ways: one is to calculate pair distribution functions (PDFs) from either neutron or x-ray scattering data, while the other is to calculate the local structure from the extended x-ray absorption fine structure (EXAFS). The controversy is that the EXAFS work exhibits a high frequency oscillation, corresponding to a longer bond length than would be expected in the fcc phase. Furthermore, no unexpected peaks appear in the PDFs obtained from neutron scattering. The former represents data exploring a region to a depth of approximately 6μ, while the latter explores the "bulk" structure. The long bond length peak observed in the EXAFS spectrum has been subject to many different explanations, ranging from the formation of a secondary phase with a body-centered cubic structure to the formation of an oxide layer. Recent EXAFS measurement at the Advanced Photon Source (APS) by Jeff Terry and Lynne Soderholm have shown that an oxide layer cannot be responsible for this unattributed peak. Those measurements utilized well characterized samples in order to understand the effects of sample cleanliness and utilized probes with different sampling depths (by using both electron yield and fluorescence detection). Unfortunately, due to a monochromator problem, it was not possible to identify conclusively the origin of the unknown peak. Resolution of this controversy is important to gain an understanding of the structure of Pu alloys.

The area of focus in this proposal is the Pu-rich portion of the phase diagram. Samples will be prepared around the minimum concentration necessary to stabilize the δ-phase. In order to determine the local atomic environment of the pluto-

CP532, Plutonium Futures – The Science, edited by K. K. S. Pillay and K. C. Kim,
2000 American Institute of Physics 1-56396-948-3

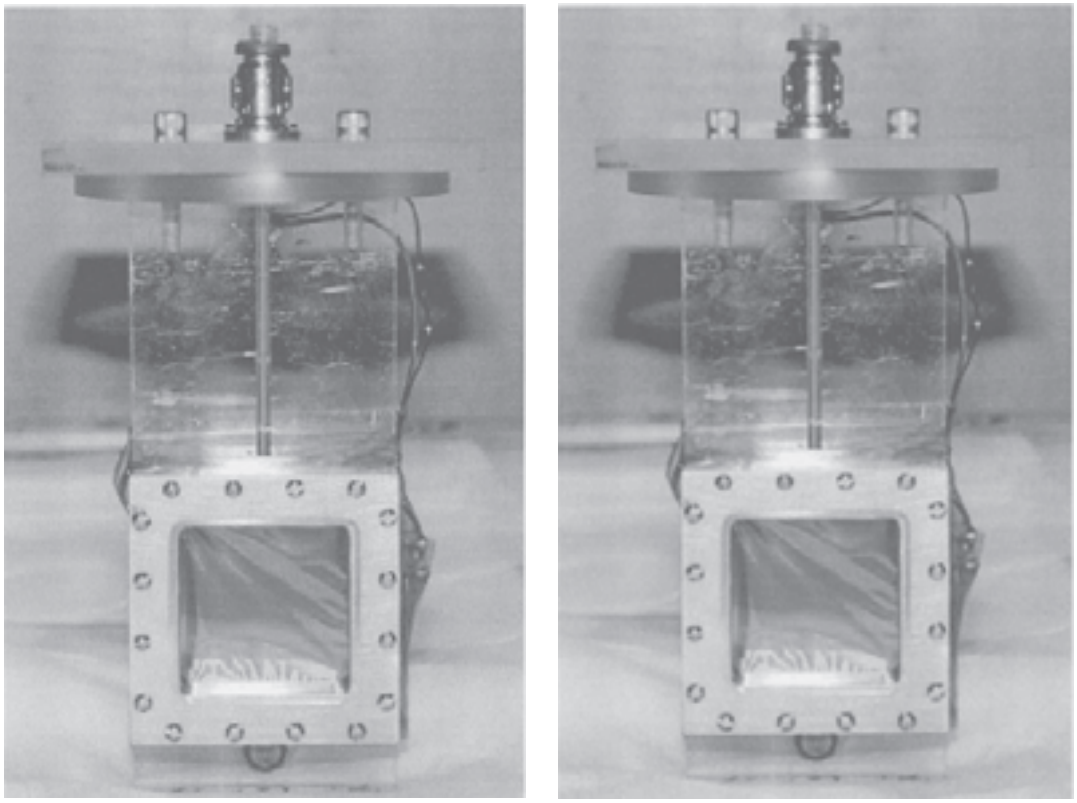

Figure 1. The electron-yield sample holder is shown.

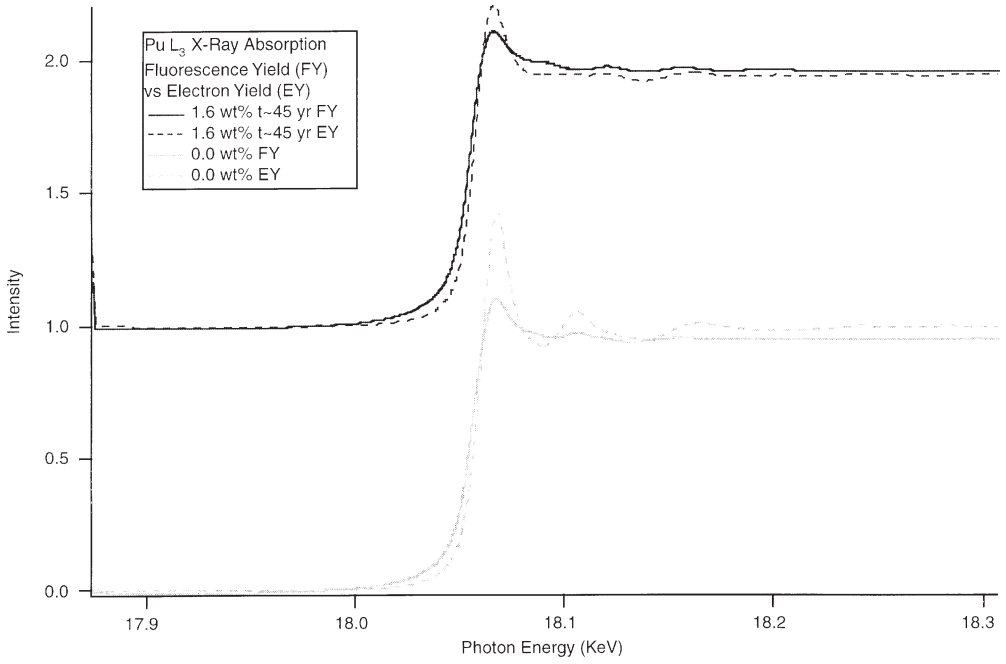

Figure 2. A comparison of the electron yield to the fluorescence yield measurement shows that the surface is partially oxidized. The extent of the oxidation was greater for the alpha sample than for the delta sample.

nium atoms, the extended X-ray absorption fine structure spectra of the Pu L_3-edge were measured. From the high Ga concentration stabilized plutonium alloys, the environment around the plutonium atoms appears to be simple fcc. The unalloyed plutonium also appears to be simple monoclinic as expected. However, differences from the ideal δ-phase spectrum were encountered near the limiting concentrations necessary for phase stability.

A 0.5 wt. % Ga-Pu alloy exhibited a higher frequency oscillation (longer bond length) than observed in the ideal δ-phase. The stability of the APS allowed the technique of principal component analysis (PCA) to be used on this series of spectra. PCA highlighted this difference and showed that the 0.5 wt. % Ga-P alloy had some similarities to the ideal δ-phase alloys, was very dissimilar from the unalloyed α-phase, and also was quite unique due to the unexplained high frequency component. To understand plutonium alloying, it is imperative to understand whether or not this peak is due to the presence of an unidentified phase. The preliminary measurements ruled out both the presence of an oxide and the presence of an α-Pu phase. While it is important to know what this component is not, and first steps have been made in this direction, high k EXAFS measurements may indicate higher shell contributions to the spectra that would allow positive identification of this new structure.

Ultimately, it is important to understand whether this high frequency oscillation, presently suggestive of an unknown phase, is unique to the Pu-Ga binary system. Other elements will also stabilize fcc, δ-phase plutonium. For example, Si, Al, In, and Ce will stabilize the d-phase of plutonium. The local atomic environment of the plutonium atoms in alloys with these elements can also be measured, again, utilizing the extended X-ray absorption fine structure spectrum of the Pu L_3-edge. If a similar high frequency oscillation is observed from these alloying agents near the region of phase instability, further clues to both its origin and the physics underlying its origin may be ascertained.

Los Alamos National Laboratory is operated by the University of California under Contract No. W-7405-ENG-36 with the U.S. Department of Energy. Use of the Advanced Photon Source was supported by the U.S. Department of Energy, Basic Energy Sciences, Office of Science, under Contract No. W-31-109-Eng-38. The Actinide Facility was supported by the Division of Chemical Sciences, Office of Basic Energy Sciences, U. S. Department of Energy under contracts W-31-109-Eng-38 and DE-AC03-76SF00098. This is LA-UR-99-6707.

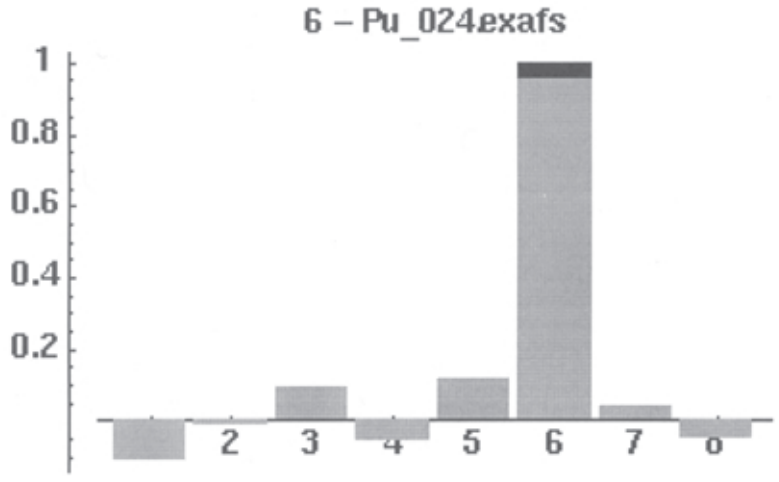

Figure 3. Uniqueness testing from the technique of principal component analysis shows that the 0.5 wt. % Ga sample was unlike the others. The magnitude of the gray bar indicates similarity.

Surface Analysis of Pu Oxide Powders: Thermal Dehydration/Water Vapor Rehydration Studies

J. Douglas Farr,
Roland K. Schulze,
Mary P. Neu,
Luis A. Morales
Los Alamos National Laboratory, Los Alamos, NM 87544, USA

Introduction

This work investigates the chemical nature of the surfaces of Pu oxide powders, primarily to help address issues that are critical for plutonium stabilization and 50-year storage. The interface between solid PuO_2 particles, adsorbed materials and the surrounding vapor phase plays a dominant role in determining reactions which affect the chemistry of the resultant atmosphere surrounding the solids. Understanding the chemistry at this interface, particularly with respect to reactions with water and water vapor, is crucial for predicting the storage behavior of these powders.

Experimental

X-ray photoelectron spectroscopy (XPS) was used to investigate the surface chemistry of a variety of samples of PuO_2 powder. The samples were studied in the as-received (atmospheric exposure) condition, in heating (dehydration) experiments up to 590° C, exposure to air after dehydration, and after controlled exposures to water vapor.

Results/Discussion

Figure 1 shows the high resolution XPS spectra of the Pu 4f and O 1s regions for a sample of PuO_2 powder that was heated to 590° C in a controlled, stepwise manner, and then exposed to water vapor. The vertical lines in these figures indicate the binding energies for lattice PuO_2 at lower binding energy (about 425.5 eV), and Pu(IV) hydroxides PuO_2 at higher binding energy (about 426.7 – 427.3 eV), based on standard spectra obtained from known compounds.[1]

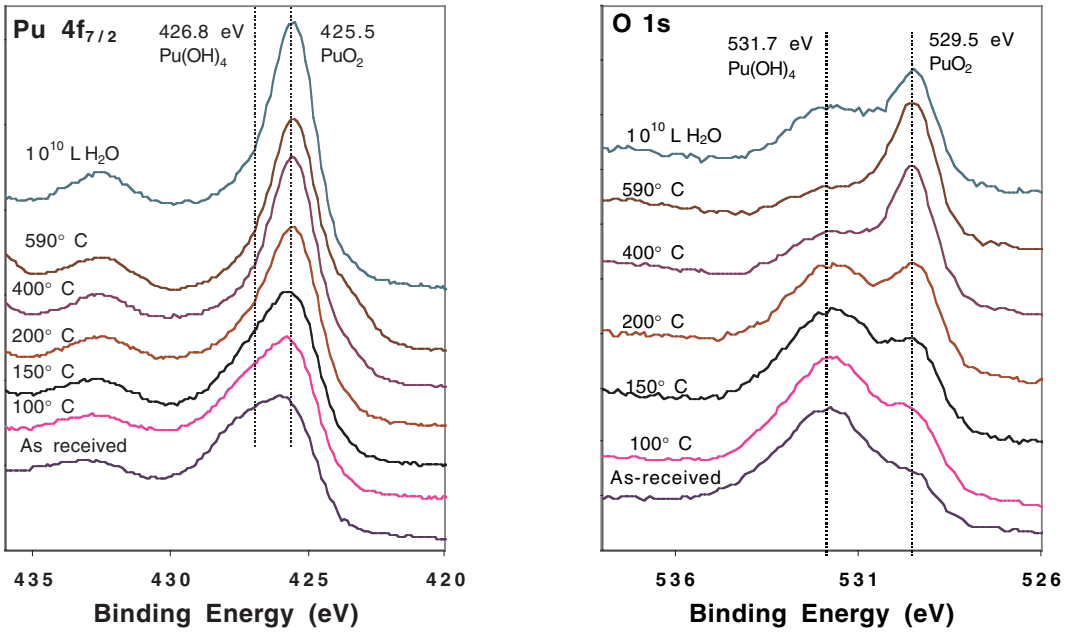

CP532, Plutonium Futures – The Science, edited by K. K. S. Pillay and K. C. Kim,
2000 American Institute of Physics 1-56396-948-3

Note the gradual decrease in intensity for the hydroxyl region in both the Pu 4f and O 1s spectra as the temperature increases. The peak due to lattice oxygen (Pu bound to O rather than OH) increases and sharpens at higher temperatures as the surface becomes more like bulk PuO_2. At 590 °C, most of the original intensity due to hydroxyl groups is gone, as seen the O 1s spectrum. The Pu 4f spectrum for 590 °C shows some increase in intensity below the main peaks in the Pu 4f region, probably due to reduction of PuO_2 to the suboxide, Pu_2O_3. After exposure to 10^{10} Langmuirs of water vapor, the suboxide feature disappears from the Pu 4f spectrum, and the broad peak due to hydroxides seen in the O 1s spectrum increases with respect to the lattice oxide peak.

The Pu $4f_{7/2}$ binding energy of 425.5 eV is slightly lower than the generally accepted value of 426.1 eV.[2] The presence of very tenacious surface hydroxides such as those observed in this work can drive this value up, as shown from our results. The binding energy for the Pu $4f_{7/2}$ peak for the as-received sample is 426.1 eV, gradually decreasing as the sample is dehydrated. Our data shows that surface hydroxylation can occur on PuO_2 powders during very low water vapor exposures, and these surface hydroxides are very stable, resisting decomposition at temperatures up to 590° C. These experiments and measurements with other Pu oxide powders and molecular compounds will be discussed in detail.

References

1. J. D. Farr, R. K. Schulze, M. P. Neu, 1997, unpublished data.

2. D. T. Larson, J. Vac. Sci. Technol., (1980) 1945.

Important New Insights into f-Electron Behavior via Ultra-high Pressure Studies of Transplutonium Elements

R. G. Haire
Oak Ridge National Laboratory, Oak Ridge, TN 37831-6375, USA

S. Heathman,
A. Lindbaum,
K. Litfin,
Y. Meressé
European Institute for Transuranium Elements, Karlsruhe, Germany

T. LeBihan
European Synchrotron Radiation Facility, Grenoble, France

Over the past two decades there have been several studies to pursue the effects of pressure on the f elements and their compounds. One issue in such studies is to ascertain how the decreasing distances brought about by applying pressure affect the electronic nature of the materials. An especially important point is whether pressure can force involvement of the f-electrons in the bonding in cases where these electrons are normally delocalized. Whereas the elements from protactinium through plutonium are accepted as having f electron involvement in their bonding at ambient pressure and temperature, in contrast the transplutonium elements do not. Thus, one goal for investigating the transplutonium elements under pressure is to ascertain if pressure can force delocalization of their normally localized f electrons.

Monitoring the structural form of materials with pressure is one experimental approach used in probing the extent of involvement of the f electrons in bonding. Although this approach requires some interpretation of the structure-bonding relationships, it has the advantage that experimentally it is possible to reach very high pressures. The structure-bonding relationships for the 4f- and 5f-electron elements have been developed both experimentally and theoretically to the level that a high degree of confidence exists with regard to such interpretation.

There has been a continued advancement in the experimental arena, due to the development of new diamond anvil cell design, detectors and the application of synchrotron radiation. Authorization to study actinides more radioactive than uranium at synchrotron sites has also advanced greatly the understanding of the bonding present in these elements. Our recent results from studies of americium, americium-curium alloys and curium under pressure have provided new insights and a better understanding of the pressure behavior of these transplutonium elements in terms of their position in the actinide series. Reviews of earlier studies of these actinides and lanthanides under pressure have been published.[1,2] There is strong evidence that the 4f-electrons of lanthanide elements in the first half of the 4f series do become delocalized under pressure. Cerium is an interesting and well-studied example, and a recent study[3] employing synchrotron radiation has enabled important new facets to be established concerning its behavior with regard to actinide behavior under pressure.

We concentrate here on the behavior of americium metal under pressure. Some work on americium metal under pressure has been published previously,[1,2] but important aspects of its structural behavior up to moderate pressures have differed in these reports. The resistivity of this metal up to 25 GPa has also been discussed[4] and provides information complimentary to that obtained from structural studies.

Americium occupies a pivotal position in the actinide series, displaying localized 5f-electron behavior while the four preceding members are recognized for their itinerant 5f-electron states. Important new insights into the nature of americium's 5f electrons with regard to metallic bonding and the relationship to that in plutonium have been acquired in our recent work. This work has employed modern

CP532, Plutonium Futures – The Science, edited by K. K. S. Pillay and K. C. Kim,
2000 American Institute of Physics 1-56396-948-3

pressure-cell designs, synchrotron radiation and an inert gas pressure-transmitting media. These have helped to provide superior resolution and intensity relationships, extended diffraction data and information for higher pressures.

As a result, we have also resolved the controversial findings reported earlier for americium in the 10-30 GPa region and have also addressed the significant difference noted between the magnitude of the theoretical and experimental relative volume collapse observed under pressure. In this recent work at ambient temperature, we found americium exhibits four different structure forms under pressure. The ambient pressure double hexagonal close packed structure first converts to a face centered cubic phase. The latter then changes to a cell having orthorhombic symmetry, which itself transforms with additional pressure to a second orthorhombic structure. The latter is stable up to one megabar. By correctly identifying the structural forms, it is also possible to establish the mechanism for the sequential conversion of the structures with pressure. A critical aspect provided by these new data is that a link can be made to the phases of plutonium.

These new findings will be presented and discussed in terms of our present understanding of the behavior of the transplutonium elements under pressure, which provides new insights for the pivotal position of americium in the series.

References

1. U. Benedict, *The Effect of Pressure on Actinide Metals*, in Handbook on the Physics and Chemistry of the Actinides, editors A. J. Freeman and G. H. Lander (North-Holland, Amsterdam, (1987) Chapter 3, pp.227-269, and references therein.

2. U. Benedict and W. B. Holzapfel, *High-Pressure Studies-Structural Aspects*, in Handbook on the Physics and Chemistry of the Rare Earths, Vol. 17: Lanthanides/Acinides: Physics I, edited by K. A. Gschneidner, Jr., L. Eyring, G. H. Lander and G. R. Choppin (North-Holland, Amsterdam, 1993) Chapter 113, pp. 245-300, and references therein.

3. M. L. McMahon and R. J. Nelmes, Phys. Rev. Letters, **78**, 3884 (1997).

4. P. Link, D. Braithwaite, J. Wittig, U. Benedict and R. G. Haire, J. Alloys and Compounds, **213/214**, 148 (1994).

Steric vs Electronic Effects in Binary Uranyl Alkoxides: A Spectroscopic Perspective

David E. Morris, Marianne P. Wilkerson, Carol J. Burns, Brian L. Scott
Los Alamos National Laboratory, Los Alamos, NM 87545, USA

Marianne P. Wilkerson, Robert T. Paine
University of New Mexico, Albuquerque, NM 87131, USA

Introduction

Electronic structure and bonding in complexes containing the linear *trans*-dioxo actinyl structural motif (AnO_2^{n+} where An = U - Am) continue to attract the attention of experimentalists and theorists alike.[1-3] The AnO_2^{n+} chromophore imparts electronic and vibrational spectroscopic characteristics that are quite sensitive to changes in symmetries and bond strengths in the equatorial plane of the "yl" moiety as well as any dative interactions involving the "yl" oxygen atoms. This is particularly true for UO_2^{2+} complexes for which optical luminescence and Raman spectroscopies have proven to be very sensitive reporters of changes in local coordination environments. However, systematic comparisons derived from spectroscopic measurements of molecular structure with electronic structure and bonding in these systems has been limited primarily to classical inorganic coordination complexes (e.g., $UO_2Cl_4^{2-}$, $UO_2(NO_3)_3^-$, etc.) as pure single crystals or doped into suitable crystalline host matrices.[1]

Recent advances in the non-aqueous alkoxide chemistry of UO_2^{2+} have provided the wherewithal to prepare and isolate a broad range of discrete molecular uranyl entities both as solids and in aprotic solvents in which it is possible to tune the ligand basicity and steric encumbrance.[4-6] Uranyl complexes have been isolated as monomers, dimers, and higher order oligomers. These complexes afford an opportunity to examine in some detail the relative importance of ligand basicity and steric demand in directing structural preferences (monomer vs. dimer, *cis* vs. *trans* isomers) and in determining electronic structural properties and relative bond strengths in the "yl" and equatorial bonds. In the present report the electronic and vibrational spectroscopic data for a series of uranyl alkoxides are correlated with molecular structural data to examine trends in electronic structure and bonding and compare these results with existing models based on the more classical uranyl coordination compounds.

Experimental

Standard inert-atmosphere techniques were used for the manipulation of all reactions. Anhydrous uranyl chloride bis(tetrahydrofuran) ($[UO_2Cl_2(THF)_2]_2$) was prepared by literature methods from uranium oxide.[4] Potassium alkoxide salts were prepared from the appropriate dry alcohol and KH in tetrahydrofuran at room temperature, and were dried in vacuo prior to use. In a typical reaction, KOR (R = $CHPh_2$, $CH(^tBu)Ph$,[2] 2,6-$^tBu_2C_6H_3$, 2,6-$Ph_2C_6H_3$, 2,6-$Cl_2C_6H_3$, 2,6-$Me_2C_6H_3$) was dissolved in THF (20 mL) and added to a slurry of $[UO_2Cl_2(THF)_2]_2$ (1.00 g, 1.03 mmol) and THF (50 mL). The solution was stirred for ~ 4 h, and then filtered over Celite. The filtrate was concentrated to ~ 5 mL, layered with ~ 5 mL hexane, and cooled to -30°C yielding the appropriate uranyl product.

Optical luminescence data (spectra and lifetimes) were collected on a SPEX Fluorolog 2 system equipped with a phosphorimeter attachment. All data were collected at liquid nitrogen temperature in an insertion dewar. Solution samples were run as ices in THF and/or benzene. Raman data were collected on solid samples only at room temperature. Data were obtained on a confocal microscope

CP532, Plutonium Futures – The Science, edited by K. K. S. Pillay and K. C. Kim,
2000 American Institute of Physics 1-56396-948-3

system using 752 nm Ti:sapphire laser excitation or on a Nicolet FT-Raman spectrometer using 1064 nm Nd:VO_4 excitation.

Results and Discussion

An example of the structural variability in uranyl alkoxide chemistry is illustrated in Fig. 1 for some of the complexes for which spectroscopic data are presented here. In the solid state only monomeric products are isolated for the more sterically demanding ligands including diphenylmethoxide, phenyl-*tert*-butylmethoxide (not shown), 2,6-di-*tert*-butylphenoxide and 2,6-diphenylphenoxide. However, for less sterically demanding ligands like 2,6-dichlorophenoxide and 2,6-dimethylphenoxide (not shown), dimeric species are isolated.

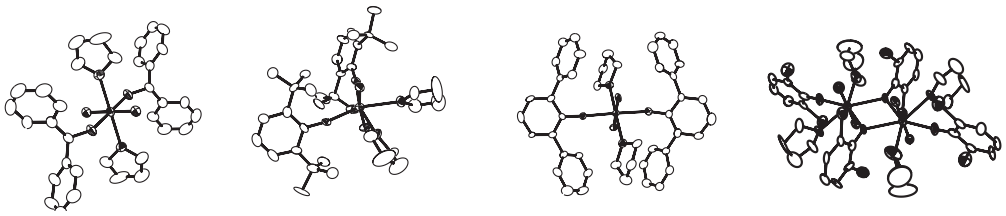

Figure1. Solid-state uranyl alkoxides (left to right) $UO_2(OCHPh_2)_2(THF)_2$, $UO_2(O\text{-}2,6\text{-}{}^tBuC_6H_3)_2(THF)_2$, $UO_2(O\text{-}2,6\text{-}Ph_2C_6H_3)_2(THF)_2$, and $[UO_2(O\text{-}2,6\text{-}Cl_2C_6H_3)_2(THF)_2]_2$.

The luminescence spectra obtained for the series of aromatic alkoxide complexes are shown in Fig. 2. For several of these complexes in solution there is a concentration dependence to the emission spectra that suggests an equilibrium exists between monomeric and dimeric forms or different conformers of monomers. Notably, for these aryloxides there is no significant trend in the energy of the electronic origin (which best reflects the HOMO - LUMO gap) as a function of the ligand basicity (pK_a range from ~ 7 to ~ 12) indicating that structure and bonding in these systems adjust to accommodate the ligand steric demand with ligand basicity *per se* having no significant impact on electronic structure. The emission spectra for the monomeric aliphatic alkoxides (pK_a values of ~ 15-16) display energies for the electronic origin similar to those for the aryloxide systems again demonstrating that steric effects dominate the bonding and diminish the anticipated electronic perturbations from increased ligand basicity.

Vibrational data extracted from the Raman spectra of the solids and/or from the vibronic resolution in the emission data provide a more sensitive correlation between ligand basicity and "yl" bond length for all the alkoxide complexes considered here. These results are consistent with the Denning model[1] that predicts longer "yl" bonds with lower "yl" vibrational energies for the totally symmetric mode as the ligand basicity increases.

Acknowledgment

Funding for this effort was made possible through the Laboratory Directed Research and Development program at Los Alamos and the Chemical Sciences Division, Office of Science of the United States Department of Energy.

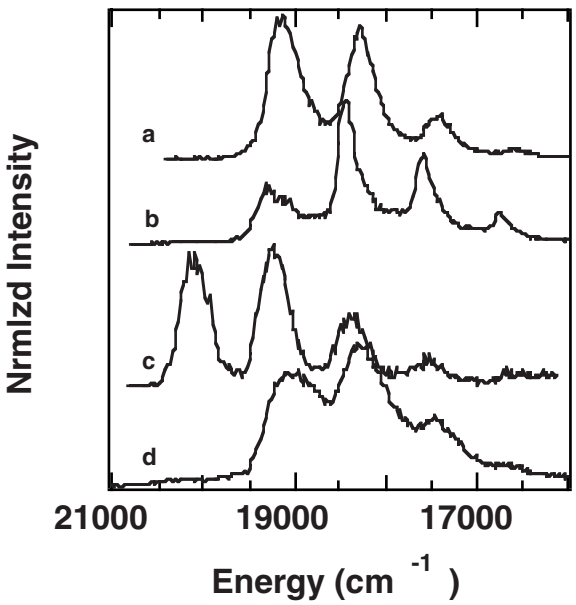

Figure 2. Luminescence spectra for (a) $[UO_2(O\text{-}2,6\text{-}Cl_2C_6H_3)_2(THF)_2]_2$, (b) $UO_2(O\text{-}2,6\text{-}Ph_2C_6H_3)_2(THF)_2$, (c) $[UO_2(O\text{-}2,6\text{-}Me_2C_6H_3)_2Cl(THF)]_2$, and (d) $UO_2(O\text{-}2,6\text{-}{}^tBuC_6H_3)_2(THF)_2$. Ligand basicity increases from top to bottom.

References

1. Denning, R. G. *Struct. Bonding* **1992**, 79, 215-76.
2. Pepper, M.; Bursten, B. E. *Chem. Revs.* **1991**, 91, 719-41.
3. Schreckenbach, G.; Hay, P. J.; Martin, R. L. *J. Comput. Chem.* **1999**, 20, 70-90.
4. Wilkerson, M. P.; Burns, C. J.; Paine, R. T.; Scott, B. L. *Inorg. Chem.* **1999**, *38*, 4156.
5. Wilkerson, M. P.; Burns, C. J.; Dewey, H. J.; Martin, J. M.; Morris, D. E.; Paine, R. T.; Scott, B. L. *Manuscript submitted.*
6. Wilkerson, M. P.; Burns, C. J.; Morris, D. E.; Paine, R. T.; Scott, B. L. *Manuscript in preparation.*

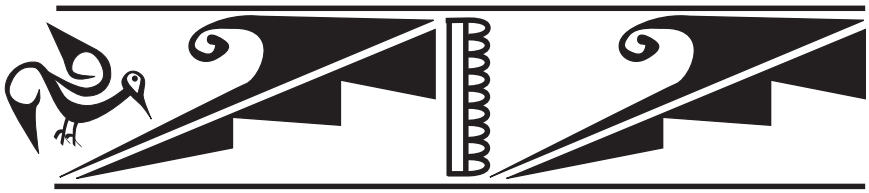

Actinide Compounds & Complexes

Structural Preferences and Reactivity of Uranyl Alkoxide Complexes Prepared in Non-Protic Media

Carol J. Burns, Marianne P. Wilkerson, David E. Morris, Brian L. Scott
Los Alamos National Laboratory, Los Alamos, NM 87545, USA

Robert T. Paine, Marianne P. Wilkerson
Department of Chemistry, University of New Mexico, Albuquerque, NM 87131, USA

Introduction

Recent reports have shown that uranyl complexes may exhibit Lewis basic or Brönsted basic behavior in electron-rich coordination environments.[1,2] In this presentation, structural, spectroscopic and chemical properties of a series of uranyl alkoxide compounds are compared in order to assess the influence of electron-donor alkoxide ligands.

Experimental Results

The preparation of uranyl alkoxide (OR, R = alkyl) complexes in nonaqueous media results in the formation of a variety of products which depend on the basicity and solubility of the ligand. These compounds can undergo ligand swapping of a uranyl oxo group for two alkoxide ligands or can generate aggregates that exhibit coordinative behavior previously not seen for actinyl species obtained from aqueous solutions. For example, it has been reported that preparation of uranyl bis-*tert*-butoxide allows for ligand redistribution to the intermediate $UO(O^tBu)_4$, which can then coordinate two more $UO_2(O^tBu)_2$ fragments to form a trimer (Figure 1).[1] The reaction of the less bulky alkoxide ligand, OCH_2CMe_3, with uranyl chloride yields a product consistent with complete oxo-alkoxide ligand redistribution, $U(OCH_2CMe_3)_6$ (Figure 2).[3] An unusual tetrameric product, $[UO_2(OCH(^iPr)_2)_2]_4$, is isolated from the reaction of potassium di-*iso*-propyl methoxide with uranyl chloride. In this aggregate, uranyl oxo groups bridge to neighboring metal centers. A series of isostructural 'ate' uranyl *iso*-propoxide complexes, $[M(THF)_x(UO_2)_3(O^iPr)_7]_2$ (M = Na, K: x = 1; M = Rb, Cs: x = 0), have been synthesized in a similar metathesis reaction. These molecules have cubane-like metal frameworks which also contain oxo bridging to neighboring Lewis acids.[4]

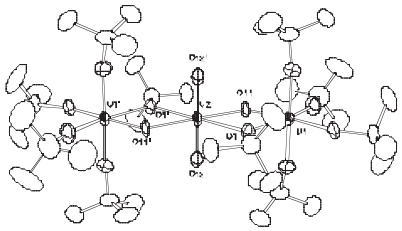

Figure 1. Thermal ellipsoid drawing of $[UO(O^tBu)_4]_2$ $[UO_2(O^tBu)_2]$.[1]

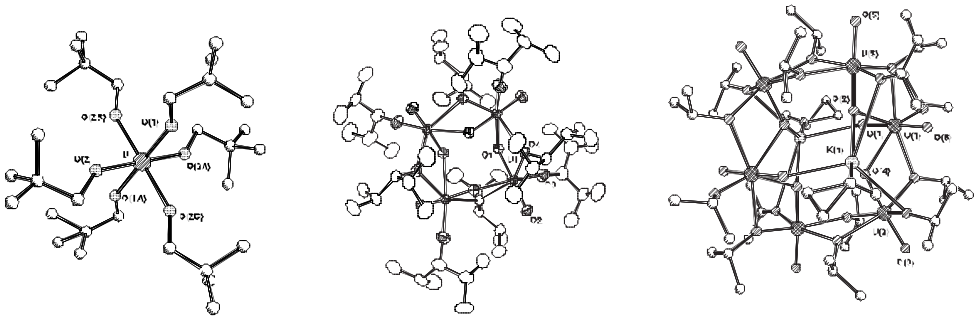

Figure 2. Thermal ellipsoid drawings of $U[OCH_2C(CH_3)_3]_6$,[3] $[UO_2(OCH(^iPr)_2)_2]_4$, and $[K(THF)(UO_2)_3(O^iPr)_7]_2$.[4]

CP532, Plutonium Futures – The Science, edited by K. K. S. Pillay and K. C. Kim,
2000 American Institute of Physics 1-56396-948-3

The coordinative behavior of these uranyl alkoxide complexes is induced by the increased basicity of the oxo groups, resulting in a weakening of the uranyl U-O bond. Raman spectroscopy may be used to probe the O=U=O bond strength. The symmetric stretch for these species uniformly appears at lower energy than that of the free ion (856 cm^{-1}). For example, n_1 for tetrameric $[UO_2(OCH(^iPr)_2)_2]_4$ is dramatically red-shifted (~ 710 cm^{-1}), whereas the red shifts of the symmetric stretch for the 'ate' complexes, $[M(THF)_x(UO_2)_3(O^iPr)_7]_2$, are a more complex function of the weakened uranyl bonds and the ionic character of the complexes.

Optical spectroscopy is a useful tool for determining the relative degree of aggregation in the solid state or solution. Comparison of the emission spectra of these compounds shows that there is a red shift in the $E_{0\text{-}0}$ transition as the degree of oligomerization is increased. Therefore, solvent induced deaggregation may be determined. Furthermore, the reactivity of these uranyl alkoxide compounds is directly related to the degree of oligomerization in solution. Aggregates that remain intact are unreactive, while those that are either monomeric or fragmented allow for the preparation of new chemical species.

Acknowledgment

This research at Los Alamos National Laboratory was supported by the Division of Chemical Energy Sciences, Office of Basic Energy Sciences, U.S. Department of Energy, and by the Laboratory Directed Research and Development Program.

References

1. Burns, C. J.; Sattelberger, A. P. *Inorg. Chem.* **1988**, *27*, 3692.

2. Clark, D. C.; Conradson, S. D.; Donohoe, R. J.; Keogh, D. W.; Morris, D. E.; Palmer, P. D.; Rogers, R. D.; Tait, C. D. *Inorg. Chem.* **1999**, *38*, 1456.

3. Wilkerson, M. P.; Burns, C. J.; Dewey, H. J.; Martin, J. M.; Morris, D. E.; Paine, R. T.; Scott, B. L. *Manuscript submitted*.

4. Wilkerson, M. P.; Burns, C. J.; Morris, D. E.; Paine, R. T.; Scott, B. L. *Manuscript in preparation*.

Synthesis and Structural Studies of Plutonium Complexes Containing Nitrogen and Sulfur Donor Ligands

John H. Matonic,
Mary P. Neu,
Brian Scott
Los Alamos National Laboratory, Los Alamos, NM 87545, USA

Marinella Mazzanti
Laboratorie de Reconnaissance Ionique, CEA-Grenoble, France

The large coordination sphere, wide range of readily accessible oxidation states, and 5f orbital/ligand interactions all make plutonium complexes very interesting systems to study. The results from such studies help us understand the basic coordination chemistry and reactivity of plutonium complexes. Specifically, we are pursuing the following goals: (1) structural characterization of plutonium complexes with relatively soft (nitrogen and sulfur) donor ligands; (2) preparation of new starting materials for the study of nonaqueous Pu(III) and Pu(IV) chemistry; (3) determining ligand affinities and coordination geometry preferences for low valent actinides. The latter allows us to evaluate complexes for extractions and other separations of these elements from lanthanides and transition metal fission products.[1]

Structural studies of plutonium coordination complexes are rare. In fact, at the end of the twentieth century, the Cambridge Data Base, which lists structurally characterized molecules that contain at least one carbon and one hydrogen, shows 16 plutonium complexes, all of which were characterized by powder diffraction. This absence of structural data severely limits the prediction of possible reaction products and reduces the accuracy of computer modeling, which relies heavily on such data. We hope to build a database of plutonium complexes in which one can find typical plutonium bond distances and coordination geometries.

The preparation of virtually all nonaqueous An(III) complexes has gone through the triiodide-tetrahydrofuran complex. We are interested in the preparation of new complexes using solvents other than tetrahydrofuran. We have prepared a few new starting materials soluble in acetonitrile, all exploiting the ease of plutonium oxidation. The preparation of a homoleptic acetonitrile complex was accomplished by reacting plutonium metal with hexachloroethane and aluminum trichloride. Trishalide-acetonitrile plutonium complexes can be made by very simply reacting plutonium metal with iodine or $PhICl_2$ in acetonitrile. All of these systems allow for a one-pot preparation of new complexes via addition of suitable ligands.

We are currently investigating the addition of nitrogen and sulfur donor ligands, including tripodal amines, thioethers, and thiolates, to these systems. Tripodal amines have shown a preference for binding actinides over lanthanides by a factor of ten. A few lanthanide complexes of tripodal amines have been structurally characterized.[2-4] Comparison of these complexes with analogous actinide complexes allows for a direct look at bonding differences between the lanthanides, and actinides and could possibly expose the reason for this preference. We have structurally characterized the product formed between trispyrazine amine and $PuI_3(MeCN)_4$ and found an eight coordinate plutonium complex containing the tripodal amine, three iodides, and a acetonitrile.

We have also studied the trispyridyl amine and trisbipyridyl amine systems. In both the trispyridyl and trispyrazine amine systems we see formation of a 1:1 and 2:1 ligand to metal product as shown by nuclear magnetic resonance (NMR) and UV-vis data. In the trisbipyridyl amine system, we see the formation of a 1:1 product.

CP532, Plutonium Futures – The Science, edited by K. K. S. Pillay and K. C. Kim,
2000 American Institute of Physics 1-56396-948-3

Figure 1. The structure of $PuI_3(TPZA)(MeCN)$.

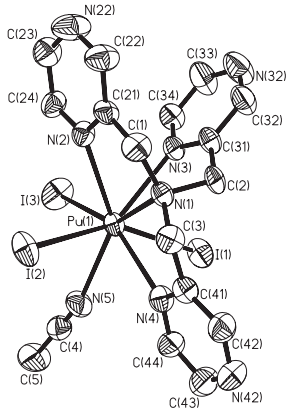

A few sulfur donor ligands show even more preference favoring the actinides. Sulfur ligands are notoriously poor ligands for the lanthanides and very few complexes are known for the actinides. We have started to probe the reactivity between some soft sulfur donor ligands and Pu(III). The ligands include phenyl dithiolates, alkyl thiolates, and sulfides. We will present the X-ray structures, electronic absorption spectra, NMR data, and cyclic voltammograms for these new Pu and Am complexes.

References

1. K. N. Nash, *Solvent Extr. Ion Exch.*, **1993**, *11*, 729.

2. R. Wietzke, M. Mazzanti, J.-M. Latour, J. Pecaut, *Inorg. Chem.*, **1999**, *38*, 3581-3585.

3. R. Wietzke, M. Mazzanti, J.-M. Latour, J. Pecaut, *J. Chem. Soc., Dalton Trans.*, **1998**, 4087-4088.

4. R. Wietzke, M. Mazzanti, J.-M. Latour, J. Pecaut, P.-Y. Cordier, C. Medic, *Inorg. Chem.*, **1998**, *37*, 6690-6697.

Structures of Plutonium Coordination Compounds: A Review of Past Work, Recent Single Crystal X-Ray Diffraction Results, and What We're Learning about Plutonium Coordination Chemistry

M. P. Neu,
J. H. Matonic,
D. M. Smith,
B. L. Scott
Los Alamos National Laboratory, Los Alamos, NM 87544, USA

Structural studies of plutonium coordination complexes are rare. In fact, the Cambridge Structural Database (CSD), which consists of molecules that have been structurally characterized using X-ray diffraction (XRD) and contain at least one carbon atom and one hydrogen atom, contains information for only 16 plutonium compounds. All of the references are to powder diffraction studies reported from 1949 to 1981. The Inorganic Crystal Structure Database, which contains all structures not in the CSD, includes 81 compounds containing plutonium, of which 78 are powder diffraction studies and the majority were reported before 1965. The compounds are also nearly all solid state materials, including 33 plutonium alloys. There are only three plutonium coordination compounds that have been characterized using single crystal XRD: the nitrate, sulfate, and carbonate, all Pu(IV) complexes. This absence of detailed structural data limits the ability to predict plutonium chemistry in general and particularly hinders the subfields of basic science, separations, environmental behavior, material processing, theory and modeling.

The reasons for this lack of structural data for plutonium coordination compounds, particularly in the last few decades, are many and varied. We and others are overcoming these obstacles and characterizing plutonium complexes using single crystal XRD and advanced spectroscopies. The single crystal structures reported in the literature are all for simple, bidentate, oxygen-donor ligands bound to Pu(IV). Plutonium(IV) sulfate was isolated by Jayadevan, *et al.* as the tetrahydrate, $Pu(SO_4)_2(H_2O)_4$, containing an eight coordinate Pu atom.[1] The plutonium nitrate complex reported by Spirlet, *et al.* is the bis ammonium salt of the hexanitrate, $(NH_4)_2Pu(NO_3)_6$, where Pu is twelve-coordinate.[2] Intermediate between these two coordination geometries is the recently reported (Clark, *et al*.) sodium salt of the limiting carbonate, $Na_6Pu(CO_3)_5$ where the Pu(IV) is ten-coordinate.[3]

The compounds we have isolated and characterized include plutonium(III) and plutonium(IV) bound by ligands with a range of donor types and denticity (halide, phosphine oxide, hydroxamate, amine, sulfide) in a variety of coordination geometries.[4] For example, we have obtained the first X-ray structure of Pu(III) complexed by a soft donor ligand. Using a "one pot" synthesis beginning with Pu metal strips and iodine in acetonitrile and adding trithiacyclononane we isolated the complex, $PuI_3(9S_3)(MeCN)_2$ (Figure 1). On the other end of the coordination chemistry spectrum, we have obtained the first single crystal structure of the Pu(IV) hexachloro anion (Figure 2). Although this species has been used in plutonium purification via anion exchange chromatography for decades, the bond distances and exact structure were not known. We have also characterized the first plutonium-biomolecule complex, Pu(IV) bound by the siderophore desferrioxamine E.

In this presentation we will review the preparation, structures, and importance of previously known coordination compounds and of those we have recently isolated. We will show the coordination chemistry of plutonium is rich and varied, well worth additional exploration.

CP532, Plutonium Futures – The Science, edited by K. K. S. Pillay and K. C. Kim,
2000 American Institute of Physics 1-56396-948-3

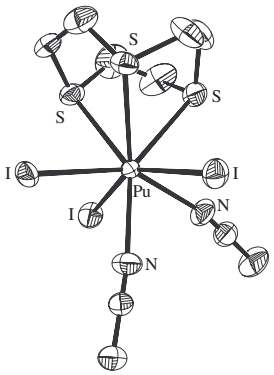

$PuI_3(9S_3)(MeCN)_2$

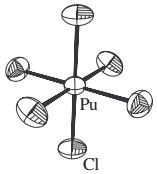

$[Et_4N]_2[PuCl_6]$

References

1. N. C. Jayadevan, K. D. Singh Mudher, D. M. Chackraburtty, *Zeitschrift für Kristallographie*, **1982**, *161*, 7-13.

2. M. R. Spirlet, J. Rebizant, C. Apostolidis, B. Kanellakopoulos, E. Dornberger, *Acta Cryst. C*, **1992**, *48*, 1161-1164.

3. D. L. Clark, S. D. Conradson, D. W. Keogh, P. D. Palmer, B. L. Scott, C. D. Tait, *Inorg. Chem.* **1998**, *37*, 2893-2899.

4. For examples see, a) PuI_3(tpza)(MeCN) – J. H. Matonic, B. L. Scott, M. P. Neu *Inorg. Chem*. submitted. b) $[Pu(NOPOPO)_2(NO_3)_2](NO_3)_2$ – E. M. Bond, E. N. Duesler, R. T. Paine, M. P. Neu, J. H. Matonic, B. L. Scott *Inorg. Chem.* submitted. c) $[Al(H_2O)_6][Pu(DFOE)(H_2O)]_2(CF_3SO_3)_5$ – M. P. Neu, J. H. Matonic, C. E. Ruggiero, B. L. Scott. *Angew. Chem*. **2000**, in press.

Characterisation of Uranium Compounds After a Fire Ignition

D. Labroche,
D. Pisson,
P. Ramel,
O. Dugne
Commissariat à l'Energie Atomique CEA/Valrho, DCC/DTE/SIM Laboratoire de Métallographie, BP111, 26702 PIERRELATTE Cedex 2, France

This paper presents the characterisation of uranium compounds after a fire occurred during handling of a calorimeter composed of uranium plates at the CERN (Nuclear Research European Centre, Geneva, Switzerland). The evaluation of the cut of ignited samples allows several hypotheses on the origin of the fire ignition.

Last year, three calorimeters were broken up. They were composed of alternating plates of poor uranium metal/organic composite matrix and copper plates, all oriented in a vertical position. The calorimeter is filled by liquid argon during the experiment.

The fire was characteristic of a metal fire. It was initiated during the suction of black powder that fell from the plates during handling. The fire was stopped by firemen using powder extinguishers.

Three specimens were examined with chemical (fluorescence, EDS), morphological (SEM) and structural (XRD) analyses to identify the origin of the fire:

- N°12: powder coming from the surface of a uranium plate in front of a fire area sampled on the ground,
- N°13: powder sampled on a surface uranium plate from a known fire area,
- sample 14: powder sampled on a uranium surface plate near a fire area.

The results show a similarity between the three specimens. They are all composed of uranium oxides UO_2, U_3O_7 and U_4O_9 within any detection of U_3O_8, UH_3 or uranium metal. With this last established fact it can be concluded that the ignition of the fire was not started by the presence of UH_3 or uranium metal.

The lack of difference between the three samples cannot permit us to conclude with certainty; however, we propose that the fire was ignited by a mechanical impact of UO_2 powder with high specific surface, produced by corrosion that occurred on the surface of uranium plates.

CP532, Plutonium Futures – The Science, edited by K. K. S. Pillay and K. C. Kim,

Solid State Chalcophosphate Compounds of Actinide Elements

Paula M. Briggs Piccoli, Ryan F. Hess, Peter K. Dorhout
Department of Chemistry, Colorado State University, Fort Collins, CO 80523, USA

Paula M. Briggs Piccoli, Kent D. Abney, Jon R. Schoonover, Peter K. Dorhout
Los Alamos National Laboratory, Los Alamos, NM 87545, USA

Introduction

Since the discovery of the transuranic elements, much of the focus of actinide solid-state chemistry has concerned binary compounds and alloys. Special attention has been given to oxide forms of the actinides, as they have applications in nuclear fuels and waste storage forms. While much information is known for these systems, relatively little study has been conducted on compounds involving heavier congeners of the oxide family (the chalcogenides) past that of the binary compounds. Most study of binary actinide chalcogenide compounds was undertaken in the late 1940s and early 1950s;[1-3] with more accurate characterization techniques, much of this early work is currently being reinvestigated.[4-7]

Description

This work involves the exploration of ternary and quaternary compounds of the actinide chalcogenides using a Zintl ion building block approach. Zintl ions are closed shell, main-group ions that can coordinate to other elements in the compound in such a way that builds up the structure. A common Zintl ion in the chalcophosphate family is the ethane-like $(P_2Se_6)^{4-}$ anion, which has been found to bond to main group, transition metal and lanthanide elements in a variety of coordination modes.[8-10] To achieve our goal of new actinide-metal Zintl phase material synthesis, we are employing a low-to-moderate temperature (300°C–800°C) molten salt technique.[11-13] This technique utilizes low-melting binary alkali chalcogen salts like K_2Se_3 in combination with excess chalcogen as the oxidizing agent for the actinide metal and other main group elements to be incorporated into the final structure. This departure from conventional (high-temperature) routes to solid-state materials allows for formation and isolation of metastable phases with complex, low-dimensional structures not seen in the binary compounds. Prior to our studies, three quaternary compounds of actinide chalcophosphates were reported in the literature: $K_2UP_3Se_9$,[14] $Rb_4U_4P_4Se_{26}$[15] and $KTh_2Sb_2Se_6$.[16] The known ternary and quaternary chalcogen compounds of the actinides have thus far exhibited rich structural chemistry.[17]

Results

Investigation of quaternary A/An/P/Q chalcophosphate systems (A = K, Rb, Cs; An = Th, U; Q = S, Se) from molten salts at moderate temperatures (700°C–750°C) has revealed at least seven new phases of material not previously seen in thorium and/or uranium chalcogenide chemistry. The molten salt flux compositions used in these syntheses have supported the formation of $(PS_4)^{3-}$ and $(P_2Se_6)^{4-}$ Zintl ions almost exclusively, although polychalcogen anions like $(Se_2)^{2-}$, $(P_2S_7)^{4-}$ and the previously unseen Zintl ion $(P_2Se_9)^{6-}$ have also been seen from these reactions. General features of these new structures include eight- and nine-coordinate actinide metal centers that either corner-share or edge-share chalcogen atoms to form "dimeric" polyhedral units. These structural units are linked together in one, two or three dimensions by the chalcophosphate anions to form the final structures. Alkali cations are found in the channels or holes created by the overall structure to charge balance the compound; one material in particular has been noted to possess ion exchange capabilities. Examination of the phase diagrams

CP532, Plutonium Futures – The Science, edited by K. K. S. Pillay and K. C. Kim,
2000 American Institute of Physics 1-56396-948-3

produced from flux composition and final products indicates that cation size and/or relative Lewis acidity or basicity of the molten salt flux has a significant influence on the final structure.[18] Differing structures from identical flux compositions will be compared, and the phase diagrams will be examined. Comparisons to relevant lanthanide structures will also be made. Structures determined by single crystal X-ray diffraction and Raman spectra will be presented. In addition to the thorium and uranium work undertaken by our group, investigations using transuranic elements (Np, Pu) are also underway.

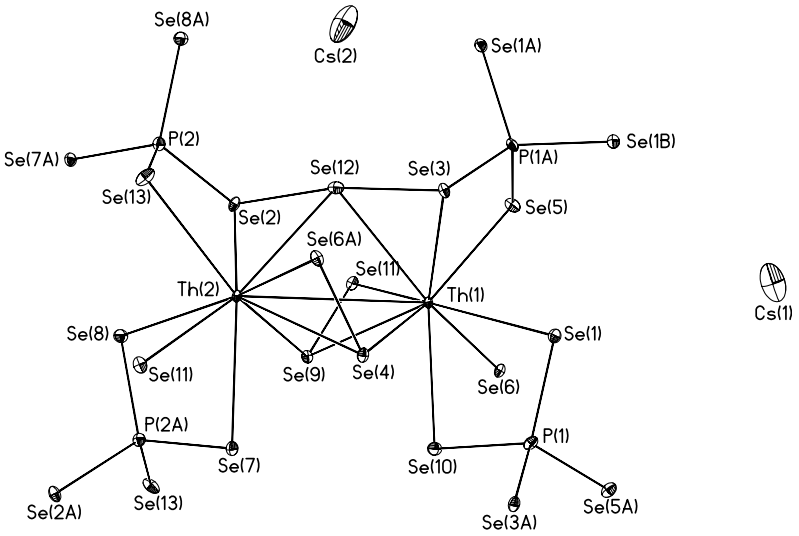

Figure 1. Thermal ellipsoid plot of the asymmetric unit of $Cs_4Th_4P_4Se_{26}$ showing the $(P_2Se_9)^{6-}$ and $(Se_2)^{2-}$ anions and immediate coordination sphere of the Th atoms.

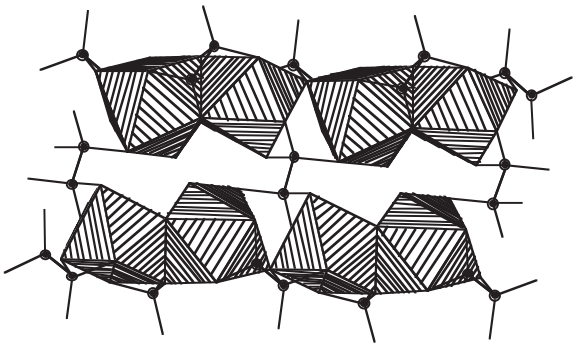

Figure 2. Double chain of corner-sharing $[Th_2Se_{13}]$ polyhedra in $Cs_4Th_2P_5Se_{17}$. The chains are held together by the ethane-like $(P_2Se_6)^{4-}$ anions. $(Se_2)^{2-}$ anions are also part of the structure but are integrated into the polyhedral units.

References

1. Zumbusch, M. *Z. Anorg. Allg. Chem.* **1940**, *243*, 322.
2. Zachariasen, W. H. *Acta Cryst.* **1949**, *2*, 288.
3. Zachariasen, W. H. *Acta Cryst.* **1949**, *2*, 57.
4. Stöwe, K. *J. Alloys Comp.* **1997**, *246*, 111-123.
5. Tougait, O.; Potel, M.; Noël, H. *J. Solid State Chem.* **1998**, *139*, 356-361.
6. Tougait, O.; Potel, M.; Nöel, H. *Inorg. Chem.* **1998**, *37*, 5088-5091.
7. Tougait, O.; Potel, M.; Levet, J. C.; Noël, H. *Eur. J. Solid State Inorg. Chem.* **1998**, *35*, 67-76.
8. Kanatzidis, M. G.; Huang, S.-P. *Coord. Chem. Rev.* **1994**, *130*, 509-621.
9. Chen, J. H.; Dorhout, P. K.; Ostenson, J. E. *Inorg. Chem.* **1996**, *35*, 5627-5633.
10. Pell, M. A.; Ibers, J. A. *Chem. Ber.* **1996**, *130*, 1-8.
11. Sunshine, S. A.; Kang, D.; Ibers, J. A. *J. Am. Chem. Soc.* **1987**, *109*, 6202-6204.
12. Kanatzidis, M. G.; Sutorik, A. C. *Prog. Inorg. Chem.* **1995**, *43*, 151-265.
13. Kanatzidis, M. G. *Curr. Opin. Solid State Mater. Sci.* **1997**, *2*, 139-149.
14. Chondroudis, K.; Kanatzidis, M. G. *C. R. Acad. Sci. Paris* **1996**, *t. 322, Serie II b*, 887-894.
15. Chondroudis, K.; Kanatzidis, M. G. *J. Am. Chem. Soc.* **1997**, *119*, 2574-2575.
16. Choi, K. S.; Iordanis, L.; Chondroudis, K.; Kanatzidis, M. G. *Inorg. Chem.* **1997**, *36*, 3804-3805.
17. Narducci, A. A.; Ibers, J. A. *Chem. Mater.* **1998**, *10*, 2811-2823.
18. Chondroudis, K.; Kanatzidis, M. G. *Inorg. Chem.* **1998**, *37*, 3792.

Thermodynamic and Structural Characterisation of the $UFeO_4$ Compound

D. Labroche,
J. Rogez,
O.Dugne
CEA-VALRHO, DCC/DTE/SIM, BP 111, 26702 Pierrelatte Cedex, France

J. P. Laval
Université de Limoges, CTM, 26 rue du 141 ème RIA, 13003 Marseille, France

In order to establish the whole ternary phase diagram (U-Fe-O), which is one of the main systems in the nuclear safety and enrichment programs, the $UFeO_4$ ternary compound must be characterised with more precision. Indeed, the knowledge of this compound is essential because an experimental determination of the isothermal section at 1300 K shows that $UFeO_4$ is involved in three-phase equilibria.

The first purpose of this work is to obtain thermodynamic data and new structural information on this ternary oxide. Even if this compound has been already studied since 1966,[1] thermodynamic data are available and the structure is partly known.[2]

The experimental thermodynamic study presented consists of the determination of the enthalpies of formation of the $UFeO_4$ compound by several solution calorimetries at two temperatures. The references are simple oxides in the binary side diagrams. The ambient solution calorimetry is performed in aqueous acid solvent and the high temperature one in borate baths. The heat capacities between the two temperatures are derived from drop calorimetry measurements. This set of complementary measurements aims to give some coherent data for further optimisation.

Some structural (XRD, neutron diffraction) and physicochemical (TEM, FPMA) characterisations are achieved to determine and check

- the temperature range of stability of $UFeO_4$,
- the crystallographic structures, and
- the nature of the structural defaults.

This information helps us in the choice of the sub-lattice selected to described the ternary phases.

The second aim is to determine new thermodynamic data on the ternary system, involving $UFeO_4$ in the equilibrium relationship. Thermogravimetric measurements are performed with a Setaram thermobalance in view to determine the oxygen potential of $UFeO_4$ in equilibrium with Fe_2O_3 and U_3O_8 for example. A specific gas system was added to provide a controlled residual pressure of oxygen.

These experiments have never been achieved before even if the existence of $UFeO_4$ has been known since 1966.[1] All these measurements permit us to complete the physicochemical description of the $UFeO_4$ compound and to determine thermodynamic data on U-Fe-O systems. These new data are introduced in the final optimisation of the (U-Fe-O) system with the Thermocalc code.

References

1. Hoekstra H. R., Marshall R. H., Some uranium-transition element double oxides, Lanthanide/Actinide Chemistry 16, 211-227 (1966)
2. Bacmann M., Bertaut M. M., Structure du nouveau composé $UFeO_4$, Bull. Soc. Fr. Minéral. Cristallogr., XC, 257-258 (1969)

CP532, Plutonium Futures – The Science, edited by K. K. S. Pillay and K. C. Kim,

Thermodynamic Properties of Pu^{3+} and Pu^{4+} Aquo Ions

F. David,
B. Fourest,
S. Hubert
IPN, Orsay, France
J. Purans
University of Riga, Riga, Lettonia
V. Vokhmin
Inst. Phys. Chem., Moscow, Russia
C. Madic
CEA Marcoule, France

The purpose of this work is to evaluate thermodynamic properties of some actinide ions in aqueous solution, particularly plutonium, taking into account their real characteristics, such as their covalent character and effective charge. The aquo ions are characterized by the charge q, crystallographic radius Rc with coordination number N, radius of the water molecule Rw and number H of molecules in the second hydration sphere. For the understanding of lanthanide and actinide aquo ion properties, we have performed EXAFS experiments on different trivalent and tetravalent ions (with concentration 7.10-3 to 0.2 M) in acidic solutions (HCl 1 M) at LURE.[1,2,3] Based on our data and different published investigations, we have defined the coordination number N and the interatomic distances d between the cation and the oxygen atoms of the primary hydration sphere for the complete series of trivalent lanthanides, for some trivalent actinides (U, Np, Pu, Am and Cf) and for the tetravalent plutonium ion.

Considering electrostriction model and experimental data relative to species with ionic character and charge from -1 to +3, we have evaluated an "ionic" distance d(ion) for each investigated ion. Consequently, we observed a decrease *d = d(ion) -d, for the two plutonium ions. This decrease is larger than the accepted standard deviation, and, therefore, significant. Moreover, it is also observed for other f elements at the beginning of the two f series, but *d is essentially nonexistent from the middle of the two series. This result could be interpreted by the existence of a covalent effect,[1,4] especially for plutonium ions.

By applying an ion-water interaction model[4] and taking into account realistic values of the characteristic parameters of the aquo ions, we have deduced an effective charge of the different ions considered. The decrease of the charge, *q, is correlated with the experimental decrease of the distance *d for ions presenting covalent character. If we accept that such a correlation is also effective in the actinide series, then effective charge could be also evaluated for actinides, and particularly plutonium species, taking into account the experimental *d value.

Finally, the free hydration energy of trivalent and tetravalent plutonium ions has been calculated based on reliable values of q, N, Rc, Rw, and H. In the case of trivalent lanthanides and tetravalent cerium an excellent agreement is observed between calculated and experimental data.

Since the hydration entropy term is expressed by the derivation versus temperature of the hydration free energy, an entropy model is proposed which is validated with experimental entropy determination. Therefore, since this model is also based on the five characteristics of the ions considered, an evaluation of the trivalent and tetravalent plutonium entropy is achieved which takes into account the covalent character of the trivalent and tetravalent ions.

CP532, Plutonium Futures – The Science, edited by K. K. S. Pillay and K. C. Kim,

References

1. F. David et al., Proceedings of the Actinide Conference XAS 98, Grenoble, 2-4 October 1998, AEA Report, 1999.

2. R. Revel et al., Inorg. Chem, 38, N° 18 (1999) 4139.

3. F. David et al., to be published.

4. F. David, V. Vokhmin, G. Ionova, in press, J. of Molecular Liquid.

Modeling the Thermodynamic Properties of Plutonium

Marius Stan
Los Alamos National Laboratory, Los Alamos, NM 87545, USA

The golden dream of any modeling enterprise is to predict the properties of the studied system in a new and often "hostile" environment. The basis of this kind of work is the careful, accurate assessment of the system properties in normal conditions. What "normal conditions" means for plutonium is an interesting question itself. This work is dedicated to modeling only a fraction of the remarkable characteristics of this "mysterious" material, that is the thermodynamic properties of its six allotropic phases (seven under pressure), the liquid phase, and the vapor phase. The goal is to provide valuable information for the calculation of alloyed plutonium phase diagrams.

Many thermodynamic calculations involve extrapolating known properties into regions where certain phases are unstable or metastable. For high temperature, the Gibbs free energy is usually expressed in a polynomial form based on the interpolation of the experimental heat capacity values.

$$C_P(T) = A + BT + CT^2 + DT^{-2} \quad \textbf{(1)}$$

A similar approach is based on measured enthalpy values. When starting the assessment, a first concern is the reliability of the input values. That is why we developed a set of computer programs that is capable of checking the self-consistency of the data set by verifying the fundamental thermodynamics relationships which involve the heat capacity at constant pressure C_p, the entropy S, the enthalpy H and the Gibbs free energy G.

If the pressure is constant, then:

$$C_p(T) = f(T)$$

$$H(T > T_1) = H_{T_0} + C_{p1}(\tau)d\tau + \Delta H_{t_1} + {}^{T}_{T_1}C_{p2}(\tau)d\tau$$

$$S(T > T_1) = S_{T_0} + \frac{C_{p1}(\tau)}{\tau}d\tau + \frac{\Delta H_{t_1}}{T_1} + \frac{{}^{T}C_{p2}(\tau)}{\tau}d\tau$$

$$G(T) = H(T) - T \cdot S(T) \ ,$$

where T_1 is the temperature of the phase transformation (if any) and T_0 is the reference temperature for enthalpy and entropy. Additional terms have been included to describe subsequent phase transformations. In many commercial databases T_0 equals 298.15 K because only high temperature properties are of interest. Our program also models properties situated bellow the room temperature. In that case, any attempt of using the common polynomial form (1) of $C_P(T)$ is most likely expected to fail. That is why we use for the heat capacity at constant volume the Einstein model, the Debye model, and the model developed by D. C. Wallace and recently applied to plutonium metal.[1]

CP532, Plutonium Futures – The Science, edited by K. K. S. Pillay and K. C. Kim,
2000 American Institute of Physics 1-56396-948-3

The thermodynamic information is stored in a relational database. Additional programs we have developed are using the information available for each phase to compute the equilibrium phase diagrams. Step by step, the user can monitor the properties of the phases and the interaction parameters. The programs can also predict metastable phases.

Figure 1 shows the enthalpy of solid plutonium for temperatures situated above the room temperature. The extrapolated values (plotted only for d and e phases, as examples) are a must for phase diagram calculations.

Throughout the course of the project we are in a continuous feedback mode, where the experimental results and the calculations are compared. The extrapolations to 0 K will be used to determine corrections to the atomic scale models which, in turn, will be incorporated to the thermodynamic calculations.

Reference

1. D. C. Wallace, Electronic and Phonon Properties of Six Crystalline Phases of Pu Metal, Phys. Rev. B, 58, 1998, p. 15433-15439.

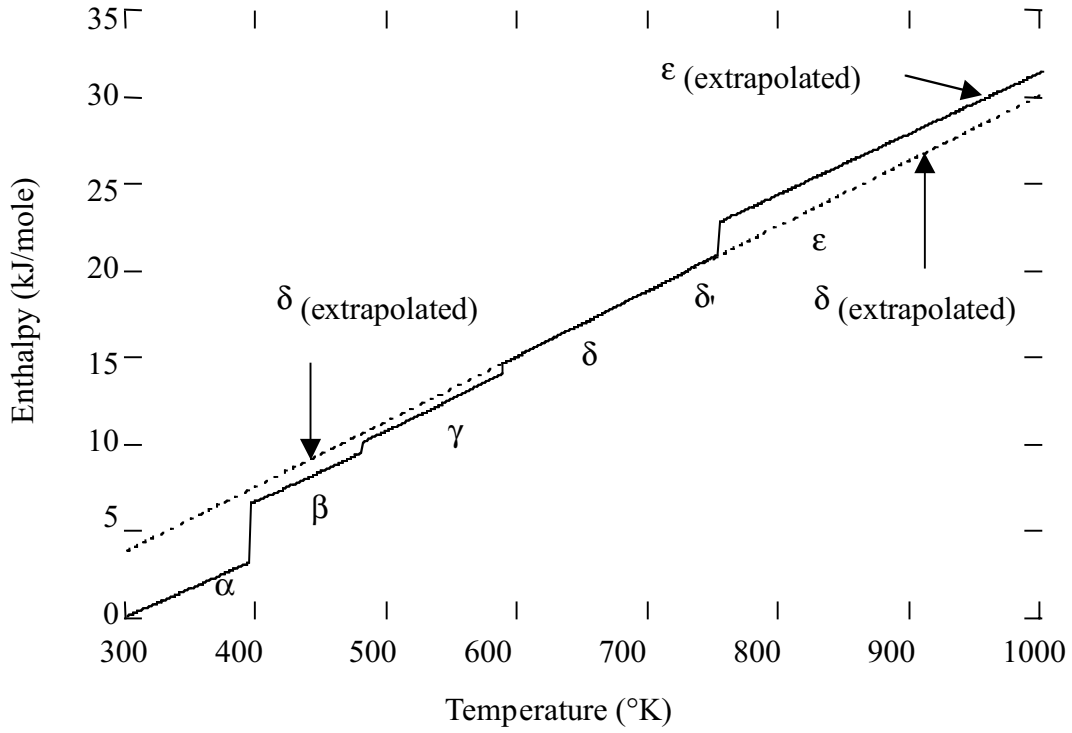

Figure 1. Modeled enthalpy of solid plutonium phases.

Theoretical Studies of Actinyl Crown Ether Inclusion Complexes

Richard L. Martin, P. Jeffrey Hay, Georg Schreckenbach
Los Alamos National Laboratory, Los Alamos, NM 87545, USA

Clark et al.[1] recently reported the synthesis of the NpO_2^+ ion encapsulated by the 18-crown-6 ligand. The $[NpO_2(18\text{-crown-6})]ClO_4$ salt was characterized crystallographically and shown to have six approximately coplanar crown ether oxygen atoms coordinated to a central NpO_2^+ unit.While the $[UO_2(18\text{-crown-6})]^{2+}$ species had been synthesized and characterized as the perchlorate salt previously,[2] this is the first example of a transuranic crown inclusion complex. Motivated by this synthetic accomplishment and the prospect of similar chemistry involving the Pu analogues, we have undertaken theoretical studies of the series of actinyl inclusion complexes $[AnO_2(18\text{-crown-6})]^{(1+,2+)}$, where An = U, Np, and Pu.

The calculations employed our previously developed relativistic effective core potentials,[3] hybrid density-functional-theory (B3LYP), and the Gaussian suite of electronic structure programs. Figure 1 depicts the optimized structure for the $[NpO_2(18\text{-crown-6})]^+$ and in Table 1 we report the actinyl bond lengths for the series The theoretical Np = O bond length for the Np(V) species $[NpO_2(18\text{-crown-6})]^+$ is in good agreement with experiment. Agreement with experiment is also good for the U = O bond length in the $[UO_2(18\text{-crown-6})]^{2+}$ species, *if* one assumes the longer of the two experimental determinations is valid. Note that for a given charge state, +1 or +2, there is very little change in the actinyl distance as one progresses from U to Pu. More significant are the changes in bond length as a function of charge. The An = O distance is typically 0.05Å shorter in the divalent cations. The theoretical distances to the crown ether oxygens, not reproduced in the table, show similar behavior as a function of actinide and charge. However, for these equatorial bonds the theoretical distances appear to be overestimated by nearly 0.1Å as judged by the Np(V) complex. We have earlier noted a tendency of the B3LYP approximation to overestimate dative bonds to H_2O in coordination to actinyl ions[4] and to the ferric ion.[5] The local-density approximation (LDA) of density-functional-theory does not seem to suffer from these problems in the cases mentioned above.Why the hybrid approach should give good actinyl distances, but poorer equatorial distances is not understood.

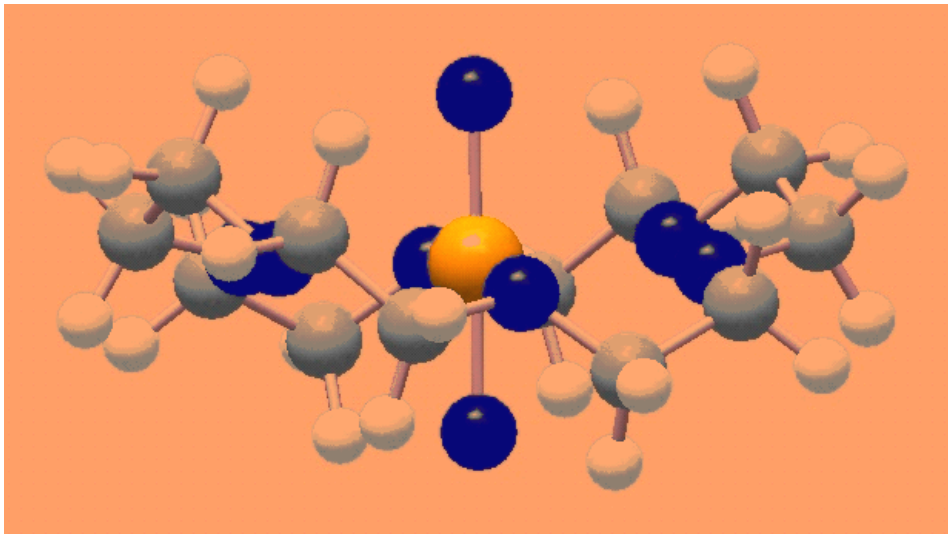

Figure 1. The structure computed for the $[NpO_2(18\text{-crown-6})]^+$ complex.

CP532, Plutonium Futures – The Science, edited by K. K. S. Pillay and K. C. Kim,
2000 American Institute of Physics 1-56396-948-3

	Calc.	*Expt.*
UO_2^+	1.81	--
NpO_2^+	1.81	1.80(1)
PuO_2^+	1.81	--
UO_2^{2+}	1.76	1.78,1.64 (2)
NpO_2^{2+}	1.76	--
PuO_2^{2+}	1.78	--

Table 1. Actinyl (18-crown-6) Bond Lengths from Relativistic Hybrid DFT Calculations (Å).

It is often the case that the actinyl stretching frequencies are a much more sensitive probe of the bond strength variations than the distances. Table 2 reports the frequencies computed for the symmetric and antisymmetric actinyl stretches. The symmetric stretch frequency of 780 cm^{-1} measured for the Np(V) crown ether complex[6] is in fortuitously good agreement with theory (776 cm^{-1}). Note that the Raman active symmetric stretch mode lies lower in frequency than the infrared active asymmetric stretch, and steadily decreases in frequency from UO_2^{q+} to PuO_2^{q+} for both the +1 and +2 charge states. The magnitude of the shift is large, the symmetric stretch being predicted to occur at 878, 839, and 623 cm^{-1} for U, Np, and Pu, respectively, in the the AnO^{2+} crown complexes, respectively.

	ω_{sym}	ω_{asym}
UO_2^+	823	891
NpO_2^+	776	877
PuO_2^+	697	855
UO_2^{2+}	878	980
NpO_2^{2+}	839	952
PuO_2^{2+}	623	847

Table 2. Actinyl (18-crown-6) Stretching Frequencies from Relativistic Hybrid DFT Calculations (cm^{-1}).

A decrease also occurs for the symmetric stretch frequency in the series of aquo complexes $AnO_2(H_2O)_5^{2+}$ (5). Again, a slight (~ 0.02 Å) contraction in the bond length occurs in going from U to Pu, accompanied by a very large *decrease* in the theoretical symmetric stretch frequency. An examination of the Mulliken atomic population gives net f and d populations of 2.71 and 1.26, respectively, in the formally f^0 case of $UO_2(H_2O)_5^{2+}$. In particular, the overlap populations show strong f_s participation in the actinyl bond. There is no strong variation in the atomic population of d and f-orbitals in moving from U to Pu (other than the expected increase in the number of actinide f-electrons), but one does observe a steady decrease in the net overlap population of about 10 percent, which we attribute to the smaller size of the 5f orbitals as the atomic number increases. The steady decrease in stretching frequency appears to correlate with this decreased overlap with the 5f orbital.

Finally, we have examined free energies for redox reactions in solution by combining thermodynamic free energies in the gas phase with a dielectric continuum model to treat solvent effects. Using this approach we have estimated redox potentials for the crown and aquo complexes. This effort has met with mixed success. Possible reasons for this will be discussed.

References

1. D. L. Clark, D. W. Keogh, P. D. Palmer, B. L. Scott, and C. D. Tait, *Angew. Chem. Int. Ed.*, **37**, 164(1998).

2. A. Dejean, P. Charpin, G. Folcher, P. Rigny, A. Navaza and G. Tsouraris, *Polyhedron,* **13**, 1725 (1987); A. Navaza, F. Villain, P. Charpinj, *Polyhedron,* **3**, 143 (1984).

3. P. J. Hay and R. L. Martin, *J. Chem. Phys.*, **109**, 3875 (1998).

4. P. J. Hay, R. L. Martin, and G. Schreckenbach, Los Alamos National Laboratory document LAUR99-6625, *J. Phys. Chem.*, submitted.

5. R. L. Martin, P. J. Hay, and L. R. Pratt, *J. Phys. Chem. A*, **102,** 3565 (1998).

6. C. D. Tait, private communication.